Final Project Report

Project Title: Development of Defluoridation Media for Contaminated Groundwater and its Lab to Field Application

Project No.: 23/43/2005-R&D/823 Dated: 29/06/2005

Sponsored by the Ministry of Water Resources and Central ground water Board (New Delhi)

Principal Investigator: Dr. Uday Chand Ghosh
Department of Chemistry,
Presidency College
Kolkata-700073

Contents

Project Title: "Development of defluoridation media for contaminated groundwater and its lab to field application"

Project No.: 23/43/2005-R&D/823 **Dated:** 29/06/2005

Sponsored by the Ministry of Water Resources and Central ground water Board (New Delhi).

Initial duration of the project: 16th August 2005 to 15th August 2007.

Time of the project had been extended to 31st December, 2007.

So, the total time for completion of the work was 16th August 2005 to 31st December, 2007.

Principal Investigator: Dr. Uday Chand Ghosh
Department of Chemistry,
Presidency College
Kolkata-700073

Chapter 1

1. Introduction

Fluoride is one often called a two edged sword. In small doses it has remarkable influence on the dental system by inhibiting dental caries, while in higher doses; it causes dental and skeletal fluorosis. It is evident from the information available that a certain quantity of fluoride is essential for the formation of caries-resistant dental enamel and for the normal process of mineralization in hard tissues. The element is metabolized from both electrovalent and covalent compounds. Low fluoride concentrations stabilize the skeletal system by increasing the size of the apatite crystals and reducing their solubility. About 95% of the fluoride in the body deposited in hard tissues and it continues to be deposited in calcified structures even after other bone constituents (Ca, P, Mg, CO_3 and citrate) have reached a steady state. Age is an important factor in deciding to what extent fluorine is incorporated into the skeletal. The uptake almost ceases in dental enamel after the age of about 30 years.

Health impacts from prolonged intake of fluoride-contaminated water have been reported as:

< 0.5 mg/L: dental carries; 0.5- 1.5 mg/L: promotes dental health;

1.5- 4.0 mg/L: dental fluorosis; > 4.0 mg/L: dental and skeletal fluorosis;

- 10.0 mg/L: crippling fluorosis

Rajib Gandhi National Drinking Water Mission (RGNDWM) published a survey report in 1998, which showed that the villagers of 8700 villages are consuming ground water contaminated with excess fluoride (1.0 to 48.0 mg/L),

and are under serious health risk. Depending on the extent of the fluoride problem, states have been categorized into three groups as following:

- **Category I: Less than 30% districts affected. Jammu and Kashmir, Kerala and Orissa.**
- **Category II: 30- 50% districts affected. Bihar, Haryana, Karnataka, Maharashtra, Madhya Pradesh and Punjub.**
- **Category III: More than 50% districts affected. Andhra Pradesh, Gujarat, Rajasthan, Tamilnadu, Uttar Pradesh.**

Thus, the supply of low fluoride-contaminated water to the villagers is an emergent need of our country.

Solution of the problem:

The supply of fluoride free or low fluoride (< 1.5 mg/L) contaminated drinking water can prevent or minimize the health problem related to fluoride toxicity. It could be possible by using the alternative drinking water sources such as supply of treated surface water and reduction of fluoride level from the contaminated ground water. The supply of surface water for drinking purpose to the dwellers of remote villagers is a distant possibility due to the huge fund requirement for technological shift. The simplest and cheapest way to have safe drinking water is the treatment of high fluoride contaminated (>1.5 mg/L) ground water. Thus the defluoridation of drinking water is the only practicable option to overcome the problem of excessive fluoride in drinking water. During the years following the discovery of fluoride as the cause of fluorosis, extensive research has been done on various methods for removal of fluoride from water and wastewater. The

methods developed for this purpose are divided into some basic types based upon the mode of action:

(1) Precipitation –coagulation (2). Sorption process (3). Ion-exchange process

(4) Membrane separation process (5). Electrochemical methods.

1.1. Based on precipitation–coagulation

Lime and alum are the most commonly used coagulants. Addition of lime leads to precipitation of fluoride as insoluble calcium fluoride and raises the pH value of water up to 11–12.

$$Ca(OH)_2 + 2F^- \rightarrow CaF_2 + 2OH^-$$

At a first step, precipitation occurs by lime dosing which is followed by a second step in which alum is added to cause coagulation. When alum is added to water, essentially two reactions occur. In the first reaction, alum reacts with some of the alkalinity to produce insoluble aluminium hydroxide [$Al(OH)_3$]. In the second reaction, alum reacts with fluoride ions present in the water. The best fluoride removal is accomplished at pH range of 5.5–7.5.

Limitations

- **The process removes only a smaller portion of fluoride (18–33%) in the form of precipitates and converts a greater portion of ionic fluoride (67–82%) into soluble aluminium fluoride complex ion, and therefore this technology is erroneous. Also, as the soluble aluminium fluoride complex is itself toxic, adoption of Nalgonda technique for defluoridation of water is not desirable.**

- **Due to use of aluminium sulfate as coagulant, the sulfate ion concentration increases tremendously and in few cases, it crosses the maximum permissible limit of 400 mg/L, which causes cathartic effect in human beings.**
- **The residual aluminium in excess of 0.2 mg/L in treated water causes dangerous dementia disease as well as pathophysiological, neurobehavioural, structural and biochemical changes. It also affects musculo skeletal, respiratory, cardiovascular, endocrine and reproductive systems.**
- **Due to organoleptic reasons, users do not like the taste of treated water.**
- **Regular analysis of feed and treated water is required to calculate the correct dose of chemicals to be added, because water matrix keeps on changing with time and season as evident from earlier studies.**
- **Maintenance cost of plant is very high.**
- **The process is not automatic. It requires a regular attendant for addition of chemicals and looking after treatment process.**
- **Large space is required for drying of sludge.**
- **Silicates have adverse effect on defluoridation by Nalgonda technique. Temperature also affects the defluoridation capacity.**

1.2. Based on sorption process

These include several bone formulations, synthetic tricalcium phosphate and hydroxy apatite and a variety of adsorbent materials. Some of them are provided below.

a) Bone charcoal

Then it is pulverized to fine powders and used as a defluoridating agent, and showed low sorption capacity.

b) Processed bone

Bone contains calcium phosphate and has a great affinity for fluoride. The bone is degreased, dried and powdered. The powder can be used as a contact bed for removal of fluoride in water. The exhausted bed is regenerated with sodium hydroxide solution. The use of this material has limitation on religious ground and low capacity.

(c) Tricalcium phosphate

The product is prepared by reacting phosphoric acid with lime. It has a capacity to remove 700 mg fluoride/L. The medium is regenerated with 1% NaOH solution followed by a mild acid rinse. However all polyvalent ions showed strong interference on fluoride sorption and difficult to use in the practical field.

(d) Florex

A mixture of tri-calcium phosphate and hydroxy-apatite, commercially called Florex, showed a fluoride removal capacity of 600 mg of fluoride per L., and is regenerated with 1.5% sodium hydroxide solution. Owing to high attritional losses, Florex was not successful and the pilot plants using this material were abandoned.

(e) Activated Carbons

Most of the carbons prepared from different carbonaceous sources showed fluoride removal capacity after alum impregnation. High fluoride removal capacities of various types of activated carbons had been reported, but not free from the limitation when applied in the field. It is not cost effective.

(f) Magnesia

Investigations were conducted to study the usefulness of magnesia in fluoride removal. The study established that magnesia removed the excess fluorides, but large doses were necessary. Moreover the pH of the treated water was beyond 10 and its correction by acidification or recarbonation was necessary. All this adds to the cost and complexity of operations. The acid requirement can be to the extent of 300 mg/L expressed in terms of $CaCO_3$/L.

Limitations

- **The high initial cost, large required concentrations, alkaline pH of the treated water and complexity of the preparation of magnesia are the inhibitive factors to render it acceptable in the field.**

(g) Tamarind Gel

The concentration of fluoride from solution of sodium fluoride of 10 mg/L could be brought down to 2 mg/L by the addition of tamarind gel alone and to 0.05 mg/L by the addition of small quantity of chloride with the tamarind gel.

(h) Serpentine

Serpentine is a mineral name, which applies to the material containing one or both of the minerals, chrysotile and antigorite. The composition of the mineral closely corresponds to the formula $Mg_6Si_4O_{10}(OH)$. The material is green or yellow and is available in Andhra Pradesh. A comparative evaluation for removal of fluoride was made using green and yellow varieties of serpentine and the results are given in Table 1. It is concluded that cost of defluoridation is prohibitive with serpentine.

Table 1: Comparative performance of green and yellow varieties of serpentine

Variety	GREEN VARIETY						YELLOW VARIETY					
Dose, g/L	0	10	20	40	60	80	0	10	20	40	60	80
Fluorides, mg/L	6.2	4.8	4.2	2.6	2.5	1.9	6.2	4.6	3.7	2.7	2.2	1.8
pH	8.8	8.4	8.6	8.7	8.8	8.9	8.4	8.4	8.6	8.8	8.8	8.9

(i) Activated alumina

Defluoridation of water by activated alumina is the method of choice in developed countries. Its affinity for fluoride is very high. However, pH and alkalinity are the factors, which affect the sorption capacity. The exhausted

material can be regenerated by washing with alkali followed by acid and finally with distilled water.

(j) Plant materials

The plant materials such as barks of *Moringa olifera* and *Emblica officinalis,* the roots of *Vetiveria zizanoides* and the leaves of *Cyanodon tactylon* were found to be poor defluoridating agents.

(k) Lime stone, special soils and clay etc.

Recently limestone and heat-treated soil were tried for fluoride removal. Attempts were made to use Kenyan soil derived from volcanic ash (ex: Ando soils or soils with andic properties) as a fluoride sorbent. Fluoride sorption studies were carried out on two clay minerals, montmorillonite KSF and kaolin, and a silty clay sediment series (SCSS, used in earthenware making). The function of fluoride concentration, clay concentration and pH in clay-water suspensions was studied and showed significant fluoride sorption. Removal of fluoride by sorption on to low-cost materials like kaolinite, bentonite, charfines, lignite and nirmali seeds was investigated.

(l) Fly Ash

Retention of fluoride ion in dynamic experiments on columns packed with fly ash was studied and found that the fly ash was not an effective sorbent especially at the concentration range that commonly found in groundwater.

1.3. Based on ion-exchange mechanism

a) Anion exchange resin

Strong base exchange resins remove fluorides either on hydroxyl cycle or chloride cycle along with anions. Some inorganic ion-exchangers, eg. Complex metal chloride silicates, formed from barium or ferric chloride with silicic acid, also exchange fluoride for chloride. Polystyrene anion exchange resins and strongly basic quaternary ammonium type resins are known to remove fluorides from water along with other anions.

b) Cation exchange resins

Cation exchange resins impregnated with alum solution have been found to act as defluoridating agents. "Avaram bark" based cation exchange resin works effectively in removing fluoride from water.

Limitations

- **Efficiency is reduced in presence of other ions like sulfate, carbonate, phosphate and alkalinity.**
- **Regeneration of resin is a problem because it leads to fluoride-rich waste, which has to be treated separately before final disposal.**

- **The technique is expensive because of the cost of resin, pre-treatment required to maintain the pH, regeneration and waste disposal.**
- **Treated water has a very low pH and high levels of chloride.**
- **It will make the water totally demineralised and hence not hygienic.**

1.4. Based on membrane process

Although various conventional techniques of water purification described earlier are being used at present to solve the problem of ground water pollution, none of them is user-friendly and cost-effective technique due to some or the other limitation and has either no or very long pay back period. In the recent years, reverse osmosis (RO) membrane process has emerged as a preferred alternative to provide safe drinking water without posing the problems associated with other conventional methods.

Limitations

- **It removes all the ions present in water, though some minerals are essential for proper growth, remineralization is required after treatment.**
- **The process is expensive in comparison to other options.**
- **The water becomes acidic and needs pH correction.**
- **Lot of water gets wasted as brine.**
- **Disposal of brine is a problem.**

1.5. Based on electrochemical method

A technology of defluoridation through electrochemical route has been developed. The process utilizes 0.3 to 0.6 kwh of electricity per 1000L of water containing 5-10 mg/L of fluoride. The anode is continuously consumed and needs to be replenished. The process generates sludge at the rate of 80–100g. per 1000L (on dry basis).

Limitations

- **Electricity is the main raw material and hence wherever electricity is not available a suitable polar panel can be installed.**

1.6. Review work on removal of fluoride:

1. C. R. Nagendra Rao, 2003, Fluoride and environment- A review, Proceedings of the third international conference on environment and health, Chennai, India, 15-17 December, 2003.
2. E. J. Underwood, 1997, Trace elements in human and animal nutrition, Academic press, New York, 545.
3. C. B. Dissanayake, 1991, The fluoride problem in the groundwater of Sri Lanka- Environmental management of health, Int. J. Environ. Studies, 19, 195- 203.
4. Y. Wang and E. J. Reardon, 2001, Activation and regeneration of a soil sorbent for defluoridation of drinking water, Appl. Geochem., 16, 531-539.

5. H. Lounici, L. Addour, D. Belhocine, H. Grib, S. Nicolas and B. Bariou, 1997, Study of a new technique for fluoride removal from water, Desalination, 114, 241- 251.
6. M. Srimurali, A. Pragathi and J. Karthikeyan, 1998, A study on removal of fluorides from drinking water by adsorption onto low-cost materials, Environ. Pollut., 99(2), 285- 289.
7. M. Hichour, F. Persin, J. Sandeaux and C. Gavach, 2000, Fluoride removal from waters by Donnan dialysis, Sep. Purif. Technol., 18, 1- 11.
8. Y. Veressinina, M. Trapido, V. Ahelik and R. Munter, 2001, Fluoride in drinking water: The problem and its possible solutions, Proc. Estonian Acad. Sci. Chem., 50(2), 81- 88.
9. J. Lina, 1999, Varjatud tervisevalem, Referent, Stockholm.
10. F. A. Smith and H. C. Hedge, 1959, Fluoride toxicity, J C Mnhler and M K Hone (Edn) " Fluorine and dental health", Indian University press, Bloomington.
11. WHO, 1984, Fluorine and fluorides, WHO Environmental Health Criteria No. 36, IPCS, Geneva.
12. J. A. Lalumandier and J. L. Jones, 1999, Fluoride concentrations in drinking water, J. AWWA, 91, 42- 52.
13. K. R. Bulusu, B. B. Sundaresan, B. N. Pathak, W. G. Nawlakhe, D. N. Kulkarni and V. P. Thergaonkar, 1979, Fluorides in water, defluoridation methods and their limitations, Journal of the Institution of Engineers (India), 60, 1- 25.

14. L. Fang, K. N. Ghimire, M. Kuriyama, K. Inoue and K. Makino, 2003, Removal of fluoride using some lanthanum (III)- loaded adsorbents with different functional groups and polymer matrices, J. of Chem. Tech. And Biotech., 78, 1038- 1047.
15. E. Oguz, 2005, Adsorption of fluoride on gas concrete materials, J. of Hazard. Mater. B117, 227- 233.
16. UNICEF's position on water fluoridation, Water environment and sanitation (WES), http://www.nofluoride.com/Unicef_fluor.htm
17. B. K. Handa, 1975, Geochemistry and genesis of fluoride containing ground waters in India, Ground water, 13, 275- 281.
18. W. W. Wanzel and W. E. H. Blum, 1992, Fluoride speciation and mobility in fluoride contaminated soils and minerals, Soil Sci., 153, 357- 364.
19. E. S. Perez and J. Sanz, 1999, Fluoride concentration in drinking water in the province of Soria, central Spain, Environ. Geochem. Hlth., 21, 133- 140.
20. V. K. Saxena and S. Ahmed, 2001, Dissolution of fluoride in ground water: a water- rock interaction study, Environ. Geology, 40(8), 1084- 1087.
21. Fluoride in water: An overview, www.unicef.org/wes/fluoride.pdf
22. Global Groundwater Information System, www.igrac.nl.
23. P. D. Namade, A. Vasudeva Rao and B. J. Alappat, 2002, Removal of fluorides from water using low cost adsorbents, Water supply, 2(1), 311- 317.
24. A.K. Susheela, 1999, Fluorosis management programme in India, Current science, 77(10), 1250- 1256.

25. W. G. Nawalakhe, D. N. Kulkarni, B. N. Pathak, K. R. Bulusu, 1975, Defluoridation of water by Nalgonda technique, Ind. J. Environ. Health, 17, 26-65.
26. P.Nayak, 2002, Review aluminium: impacts and disease, Environ. Res. Sec., A89, 101–115.
27. Meenakshi, R. C. Maheshwari, 2006, Fluoride in drinking water and its removal, J. Hazard. Mate., B137, 456–463.
28. W. H. MaC Intire and J. W. Hammond, 2001. Removal of Fluorides from Natural Water of Calcium Phosphate, Industrial Engineering Chemistry, 30, 100.
29. T. S. Bhakuni and N. N. Sharma, 1962, Studies on Defluoridation, Indian J. of Environ. Health, IV, 11-16.
30. E. Elvolve, July 1940, U S Patent No.2207725, Chemical Abstracts, 34, 8129.
31. C. Zevenbergen, L. P. vanReeuwijk, G. Frapporti, R. J. Louws and R. D. Schuiling, 1997, A simple method for defluoridation of water at village level by adsorption on Ando soil in Kenya, Fluoride J. International Society for Fluoride Research, 30(2), 128.
32. M. Agarwal, K. Rai, S. Srivastava, M. M. Srivastava, S. Prakash, , R. Shrivastav and S. Dass, 1998, Fluoride sorption on clay and clay minerals: An attempt to search for viable Defluoridating agent, Fluoride J. International Society for Fluoride Research, 31(3), S30.
33. R. Piekos and S. Paslawska, 1999, Fluoride uptake Characteristics of Fly Ash, Fluoride J. International Society for Fluoride Research, 32(1), 14-19.

34. W. Runaska, M. Kawane and T. Kajima, 1951, Removal of Fluoride Ion by Anion Exchange Resin, Chemical Abstracts, 45, 5033.

35. Z. Amer, B. Bariou, N. Mameri, M. Taky, S. Nicolas, A. Elmidaoui, 2001, Fluoride removal from brackish water by electrodialysis, Desalination, 33, 215–223.

36. A. Dieye, C. Larchet, B. Auclair, C. Mar-Diop, 1998, Elimination des fluorures par la dialyse ionique croisee, Eur. Polym. J., 34, 67–75.

37. Electrochemical Deflkuoridation, http://www.tifac.org.in/offer/tsw/cecri1.htm

38. X. Fan, D. J. Parker and M. D. Smith, 2003, Adsorption kinetics of fluoride on low cost materials, Water Res., 37(20), 4929- 4937.

39. M. G. Sujana, R. S, Thakur and S. B. Rao, 1998, Removal of Fluoride from Aqueous Solution by using Alum Sludge, J. Coll. Interface Sci., 206(1), 94- 101.

40. N. Das, P. Pattanaik and R. Das, 2005, Defluoridation of drinking water using activated titanium rich bauxite, J. Colloid Interf. Sci., 292, 1-10.

41. D. Mohapatra, D. Mishra, S. P. Mishra, G. Roy Choudhury and R. P. Das, 2004, Use of oxide minerals to abate fluoride from water, J. Colloid Interf. Sci., 275(2), 355- 359.

42. Y-M. Xu, A-R. Ning and J. Zhao, 2001, Preparation and defluoridation performance of activated cerium(IV) oxide/ SiMCM-41 adsorbent in water, J. Colloid Interf. Sci., 235, 66- 69.

43. Y. Kojima, A. Kumar, D. Kuchar, M. Kuboto, H. Matsuda, 2006, Uptake of fluoride by Al^{3+} pretreated low-silica synthetic zeolites, Sep. Sci. Technol., 41(4), 683- 704.

44. Y. Ku, H.-M. Choi, W. Wang, 2002, The removal of fluoride ion from aqueous solution by a cation synthetic resin, Sep. Sci. Technol., 37(1), 89- 103.
45. D. P. Das, J. Das and K. Parida, 2003, Physicochemical characterization and adsorption behavior of calcined Zn/Al hydrotalcite-like compound (HTlc) towards removal of fluoride from aqueous solution, J. Colloid Interf.. Sci., 261, 213- 220.
46. A. V. Jamode, V. S. sapkal and V. S. Jamode, 2004, Defluoridation of water using inexpensive adsorbents, J. Ind. Inst. Sci., 84, 163- 171.
47. L. Pietrelli, 2005, Fluoride wastewater treatment by adsorption onto metallurgical grade alumina, Annali di chimica, 95(5), 303- 312.
48. A. M. Raichur, M. J. Basu, 2001, Adsorption of fluoride onto mixed rare earth oxide, Sep. Sci. Technol., 24, 121- 127.
49. M. Mahramanlioglu, I. Kizilcikli and I. O. Bicer, 2002, Adsorption of fluoride from aqueous solution by acid treated spent bleaching earth, J. Fluorine Chemistry, 115, 41- 47.
50. A. K. Yadav, C. P. Kaushik, A. K. Haritash, A. Kansal and N. Rani, 2006, Defluoridation of ground water using brick powder as an adsorbent, J. Hazard. Mater., B128, 289–293.
51. L. Ruixia, G. Jinlong and T. Hongxiao, 2002, Adsorption of fluoride, phosphate, and arsenate ions on a new type of ion exchange fibre, J. Colloid Interf. Sci., 248(2), 268- 274.
52. Y. H. Li, S. Wang, X. Zhang, J. Wei, C. Xu, Z . Luan, D . Wu, B. Wei, 2003, Removal of Fluoride from Water by Carbon Nanotube Supported Alumina, Environmental Technology, 24(3), 391-398.

53. D. A. P. Tanaka, S. Kerketta, M.A. L. Tanco, T. Yokoyama and T. M. Suzuki, 2002, Adsorption of fluoride on the Zirconium(IV) complexes of the chelating resins functionalised with amine-N-acetate ligands, Sep. Sci. Technol., 37(4), 877-894.
54. A. L. Valdivieso, J. L. R. Bahena, S. Song, R. H. Urbina, 2006, Temperature effect on the zeta potentia; and fluoride adsorption at the α- Al_2O_3/ aqueous solution interface, J. Colloid Interf. Sci., 298(1), 1- 5.
55. S. Ghorai and K. K. Pant, 2005, Equilibrium, kinetics and breakthrough studies for adsorption of fluoride on activated alumina, Sep. and Purif. Technol., 42(3), 265- 271.
56. S. M. Maliyekkal, A. T. Sharma, L. Philip, 2006, Manganese-oxide-coated alumina: A promising sorbent for defluoridation, Water Res., 40(19), 3497- 3506.
57. N. I. Chubar, V. F. Samanidou, V. S. Kouts, G. G. Gallios, V. A. Kanibolotsky, V. V. Strelko and I. Z. Zhuravlev, 2005, Adsorption of fluoride, chloride, bromide and bromate ions on a novel ion exchanger, J. Colloid Interf. Sci., 291(1), 67-74.
58. B. Shimelis, F. Zewge and B. C. Singh, 2006, Removal of excess fluoride from water by aluminium hydroxide, Bulletin of the chemical society of Ethiopia, 20(1), 17- 34.
59. Y. Cengeloglu, E. Kir and M. Ersoz, 2002, Removal of fluoride from aqueous solution by using red mud, Sep. Purif. Technol., 28(1), 81- 86.
60. Y. H. Li, S. Wang, A. Cao, D. Zhao, X. Zhang, C. Xu, Z. Luan, D. Ruan, J. Liang, D. Wu and B. Wei, 2001, Adsorption of fluoride from water by amorphous

alumina supported on carbon nanotubes, Chemical physics letter, 350(5), 412-416.

61. L. Lv, J. He, M. Wei, D. G. Evans and X. Duan, 2006, Factors influencing the removal of fluoride from aqueous solution by calcined Mg–Al–CO_3 layered double hydroxides, J. Hazard. Mater., 133(1- 3), 119- 128.
62. A. K. Chaturvedi, K. P. Yadav, K. C. Pathak and V. N. Singh, 1990, Defluoridation of water by adsorption on fly ash, Water, Air and soil Pollut., 49, 51- 61.
63. A. Sivasamy, K. P. Singh, D. Mohan and M. Muruthamuthu, 2001, Studies on defluoridation of water by coal-based sorbents, J. Chem. Tech. Biotech., 76, 717-722.
64. R. L. Ramos, J. Ovalle-Turrubiartes, M. A. Sanchez-Castillo, 1999, Adsorption of fluoride from aqeous solution on aluminium-impregnated carbon, Carbon, 37(4), 609- 617.
65. M. Agarwal, K. Rai, R. Shrivastav, S. Dass, 2002, A study on fluoride sorption by Montmorillonite and Kaolinite, Water, Air and Soil Pollut., 141(1-4), 247-261.
66. C. Caste, M. Schweizer, M. O. Simonnot, M. Sardin, Selective removal of fluoride ions by a two-way ion-exchange cyclic process Chem. Eng. Sci, **55,** 3341 – 52 (2000).
67. Y. Cengeloglu, E. Kir, M. Ersoz.M, Removal of fluoride from aqueous solution by using red mud, Separ. Purif. Technol., **28**, 81 – 6 (2002).
68. S. Dey, S. Goswami, U. C. Ghosh, Hydrous ferric oxide (HFO) – A scavenger for fluoride from contaminated water, Water, Air and Soil Pollu., **158**, 311 – 23 (2004).
69. X. Fan, D. J. Parker, M. D. Smith, Adsorption Kinetics of fluoride on low cost materials, Water Res., **37**, 4929 – 37 (2003).

70. S. Ghorai, K. K. Pant, Equilibrium, kinetics and breakthrough studies for adsorption of fluoride on activated alumina, Sep. Purif. Technol., **42** (3), 265-71 (2005).

71. S. Goswami, S. Dey, U. C. Ghosh, Studies on removal of fluoride by hydrated zirconium oxide (HZO), Chem.Environ.Res., **13**, 117 – 26 (2004).

72. M. Srimurali, A. Pragathi, J. Karthikeyan, A study on removal of fluorides from drinking water by adsorption onto low cost materials, Environ. Pollu., **99**, 285–9 (1998).

73. Tramfloc. Inc "Fluoride removal by activated alumina" PO Box 350, Tempe, AZ 85280 – 0350, water@tramfloc.com, copy right© 1997 – 2005, Tramfloc, Inc. (2005).

74. S. A. Wasay, Md. J. Haron, S. Tokunaga, Adsorption of fluoride, phosphate and arsenate ions on lanthanum impregnated silica gel, Water Environ. Res., **68**, 295–300 (1996).

75. M. Yang, T. Hashimoto, N. Hoshi, H. Myoga, Fluoride removal in a fixed bed packed with granular calcite, Water Res., **33**(16), 3395 – 402 (1999).

76. C. L. Yang, R. Dluhy, Electrochemical generation of aluminium sorbent for fluoride adsorption, J. Hazardous Mater., **94**(3), 223-38 (2002).

1.7. Objectives of the project:

I. To synthesis of pure/mixed oxides of polyvalent metals.

II. To study the adsorption behaviors of fluoride on to the synthetic oxides.

III. To study the interfering effect of some other ions viz,. Chloride, sulfate, bicarbonate, phosphate, iron(III), calcium and magnesium.

IV. To study the column test in removing fluoride using synthetic hydrous oxide packed column with varying down flow rate, bed height, bed volume etc.

V. To study regeneration of fluoride adsorbed oxide and reuse of the oxide.

VI. To study fluoride removal using field sample

VII. To study fluoride removal in pilot-scale in the field using developed best medium.

1.8. Summary of work done:

During the working period of the project four effective low cost defluoridation media were synthesized. The physical characteristic like FTIR, XRD, SEM, TGA, DTA etc. for all the four media were carried out. The fluoride adsorption studies were performed with three media out of the four synthesized media.

The four synthesized media are:

(1) Iron(III)-Zirconium(IV) Mixed Oxide, (2) Iron(III)-Aluminium(III) Mixed Oxide

(3) Iron(III)-Tin(IV) Mixed Oxide and (4) Iron (III)-Chromium (III) Mixed Oxide.

Adsorption Kinetics of Fluoride on Iron(III)-Zirconium(IV) Hybrid Oxide

Fluoride occurs in some drinking water sources at levels that are hazardous to health. Tests were conducted to assess the ability of a mineral-based adsorbent to take-up fluoride ion. Consequently, in search of novel adsorbent media, crystalline and hydrous iron(III)-zirconium(IV) hybrid oxide (IZHO) was synthesized, and tested to determine its capacity and kinetics for fluoride adsorption. The Fourier Transform Infrared (FTIR) spectrum of IZHO indicated the presence of Fe-O-Zr linkage which showed hybrid nature of the synthetic oxide. The optimum pH range for fluoride adsorption was ranged between 4.0 and 7.0. The analyses of the isotherm equilibrium data using the Langmuir and the Redlich-Peterson model equations by linear and non-linear methods showed that the data fitted better with latter model than the former. Thermodynamic analysis showed spontaneous nature of fluoride adsorption, and that took place with the increase of entropy. The kinetic data obtained for fluoride adsorption on IZHO at pH 6.8 (± 0.1) and room temperature (303±2 K) described both the pseudo-first order and the reversible first-order equations equally well (r^2 = ~0.98-0.99), and better than pseudo second order equation (r^2 = ~0.96-0.98) for higher concentrations (12.5 and 25.0 mg/dm^3) of fluoride. The kinetics of fluoride adsorption on the mixed oxide took place with boundary layer diffusion. External mass transport with intra-particle diffusion phenomena governed the rate limiting process, which has been confirmed from the Boyd poor non-linear kinetic plots.

ADSORPTION OF FLUORIDE ON SYNTHETIC IRON (III), ZIRCONIUM (IV) AND BINARY IRON (III)-ZIRCONIUM (IV) OXIDES: COMPARATIVE ASSESMENT ON PH-EFFECT AND ISOTHERM

Fluoride is an accumulative poison at high dose of intake for human and animals. Here, the sorption of fluoride from aqueous solution has been investigated on synthetic hydrous ferric oxide (HFO), hydrous zirconium oxide (HZO) and hydrous zirconium(IV)-iron(III) oxide (HZFO) by batch mode experiments. Both HFO and HZFO were crystalline and HZO was amorphous in nature. The parameter studied were the effect of pH and sorption equilibriums. Results show the increase of fluoride-sorption with increasing pH from nearly 2.0 to 5.0, 4.6 and 6.8 for HFO, HZO and HZFO, respectively. Analysis of temperature dependent sorption data obtained at equilibrium solution pH 6.8 (± 0.2) has been described by the Langmuir, Freundlich, Temkin and Redlich-Peterson isotherm model equations. The present sorption data fit, in general, are very well with the Langmuir and Redlich-Peterson models; and the fit of present data for HZFO and HFO increased but that for HZO decreased with increasing temperature. The computed thermodynamic parameters such as ΔG^0, ΔH^0 and ΔS^0 from the Langmuir equilibrium constant (b, L/mg) values show that the fluoride-sorption on HZFO was more spontaneous and endothermic process compared with that on HFO. The ΔH^0-value obtained for fluoride adsorption on HZO shows exothermic in nature.

Adsorption of Fluoride from Aqueous Solution by Synthetic

Iron(III)-Aluminum(III) Mixed Oxide.

This paper presents the synthesis of iron(III)-aluminum(III) mixed oxide with some of its physicochemical characteristics and fluoride adsorption behavior thereon. Results showed that the optimum initial pH for fluoride adsorption is 4.0-10.0, and the equilibrium time required is 1.5 h. The isotherm data follow the order: Redlich-Peterson ≥ Langmuir > Freundlich > Temkin. The Langmuir monolayer adsorption capacity of the adsorbent is found to be 17.73 mg/g, and it is higher than either of the pure oxides. The enthalpy change (ΔH^0) and entropy change (ΔS^0) for the adsorption reaction are +29.31 $kJmol^{-1}$ and +116.75 J $mol^{-1}K^{-1}$ respectively. The adsorption is endothermic in nature. The kinetics followed is pseudo-second order rate equation, and the reaction rate is multistage controlled diffusion process. The activation energy for this adsorption reaction is 6.35 $kJmol^{-1.}$

Fluoride Adsorption for Removal by Hydrous Iron(III)-Tin(IV) Bimetal Mixed Oxide from the Aqueous Solutions.

Fluoride occurs in some drinking water sources at a level that are hazardous to health. Tests were conducted to assess the ability of a mixed oxide adsorbent to take up fluoride ion. Consequently, in search of novel adsorbent media, hydrous iron(III)-tin(IV) mixed oxide (HITMO) was synthesized by a simple method and characterized. The X-ray diffraction (XRD) and the scanning electron microscopic (SEM) image showed HITMO was amorphous with irregular surface morphology. This material was tested for fluoride adsorption for removal from water. The pH effect showed the decrease of fluoride

adsorption capacity with increasing pH from 3.0 to 5.0, and remained constant up to pH 7.5.The kinetic data described the pseudo-second order model very well and, the adsorption rate was multi-stage controlled. The equilibrium data described the Langmuir isotherm model well, and the monolayer adsorption capacity obtained was ~10.50 mg g^{-1}. The mean energy computed (9.05 kJ mol^{-1}) from D-R isotherm suggested the ion exchange mechanism for fluoride adsorption. The thermodynamic parameters evaluated for the present reaction showed the ΔH^0, ΔS^0 and ΔG^0 values are positive indicating the fluoride adsorption by HITMO was endothermic and non-spontaneous process. The fluoride-rich material was regenerated up to ~75% with a pH 13.0 solution. The HITMO when applied for scavenging fluoride from the spiked (2.97 mg L^{-1}) natural water sample by batch technique showed 2.0 g material reduced the level down to 1.5 mg F^- L^{-1}.

Analysis of some field sample:

Some field samples were analyzed for fluoride for selection of spot to carry out the field test of our material.

Chapter 2

Materials and Methods

2.1. Reagents

Sodium fluoride (AR, BDH) was used for the preparation of the standard fluoride (1000 mg/dm^3) stock solution. Sodium 2-(para sulfophenyl azo)-1,8-dihydroxy-3,6-naphthalene disulfonate (SPADNS) and zirconyl oxychloride used for fluoride analysis were of GR (E. Merck) grade. Other chemicals used were of reagent grade.

2.2. Instruments

A pH-meter (Model: LI-127, ELICO India) was used for pH measurements throughout the experiments. UV-VIS spectrophotometer (Model: U3210, Hitachi Japan)

was used for fluoride determination. X-ray diffraction (XRD) of the synthetic oxide was obtained from a Philips Mat, Holland, PW1730/10 diffractometer. Scanning Electron Microscopy (SEM) of the oxide was taken by using Cambridge-360 scanning electron microscope. Perkin Elmer-RXFT Spectrophotometer was used for Fourier Transform Infra Red (FTIR) analysis of the synthetic oxide. Simudza made thermal analyzer was used for thermal analysis of the synthetic oxide.

2.3. Adsorption experiments

Batch adsorption experiments were conducted separately for evaluating the (i) effect of pH at 303 (±2)K for the concentrations 5.0, 12.5 and 25.0 mg F^-/dm^3 in the pH range 2.0 to 10.0, and (ii) isotherm equilibrium at pH 6.8 (± 0.1) and at temperatures 283 , 293 and 303 K in the concentration range 5.0 to 50.0 mg F^-/dm^3 by shaking (speed: 290 ± 10 rpm) the reaction mixture taken into 125 cm^3 capped polythene bottles. Here, 0.1g of the mixed oxide (particle size: 140-290 μm) was thoroughly mixed with 50 cm^3 fluoride solutions. The pH of the solutions was adjusted with 0.1 M hydrochloric (HCl) and/or 0.1 M sodium hydroxide (NaOH), as required. Intermediate major pH change, if any, noted was controlled with above acid/alkali solution for determining optimum pH-range for fluoride adsorption.

The batch adsorption kinetic experiments were carried out by shaking (290 ± 10 rpm) 0.1g of the mixed oxide with 50 cm^3 solution of the adsorbate (concentrations: 5.0, 12.5 and 25.0 mg F^-/dm^3) at a pH 6.8 (± 0.1) and at a temperature 303 (±2)K. The reaction mixtures were taken into ten separate 125 cm^3 polythene bottles for each concentration. The major pH change, if any, noted during the run of experiment was adjusted using above acid or alkali solution, as required. The reaction mixtures with bottles were withdrawn regularly at a desired time interval, and filtered immediately using 0.45 μm membrane filters. The filtrates were analyzed for residual fluoride by using the standard methods [1].

2.4. Theory

2.4.1. Isotherm modeling

For analysis of the equilibrium data obtained at pH 6.9 (± 0.2) and a temperature 28 (±1) ºC for fluoride adsorption onto the synthetic mixed oxide, the following isotherm model equations are used:

The Langmuir isotherm [2]:

The basic Langmuir isotherm model based on monolayer coverage of adsorbent surfaces by the adsorbate is:

$$q_e = \theta b C_e/(1+bC_e) \quad \ldots\ldots\ldots\ldots\ldots\ldots(1)$$

where q_e and C_e, respectively, are the equilibrium adsorption capacity (mg g^{-1}) and the equilibrium adsorbate concentration (mg L^{-1}), θ is the monolayer surface coverage(mg g^{-1}) and b is the equilibrium adsorption constant (L mg^{-1}).

To evaluate the adsorption capacity for a particular range of adsorbate concentration, the above equation (Eq.1) can be used as a linear form as follows:

$$C_e/q_e = 1/(\theta b) + C_e/\theta \quad \ldots\ldots\ldots\ldots\ldots\ldots(2)$$

The θ value i.e. monolayer surface coverage (mg g^{-1}) was calculated from the slope of the linear plot of C_e/q_e versus C_e.

The Freundlich isotherm [3]:

The basic isotherm model equation developed by Freundlich (1906) based on multilayer adsorption of an adsorbate on to the heterogeneous surfaces of an adsorbent is:

$$q_e = K_F C_e^{1/n} \quad \ldots\ldots\ldots\ldots\ldots\ldots(3)$$

where q_e and C_e have the same meaning as noted above, K_F and n are empirical constants dependent on several environmental factors. The linear form of the Freundlich equation (Eq.3) which is commonly used to describe adsorption isotherm data is:

$$\log q_e = \log K_F + 1/n \log C_e \quad \text{.....(4)}$$

The plot of $\log q_e$ versus $\log C_e$ of the equation (Eq. 4) should result a straight line. From the slope and intercept of the plot, the values for n and K_F are to be obtained.

Temkin isotherm [4]:

The simple form of Temkin adsorption isotherm model developed considering chemisorption of an adsorbate onto the adsorbent is represented as:

$$q_e = a + b \log C_e \quad \text{.....(5)}$$

where q_e and C_e have the same meaning as above, and other parameters are called the Temkin constants. The plot of q_e versus $\log C_e$ will generate a straight line. The Temkin constants, a and b can be calculated from the slope and intercept of the linear plot of q_e versus $\log C_e$.

The Redlich- Peterson isotherm [5]:

Jossen et al.[26] suggested that the Redlich-Peterson isotherm model with three parameters contains the features of both the Langmuir and the Freundlich isotherms.

The basic form of the model is

$$q_e = X C_e / (1 + Y C_e^{g}) \quad \text{.....(6)}$$

It has three isotherm constants, namely X, Y and g ($0<g<1$) those characterized the model. The above equation becomes the Langmuir equation for g =1 and the Henry's law form for g = 0.

The above equation (Eq. 6) can be arranged to the following linear form as:

$$C_e/q_e = \alpha + \beta C_e^{g} \quad \text{.....(7)}$$

where α ($=X^{-1}$, mg L^{-1}) and β ($= YX^{-1}$, mg L^{-1}) are the Redlich-Peterson constants. The three parameters equation (Eq. 7) has been used to analyze the present data by linear

regression of C_e^g on C_e/q_e with trial and error optimization of g for yielding maximum regression coefficient (r^2) value.

2.5. Adsorption kinetics:

To express the mechanism of fluoride adsorption onto the surface of iron(III)-aluminum(III) mixed oxide, the following kinetic model equations are used to analyze the present adsorption data for determining the related kinetic parameters.

The pseudo-first order model [6]:

The Lagergren (1898) rate equation is most widely used as a rate equation for assigning the adsorption of an adsorbate from a liquid phase. The pseudo-first order equation is represented as:

$$dq_t/dt = k_1 (q_e - q_t) \text{ …….. (8)}$$

where q_e and q_t are the adsorption capacity (mg g^{-1}) at equilibrium and time t respectively, k_1(time^{-1}) is the rate constant of pseudo-first order adsorption reaction . The integrated pseudo- first order rate equation at boundary conditions (t=0 to t = t and q_t =0 to q_t =q_t) can be written as:

$$\log (q_e - q_t) = \log q_e - k_1 t / 2.303 \text{ ……..(9).}$$

The plot of log (q_e-q_t) versus t should give a straight line from which k_1 and q_e can be calculated from the slope and intercept of the plot, respectively.

The pseudo-second order model [7]:

Ho and McKay (1998) developed a pseudo-second order kinetic expression for describing the adsorption of some metal ion onto the adsorbent.

The form of the pseudo-second order adsorption kinetic rate equation is expressed:

$$(dq_t/dt) = k_2 (q_e - q_t)^2 \quad \ldots\ldots\ldots\ldots\ldots\ldots (10)$$

where q_e and q_t have the same meaning as mentioned above. k_2 (g. mg^{-1} $time^{-1}$) is the rate constant for the pseudo–second order adsorption reaction. The integrated pseudo- second order rate equation at boundary conditions (t = 0 to t = t and q_t = 0 to q_t = q_t) can be written as:

$$1/(q_e - q_t) = 1/ q_e + k_2 t \quad \ldots\ldots\ldots\ldots\ldots\ldots\ldots\ldots\ldots\ldots (11)$$

The above equation (Eq. 11) can be rearranged to obtain the linear form (Eq. 12) as:

$$t/q_t = 1/(k_2 q_e^2) + t/q_e \quad \ldots\ldots\ldots\ldots\ldots\ldots\ldots\ldots\ldots\ldots (12)$$

The value of q_e and the pseudo-second order rate constant (k_2) can be calculated from the slope and intercept of the straight line obtained from the plot of t/q_t versus t .The initial adsorption rate can be obtained as q_t /t when t approaches to zero.

$$h_0 = k_2 q_e^2 \quad \ldots\ldots\ldots\ldots\ldots\ldots (13)$$

where h_0 is the initial adsorption rate (mg g^{-1} $time^{-1}$).

Intra particle diffusion model [8, 9]:

The adsorbate moves from the solution phase to the surface of the adsorbent particles in several steps. The overall adsorption process may be controlled by either one or more steps, e.g. film or external diffusion, pore diffusion, surface diffusion and adsorption on the pore surface or a combination of more than one step. In a rapidly stirred batch process of adsorption, the diffusive mass transfer can be related by an obvious diffusion coefficient, which will fit experimental adsorption rate data. Normally, a

process is diffusion controlled if its rate is dependent upon the rate at which components diffuse towards one another. The possibility of intra particle diffusion was explored by using the intra particle diffusion model:

$$q_t = k_{id} t^{1/2} + C \quad \text{.....(14).}$$

where k_{id} is the intra-particle (pore) diffusion rate constant (mg g^{-1} $time^{-0.5}$) and C is the intercept that gives an idea about the thickness of the boundary layer. Larger the value of C the greater is the boundary layer effect.

Chemical Phenomenon model [10]

Boyd et al. [30] developed this equation from the pseudo-first order rate equation for adsorption reaction based on diffusion through the boundary liquid film and adsorption kinetics as a chemical phenomenon. The rate equation, obtained is as expressed below:

$$\log(1-F) = (k_D/2.303)\, t \quad \text{.....(15)}$$

where $F = q_e/q_t$ and q_e and q_t have the same meaning as given in the section of the pseudo-first order model and k_D is a rate constant. A rate equation for diffusion through a boundary liquid film (Eq.16) is derived from the pseudo-first order rate equation of Lagergren:

$$\log (1-F) = -(k_R/2.303)\, t \quad \text{.....(16)}$$

where k_R is a rate constant, and it is equal to the negative value of k_D. If the adsorption is due to ion- exchange, the constant of the equation will depend only on the concentrations of the ions in solution and temperature.

Elovich model:

The Elovich kinetic model based on chemisorption phenomena is expressed as :

$$dq_t/dt = \alpha \exp(-\beta q_t) \quad \text{.....(17)}$$

To simplify the Elovich equation (Eq. 17), Chine and Clayton [11] assumed ($\alpha\beta t$) >>1, and on applying the boundary conditions $q_t = 0$ at t = 0 and $q_t = q_t$ at t = t, the above equation as described by Sparks [12] becomes

$$q_t = 1/\beta \ln(\alpha\beta) + 1/\beta \ln t \quad \text{.....(18)}$$

where, α is the initial adsorption rate and β is the adsorption rate. The equation (Eq. 18) can be rearranged as:

$$q_t = A_1 + 2.303\, B_1 \log t \quad \text{.....(19).}$$

where A_1 [=1/β ln ($\alpha\beta$)] and B_1 [=1/β] are Temkin constants, and have their usual significance. From the intercept and slope of the straight line obtained from the plot q_t versus logt, the value for A_1 and B_1 were calculated.

2.6. References

[1] APHA, AWWA, WEF, Standard Methods for the Examination of Water and Wastewater, 20th Edn, Washington USA. (1998).

[2] I. Langmuir, The constitution and fundamental properties of solids and liquids, J. Am. Chem. Soc., **38**, 2221 – 95 (1916).

[3] H. M. F Freundlich, über die adsorption in lösungen, Zeitsschrift fur (J. Phys. Chem.) **57**, 385 -470 (1906).

[4] C. Aharoni, M. Ungarish, Kinetics of Activated Chemisorptions. Part 2. Theoretical Models. *J. Chem. Soc. Faraday Trans*. **1977**, *73*, 456.

[5] O. Redlich, D. L. Peterson, A useful adsorption isotherm, J. Phys. Chem., **63,** 1024 (1959).

[6] S. Lagergren, Zur theorie der sogenannten adsorption gelöster stoffe, Kungliga Svenska Vetenskapsakademiens, Handlingar, **24 (4)**, 1-39 (1898).

[7] Y. S. Ho, G. Mackay, Sorption of dye from aqueous solution by peat, Chem. Eng. J., **70**, 115 – 24 (1998).

[8] A. K. Bhattarcharya, C. Venkobachar, Removal of cadmium(II) by low costadsorbents, J. Environ. Eng. Div., ASCE Proc., **110**, 110 – 22 (1984).

[9] W.J. Weber Jr., J.C. Morris. Kinetics of adsorption on carbon from solution, J. Sanit. Div. Am. Soc. Civ. Eng. 89 (1963) 31- 60.

[10] G. E. Boyd, A. W. Adamson, L. S. Mayers (Jr.). The exchange adsorption of ions from aqueous solutions on organic zeolites. Kinetic II. J. Am. Chem. Soc., 69**, 2836 (1947).**

[11] S. H. Chien, W. R. Clayton. Application Elovich equation to the kinetics of phophate release and sorption on soils. Soil Sci. Soc. Am. J. 44**, 265 (1980).**

[12] D. L. Sparks, Kinetics of reactions in pure and mixed systems in soil physical chemistry. CRC Press, Boca Raton, FL, 1986.

Chapter 3

Adsorption Kinetics of Fluoride on Iron(III)-Zirconium(IV) Hybrid **Oxide**

Synthesis of the material:

3.1. Iron(III)-Zirconium(IV) mixed oxide synthesis

A mixture of 0.1 M Ferric chloride (in 0.01 M HCl) and 0.1 M zirconium oxychloride (in 0.01 M HCl) solutions (v/v = 9:1) was warmed at ~80^{o} C, and hydrolyzed

by drop wise addition of 0.1 M NaOH solution. The brown gel-like precipitate formed was aged with supernatant for 5 d at room temperature. The filtered precipitate was washed with water to remove chloride, and dried at 50-60^{o}C in an air oven. The dry product when treated with cold water converted into smaller particles. The particles ranged in140-290 μm were used for the experiments.

3.2. Results and Discussion

3.2.1. Physicochemical characterization

The X- ray diffraction (XRD) pattern (Fig.1) of iron(III)-zirconium(IV) hybrid oxide (IZHO) obtained between start and end angle ($^{o}2\theta$), 10^{o} and 80^{o}, showed eighteen peaks, and most significant are at 35.33^{o}, 26.9^{o}, 56.14^{o}, 11.56^{o} and 39.45^{o} with relative intensity >30%. The results indicated that IZHO is crystalline in nature. The scanning electron micrograph (SEM) image (Fig. 2) of IZHO showed the agglomerated surface morphology with irregular shape and porous nature, which indicates high surface area. The chemical composition of the oxide synthesized was analyzed and found the mole ratio of iron to zirconium 9:1, which is as per mole ratio added for synthesis. The isoelectric point (pH_{zpc}) determined for the oxide surface by pH titration is 7.1-7.2. The Fourier Transform Infrared (FTIR) spectrum (Fig. 3) for the synthetic oxide showed nine absorption bands at wave numbers (cm^{-1}) around 3754, 3393, 2926, 2367, 2075, 1619, 980, 676 and 485. The bands around 3754, 3393 and 1619 cm^{-1} are due to the stretching and bending modes of coordinated water and O-H bond, respectively. The sharp band at around 2367 cm^{-1} is for CO_2, which was presumably present in alkali used for synthesis of the mixed oxide. The weak band around 980 cm^{-1} is for Zr-O bond. The bands obtained at 676 and 485 cm^{-1} are the stretching and bending modes for Fe-O-Zr. As the band positions are shifted to higher and lower value compared to that of M-O in hydrous ferric oxide (671 and 461cm^{-1}) indicated the formation of hybrid oxide. The extra two bands found at ~ 2926 and ~ 2075 cm^{-1} are presumably for stretching of symmetrical hydrogen bonded OH and the bending of lattice hole trapped OH, respectively**.** The two steps weight loss found in thermo gravimetric (TG) analysis, ~ 16.7 and ~ 11.4% at ~100^{o} and <200^{o} – 600^{o} C, respectively correspond to physically adsorbed water and dehydroxylation from OH groups. The differential thermal (DT) analysis showed a sharp endothermic peak around 90 – 100^{o}C

and a weak endothermic peak at >200 - < 300^{o}C, which correspond to the two steps weight loss. The results indicated the hydrous nature of the synthetic oxide.

3.2.2. Effect of pH

Fig. 4 showed the results of fluoride adsorption on IZHO with varying pH at 303 (±2) K. The adsorption of fluoride from aqueous solution by IZHO increased with increasing solution pH from 2.0 to 4.0 and remained up to pH 7.0, and decreased thereafter. In acid pH range, IZHO surface remains positive due to the reaction either (i) or (ii).

$$MOH + H_3O^+ \rightarrow MOH_2^+ + H_2O \text{ ---------- (i)}$$
$$MOH + H_3O^+ \rightarrow M^+ + 2H_2O \text{ ---------- (ii)}$$

Available fluoride ion in solution binds on the solid surface of the adsorbent with columbic forces, and results outer (iii) or inner sphere (iv) complex reaction. Less adsorption of fluoride in strong acid pH-range is due to (a) the equilibrium, $HF_{(aq)} \rightarrow H^+_{(aq)} + F^-_{(aq)}$ shifts left for the common-ion effect, and effective available fluoride concentration for adsorption is lower than added (pK_a^{HF} = 2.95), and (b) the solubility loss of the adsorbent.

$$MOH_2^+ + F^-_{(aq)} \rightarrow MOH_2^+ \text{-- } F^- \text{ ---------- (iii)}$$
$$M^+ + F^-_{(aq)} \rightarrow M^+ \text{ -- } F^- \text{ ---------- (iv)}$$

The increased adsorption of fluoride with increasing pH is due to the increase of available fluoride concentration in above dissociation reaction of HF and decrease in solubility of the oxide. However, the decreased fluoride adsorption on IZHO at pH > 7.0 is due to change of surface nature of the oxide. At pH > pH_{zpc} (7.1-7.2), the mixed oxide surface becomes negative; and the sodium ion (Na^+), available in solution with fluoride ion, adsorbs on negative surface sites of the solid (first sphere of adsorption) and fluoride ion adsorbs thereon (in secondary adsorption sphere) competing with OH^-.

$$MOH + Na^+ + F^- + OH\text{-} \rightarrow MO^- \text{ -- } Na^+ \text{-- } F^- + H_2O \text{ ---------- (v)}$$

The optimum pH range obtained for fluoride adsorption is 4.0 to 7.0. Thus, the remaining experiments were conducted at pH 6.8 (± 0.1), which is typically a value in drinking water pH-range.

3.2.3. Adsorption isotherm

The equilibrium adsorption isotherm capacity (q_e, mg/g) determined for fluoride at pH 6.8 (± 0.1), and at three different temperatures (283, 293 and 303K) are shown as in **Fig. 5** as data points against equilibrium fluoride solution concentration (C_e, mg/dm^3). As the isotherm analysis is important to know the equilibrium adsorption capacity and affinity of adsorbent, the experimental isotherm data shown (**Fig. 5**) have been analyzed separately by linear as well as non-linear methods for the Langmuir (Eq. 1) and the Redlich-Peterson (Eq. 2) isotherm model equations. The isotherm parameters obtained from linear and non-linear analyses are presented in Table 1A and 1B, respectively. The analysis of the parameters on the basis of r^2-value for linear method or on the basis of average absolute error (AAE) and average absolute percent error (AAPE) obtained for the non-linear fitting showed that the present data have fitted better with the Redlich-Peterson isotherm model equation (shown in **Fig. 5**) than the Langmuir, but the quality of the data fit became progressively somewhat poorer with increasing temperature. The value for the Redlich-Peterson exponent, $n_{RP,}$ obtained is ranged from 0.72 to 0.89, and deviation from the unity indicating fewer tendencies to exhibit saturation behavior, as implied by the Langmuir isotherm. This is consistent with the lower quality of fit for the higher temperature. The increase of both the A_{RP} and A_L values with increasing temperature on the adsorption reaction indicates the increase of fluoride adsorption affinity of IZHO with rising temperature.

The equilibrium parameter R_L, which is defined as $R_L = 1 / (1+ B_L C_i)$ where C_i is the initial concentration of adsorbate, was calculated in the concentration range (5 – 50.0 mg/dm^3) studied, and found the values lay in the range $0< R_L < 1$. This indicated the fluoride adsorption on IZHO is favorable under the conditions of experiments.

The fluoride adsorption performance of IZHO at room temperature has been assessed by comparing the monolayer adsorption capacity (q_m, mg/g), though the value is temperature dependent, with some literature available data (**Table-2**). The results obtained showed that IZHO has greater affinity for fluoride than either of the reported

data excepting metallurgical grade alumina. Though different forms of aluminum oxide have been studied for fluoride adsorption by different authors and showed different efficiency, the trace solubility of aluminum as fluorocomplex might occur and long term drinking of such water is presumably the root of increasing Alzheimer's disease, a neurological problem, for the persons especially those who have poor kidney function. In this light the present adsorbent has promising prospect in this area.

3.2.4. Thermodynamics parameters

Thermodynamics parameters such as the changes of Gibbs free energy (ΔG^0), enthalpy (ΔH^0) and entropy (ΔS^0) for the adsorption of fluoride on IZHO are calculated by using the Eqs. 12 to 14.

$$\Delta G^0 = - 2.303\ RT \log_{10} B_L \text{ ----------} \quad (12)$$

$$\log_{10} B_L(T_2) - \log_{10} B_L(T_1) = - (\Delta H^0 / 2.303\ R) [1/T_2 - 1/T_1] \text{ ----------} \quad (13)$$

$$\Delta S^0 = (\Delta H^0 - \Delta G^0) / T \text{ ----------} \quad (14)$$

where R is the universal gas constant (8.314 J/mol/K**),** T is the absolute temperature (K) and B_L is the Langmuir equilibrium constant.

The Gibbs free energy change values (kJ/mol) calculated using the Langmuir equilibrium constant (B_L), obtained by linear analysis, are – 21.51 and – 24.81, respectively at 293 and 303 K. The Gibbs free energy change values obtained for the adsorption of fluoride on IZHO indicated the adsorption process is spontaneous in nature, and the spontaneity of adsorption reaction increases with increasing temperature. Again, the high positive ΔH^0 value (+ 65.04 kJ/mol) calculated indicates the adsorption of fluoride onto the IZHO is endothermic. The calculated positive ΔS^0 value (+ 0. 2962 kJ/mol/K) indicates the increase in entropy indicating the adsorption phenomenon takes places with increasing number of molecules/ions at solid-liquid interface. This is presumably due to the increase in solvent molecule at the solid-liquid interface because when hydrated fluoride ion adsorbs onto the solid surface, the water molecules released at the solid-liquid interfacial position, which is greater in moles than the fluoride ions being adsorbed by the solid.

3.2.5. Adsorption kinetics

The time dependent fluoride adsorption data on IZHO at room temperature (303 ± 2) K are shown in **Fig. 6** which shows that ≥ 90% of adsorbed fluoride took place in 45 min

of contact, and the adsorption reaction was taken ~ 60 min for reaching equilibrium at the concentration range (5.0 – 25.0 mg/dm^3) studied. However, the equilibrium time required for adsorption of fluoride from 5.0 mg F^-/dm^3 solution was ~ 45 min, and that increased with increasing initial fluoride concentration; but the rapid adsorption was noted with increasing load of adsorbate in solution. Thus, the higher equilibrium time required for adsorption of fluoride with increasing concentration is presumably due to (i) the increase of columbic repulsion between adsorbed fluoride ions and the fluoride ions approaching the solid for adsorption from the solid-liquid interface, and (ii) slow intra-particle diffusion which is concentration gradient dependent.

The present adsorption data were analyzed by using pseudo-first order (Eq.4), pseudo-second order (Eq.7) and reversible first order (Eq.11) kinetic equations. The kinetic parameters calculated from the slope and intercepts of linear plots (Fig. 7-9) are shown in **Table-3**. The present kinetic data for fluoride adsorption on IZHO are described better by both the pseudo-first order and reversible first-order equations (r^2 = ~0.99 and ~0.98) than the pseudo-second order equation (r^2 = ~0.98 and ~0.96) for the studied higher two concentrations (12.5 and 25.0 mg/dm^3) of fluoride. However, the kinetic data obtained for 5.0 mg/dm^3 of fluoride solution are better described by the pseudo-second order equation (r^2 = ~0.99) than the other two equations (r^2 = ~0.98). Thus, the orders, based on r^2, obtained to describe the kinetics of fluoride adsorption are:

Pseudo-second order > pseudo-first order ≈ reversible first order for 5.0 mg/dm^3, and pseudo-first order ≈ reversible first order > pseudo-second order for 12.5 and 25.0 mg/dm^3 of fluoride solutions. The other two kinetic model equations frequently used by some authors viz. power function ($\log q_t = \log a + b \log t$) and simple Elovich ($q_t = a + 2.303b \log t$), are also used to analyze the present data (plots not shown). The linear regression coefficient (r^2) values obtained reveal that both the power function and the simple Elovich equations explain the present kinetic data less well (r^2 = 0.94 to 0.98 for power function and 0.89 to 0.96 for simple Elovich equations) compared to the used other three equations. However, the data described both the power function and Elovich equations increasingly well with decreasing fluoride concentration in solution.

3.2.6. Film and intra particle diffusion

In order to asses the nature of the diffusion process responsible for adsorption of fluoride on the IZHO, attempts were made to calculate the coefficients of the process. If film diffusion is to be the rate determining step in the present adsorption kinetic study, the value of film diffusion coefficient (D_f) should be in the range 10^{-6} to 10^{-8} cm^2/s. If pore diffusion is to be the rate limiting, the pore diffusion coefficient (D_p) should be in the range 10^{-11} – 10^{-13} cm^2/s (Michelson et al., 1975). Assuming spherical geometry for the adsorbent particles, the overall rate constant of the process can be correlated with the film diffusion coefficient and pore diffusion coefficient independently in accordance with the expressions (Bhattacharya and Venkobachar, 1984).

Pore diffusion coefficient (D_p) = 0.03 (r_0^2 /$t_{1/2}$),

Film diffusion coefficient (D_f) = 0.23 ($r_0 \partial C_S / t_{1/2} C_L$),

where r_0 is the mean radius of the adsorbent particles (1.125 x 10^{-2} cm), ∂ is the film thickness (10^{-3} cm) (Helfferich, 1946), C_S and C_L are the concentrations of adsorbate in solid and liquid phase at t = t and t = 0, respectively; and $t_{1/2}$ is time required for 50% adsorption. Inserting calculated $t_{1/2}$ value from the appropriate reaction kinetic equation and other appropriate present data, the film and pore diffusion coefficients were calculated (**Table 4**) for studied three different concentrations of fluoride in solution. The calculated D_f-values, (0.8 to 3.6) × 10^{-9} cm^2/s, are found to be lesser than 10^{-8} cm^2/s, and the D_p-values (10^{-8} to 10^{-9} cm^2/s) are clearly higher than $10^{-11} cm^2/s$. Thus, it could be suggested that the adsorption kinetics of the present reaction is controlled mainly by film (boundary layer) diffusion with some possibility of intra-particle transport, as D_f-values obtained are in between 10^{-8} and 10^{-11} cm^2/s. This is confirmed from the plots of the experimental data according to the intra-particle diffusion model which is defined as follows:

$q_t = k_i (t^{0.5})$ ---------- (15)

where the parameter, k_i ($mg/g.min^{0.5}$), is the diffusion rate constant. In theory the plot between q_t and $t^{0.5}$ is given by multiple regions representing the external mass transfer followed by intra-particle diffusion in macro, meso, and micro pores (Kumar et al., 2005). The **Fig. 10**, the plot of q_t versus $t^{0.5}$ indicated two linear portions which suggest clearly two stage diffusion of fluoride onto the IZHO at studied highest concentration. The slope of the second linear portion characteristics the rate parameter corresponding to

the intra-particle diffusion, whereas the intercept of this second linear portion is proportional to the boundary layer thickness.

3.2.7. Boyd kinetics

In order to determine the actual rate-controlling step involved in the fluoride adsorption process, the adsorption data were further analyzed using the kinetic expression developed by Boyd et al. (Kumar et al., 2005; Gupta et al., 2001)

$F = 1 - (6/\pi^2) \exp(-Bt)$ ---------- (16)

where F ($= q_t/q_e$) is the fraction of solute adsorbed at different times t and Bt is a mathematical function of F. q_t and q_e are the amount adsorbed (mg/g) at any time t and at equilibrium. Simplifying the Eq. (16), the kinetic expression becomes

$Bt = -0.4985 - \ln(1 - q_t/q_e)$ ---------- (17)

Taking measured q_e and q_t, the Bt values are calculated from Eq. (17) for each value of F, and plotted against time as shown in **Fig. 11**. The poor non-linearity of Boyd plots (**Fig.11**) indicated the external mass transport with intra-particle diffusion controlled the rate-limiting process of adsorption, which is different from the conclusion drawn by Wang and Li (2005) on adsorption of dye on unburned carbon.

3.2.8. Conclusion

The synthetic IZHO was crystalline and of hydrous nature. The optimum pH range where fluoride adsorption was good is between 4.0 and 7.0. Both linear and non-linear analyses showed the present isotherm equilibrium data fit is better with the Redlich-Peterson model than the Langmuir model, and the goodness of fit decreased with increasing temperature for non-linear analysis. The adsorption of fluoride on to the solid was spontaneous, and took place with the increase of entropy. The kinetic data for fluoride adsorption on IZHO obtained at 303 (± 2) K described both the pseudo-first order and the reversible first-order equations equally good with correlation coefficient value (~0.98 – 0.99) for higher two concentrations while those described the pseudo-second order equation better ($r^2 > 0.98$) than former two equations for 5.0 mg/dm^3 of fluoride. However, the same kinetic data described the other tested kinetic equations less well ($r^2 =$

0.94 to 0.98 for the power function and 0.89 to 0.96 for the simple Elovich equations) compared to the other three used equations. The kinetics of fluoride adsorption on the mixed oxide was found to take place not so clearly with boundary layer diffusion. External mass transport with intra-particle diffusion phenomena controlled the rate limiting process, which has been confirmed from Boyd poor non-linear kinetic plot.

3.2.9. References

Bhattarcharya.A.K, and Venkobachar.C "Removal of cadmium(II) by low costadsorbents" J. Environ. Eng. Div., ASCE Proc., **110**, 110 – 22 (1984).

Gupta.V.K and Ali.I "Removal of DDD and DDE from wastewater using bagasse fly ash, a sugar industry waste" Water Res., **35**, 33 – 40 (2001)

Helfferich.F "Ion-Exchange", New York, NY, McGraw Hill (1962).

Kumar.V.K, Ramamurthi.V and Sivanesan.S "Modeling the mechanism involved during the sorption of methylene blue onto fly ash" J. Colloid Interface Sci., **284,** 14 – 21 (2005).

Michelson.L.D, Gideon.P.G, Pace.E.G and Kutal.L.H "Removal of soluble mercury from wastewater by complexing techniques" Bull No. 74., US Dept. Industry, Office of Water Research and Technology (1975).

Pietrelli L. "Fluoride wastewater treatment by adsorption onto Metallurgical grade alumina" Annali di Chimica, **95** (5), 303-12 (2005).

Fan.X, Parker.D.J and Smith.M.D "Adsorption Kinetics of fluoride on low cost materials" Water Res., **37**, 4929 – 37 (2003).

Ghorai. S. and Pant. K.K. "Equilibrium, kinetics and breakthrough studies for adsorption of fluoride on activated alumina" Sep. Purif. Technol., **42** (3), 265-71 (2005).

Reardon.E.J and Wang.Y "Limestone reactor for fluoride removal from wastewaters" Environ. Sci. Technol., **34**(15), 3247 – 53 (2000).

Sivasamy. A, Singh K.P, Mohan D and Muruthamuthu "Studies on defluoridationof water by coal-based sorbents" J. Chem. Tech. Biotech, **76**, 717-22 (2001).

Sujana. M.G., Thakur. R.S.and Rao. S.B. "Removal of fluoride from aqueous solution by using alum sludge" J. Colloid Interf. Sci., **206** (1), 94-101 (1998).

Table 1A: Linear isotherm parameters of fluoride adsorption on IZHO at pH 6.8(±0.1)

Temperature (K)	Langmuir				Redlich-Peterson			
	A_L(dm^3/g)	q_m(mg/g)	B_L(dm^3/mg)	r^2	A_{RP} (dm^3/g)	B_{RP} (dm^3/mg)	n_{RP}	r^2
283	1.2113	7.50	0.1615	0.9886	1.44	0.260	0.920	0.9934
293	2.6983	7.51	0.3593	0.9909	3.75	0.669	0.921	0.9952
303	8.1903	8.21	0.9976	0.9986	16.16	2.606	0.922	0.9997

Table 1B: Non-linear isotherm parameters of fluoride adsorption on IZHO at pH 6.8 (±0.1)

Temperature (K)	Langmuir, $q_e = A_L C_e/(1+ B_L C_e)$				
	A_L (dm^3/g)	B_L (dm^3/mg)	q_m (mg/g)	AAE*	AAPE** %
283	1.2333	0.1655	7.454	0.254	6.891
293	3.8641	0.5584	6.920	0.314	6.038
303	54.5108	7.6520	7.124	0.619	10.971

Temperature (K)	Redlich-Peterson, $q_e = A_{RP} C_e / (1+ B_{RP} C_e^{n_{RP}})$				
	$A_{RP}(dm^3/g)$	$B_{RP}(dm^3/mg)^{n_{RP}}$	n_{RP}	AAE*	AAPE** %
283	3.7237	1.4253	0.7225	0.130	3.096
293	3.9609	1.8805	0.8511	0.234	5.950
303	152.454	28.3337	0.8875	0.369	8.596

AAE*: Average absolute error.
AAPE: Average absolute percent error.**

Table-2: A comparative assessment on fluoride adsorption performance of IZHO with some literature available data.

Adsorbent	*q_m, mg/g	Reference
Metallurgical grade alumina Active alumina	12.57 7.08	Pietrelli L. (2005)
Alum sludge	5.394	Sujana et al. (1998)
Hydroxyapatite Fluorspar Activated quartz Calcite Quartz	4.54 1.79 1.16 0.39 0.19	Fan et al. (2003)
Activated alumina	2.41	Ghorai and Pant (2005)
Lignite Bituminous coal	7.09 7.44	Sivasamy et al. (2001)
Iron-Zirconium Hybrid Oxide (IZHO)	8.21	Present work
Hydrous ferric oxide	7.50	Estimated by the authors under same conditions of present work
Hydrous zirconium oxide	10.21	Estimated by the authors under same conditions of present work

*q_m value is compared taking the value obtained from the linear analysis of Langmuir model as other values shown are given from the analysis of same model.

Table 3: Kinetics parameters for fluoride adsorption on IZHO at pH 6.8 (±0.1) and at temperature 303 (±2)K.

Fluoride concentration (mg/dm^3)	Pseudo-first order			Pseudo-second order				Reversible first order	
	$k_1 \times 10^{-2}$ min^{-1}	q_e mg/g	r^2	$k_2 \times 10^{-2}$ g/(mg.min)	$h \times 10^{-2}$ mg/(g.min)	q_e mg/g	r^2	$k_B \times 10^{-2}$ min^{-1}	r^2
5.0	5.06	2.12	0.9786	3.37	26.23	2.79	0.9867	5.09	0.9784
12.5	5.25	4.21	0.9923	2.60	82.41	5.63	0.9835	5.25	0.9924
25.0	4.47	5.64	0.9767	1.77	88.99	7.09	0.9608	4.45	0.9763

Table 4. Diffusion coefficients of fluoride removal on the IZHO.

Fluoride concentration (mg/dm^3)	Film diffusion coefficient, D_f, (cm^2/s)	Pore diffusion coefficient, D_p, (cm^2/s)
5.0	3.66×10^{-9}	1.05×10^{-8}
12.5	1.40×10^{-9}	4.79×10^{-9}
25.0	0.8×10^{-9}	4.08×10^{-9}

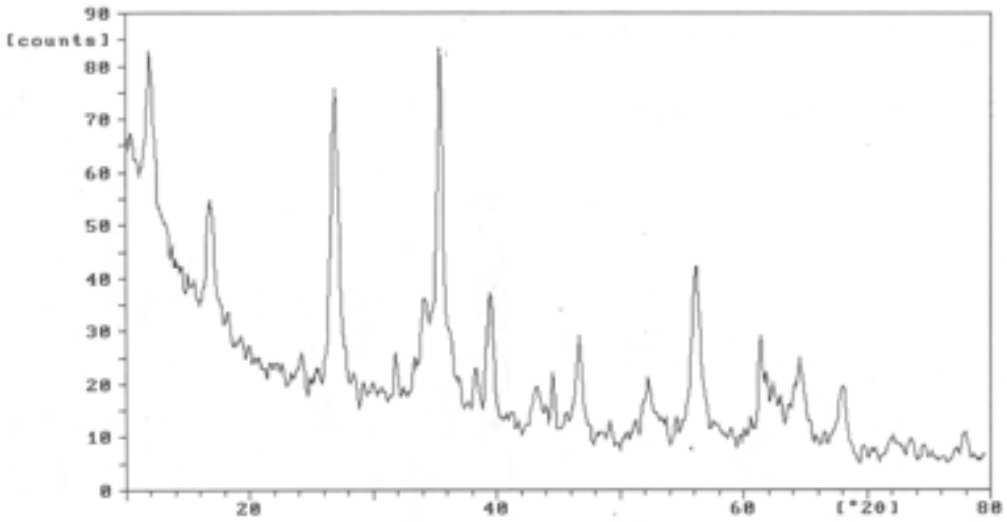

Fig. 1: X-ray diffraction pattern of IZHO

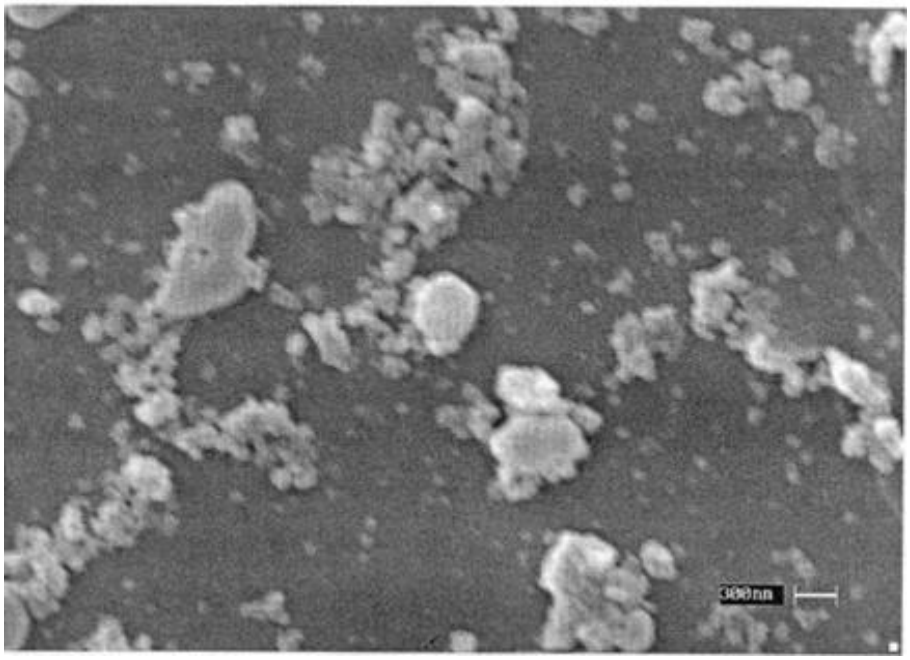

Fig. 2: Scanning electron micrograph (SEM) image of IZHO

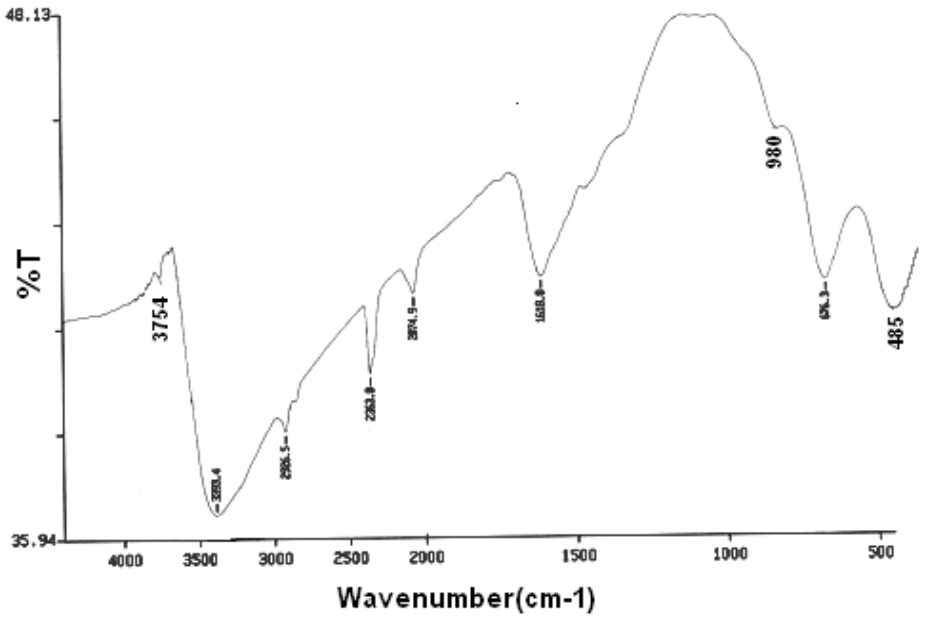

Fig. 3: Fourier Transform Infrared spectrum of IZHO

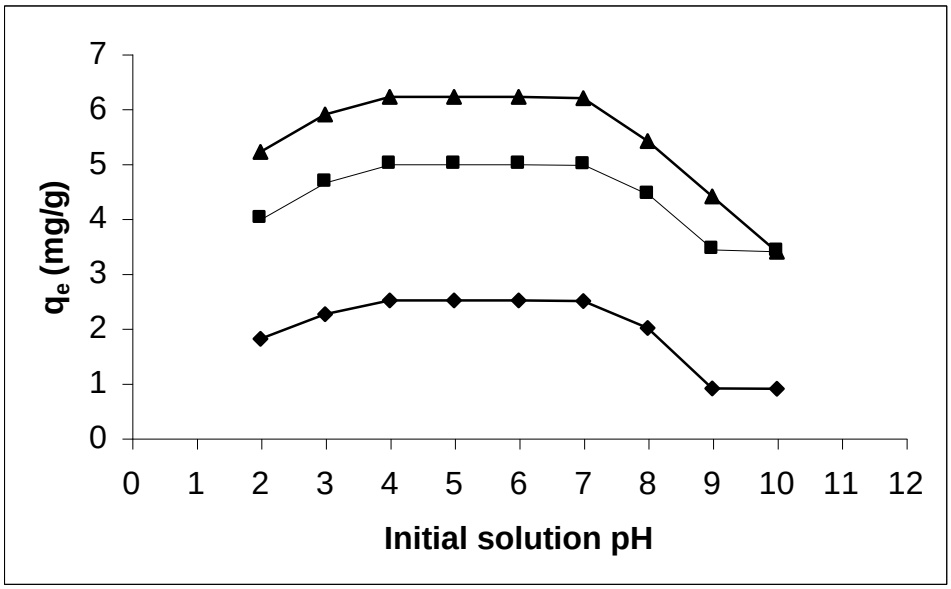

Fig. 4: Effect of initial pH on fluoride adsorption by IZHO at 303 K.

Initial fluoride concentration (mg/dm^3) used: ♦5.0, ■ 12.5 and

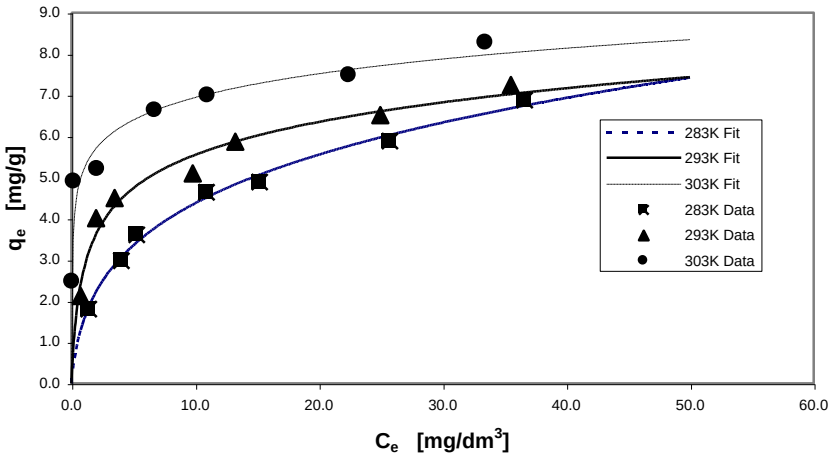

Fig. 5: Non-linear Redlich-Peterson isotherm (R-PI) plots for adsorption of fluorideat pH 6.8 (± 0.1) on IZHO. Experimental data points at 303 K (♦), 293 K (▲), and 283 K(■); R-PI modeled fits: ····· (283 K), —— (293 K) and – – (303 K).

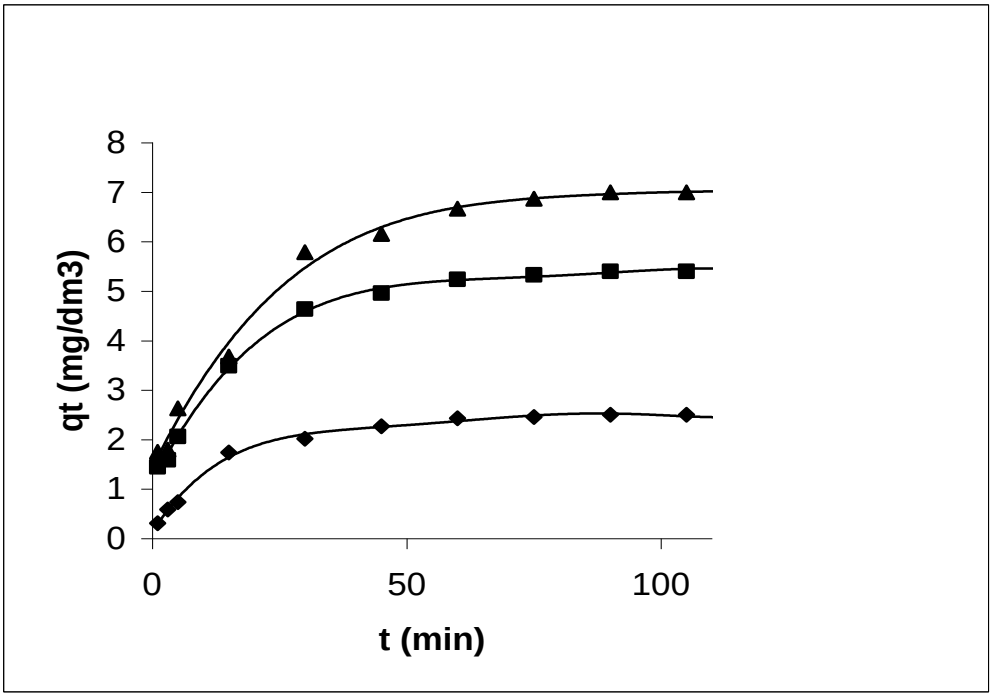

Fig.6: Kinetic data for fluoride adsorption on IZHO at 303 (±2)K and pH 6.8 (±0.1) Initial fluoride concentration (mg/dm^3) used: ♦5.0, ■12.5 and ▲25.0

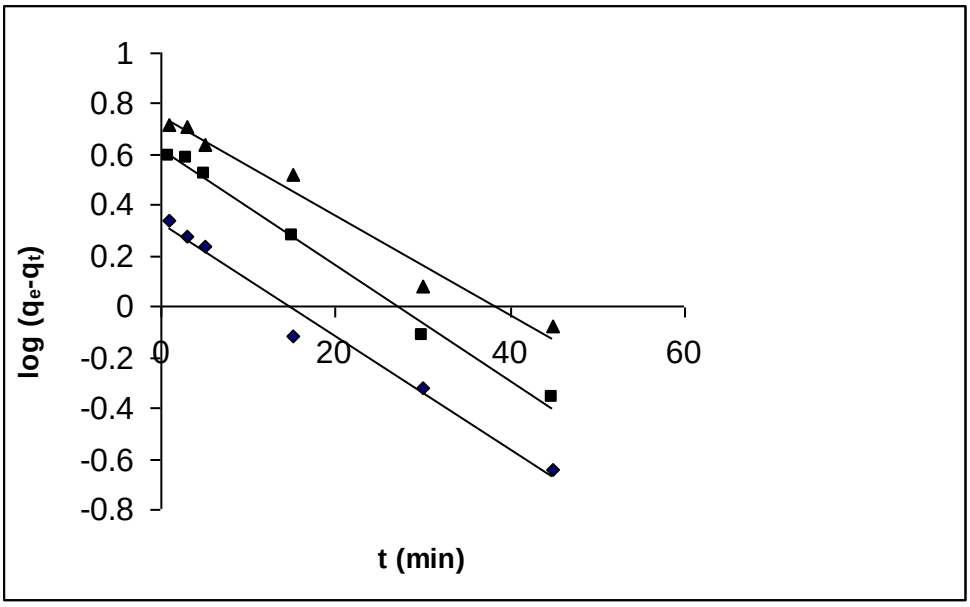

Fig. 7: Pseudo-first order kinetic plot for fluoride adsorption data on IZHO at 303 (± 2) K and at pH 6.8 (± 0.1). Initial fluoride concentration (mg/dm^3) used: ♦5.0, ■12.5 and ▲25.0.

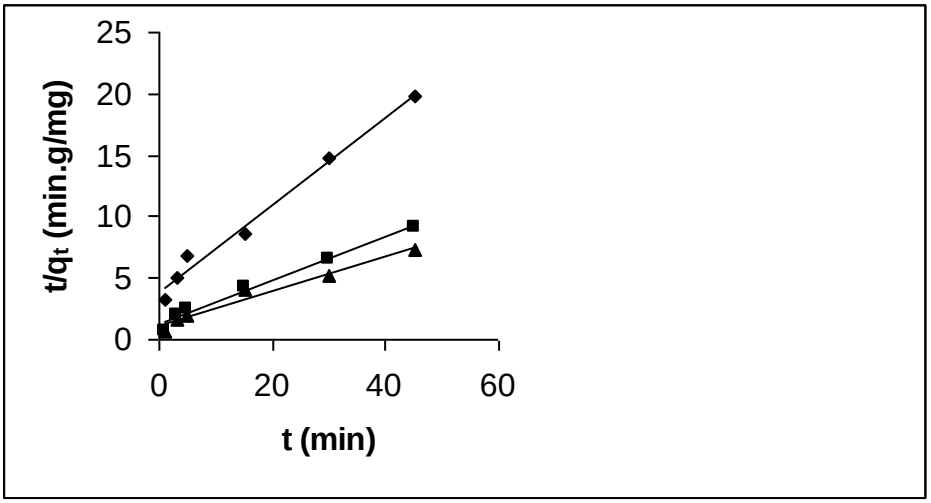

Fig. 8: Pseudo-second order kinetic plot for fluoride adsorption data on IZHO at 303 (±2) K and at pH 6.8 (± 0.1). Initial fluoride concentration (mg/dm^3) used: ♦5.0, ■12.5 and ▲25.0.

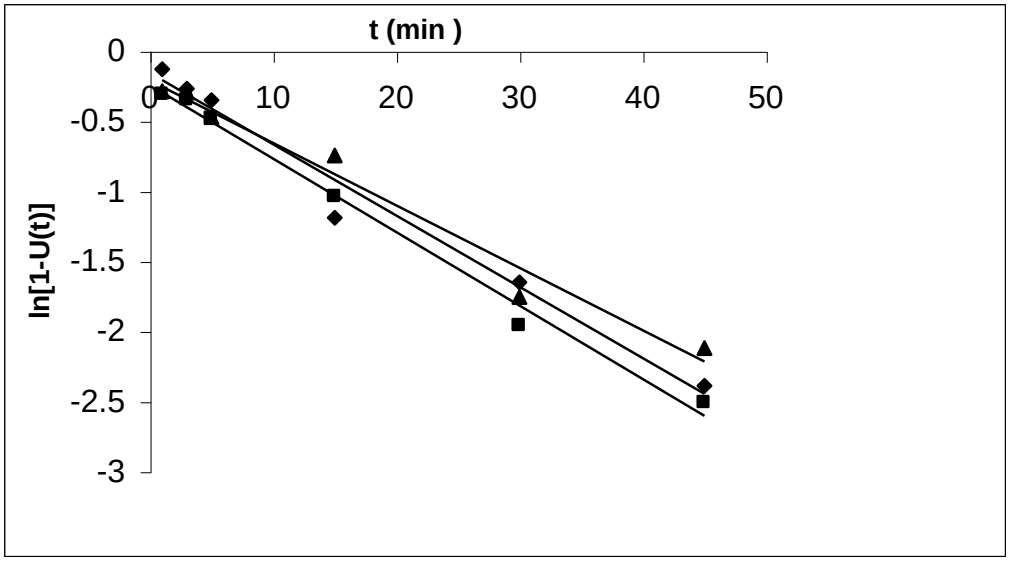

Fig. 9: Reversible first order kinetic plot for fluoride adsorption data on IZHO at 303 (±2)K and at pH 6.8 (± 0.1). Initial fluoride concentration (mg/dm^3) used: ♦5.0, ■ 12.5 and ▲25.0.

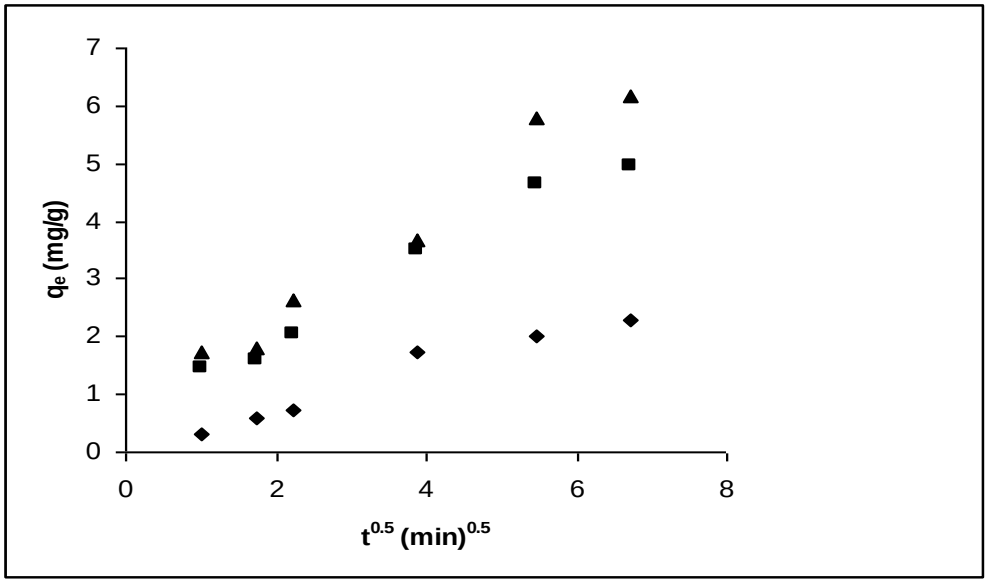

Fig. 10: q_t versus $t^{0.5}$ plot for fluoride adsorption data on IZHO at 303 (± 2)K and at pH 6.8 (±0.1). Initial fluoride concentration (mg/dm^3) used: ♦5.0, ■ 12.5 and ▲25.0.

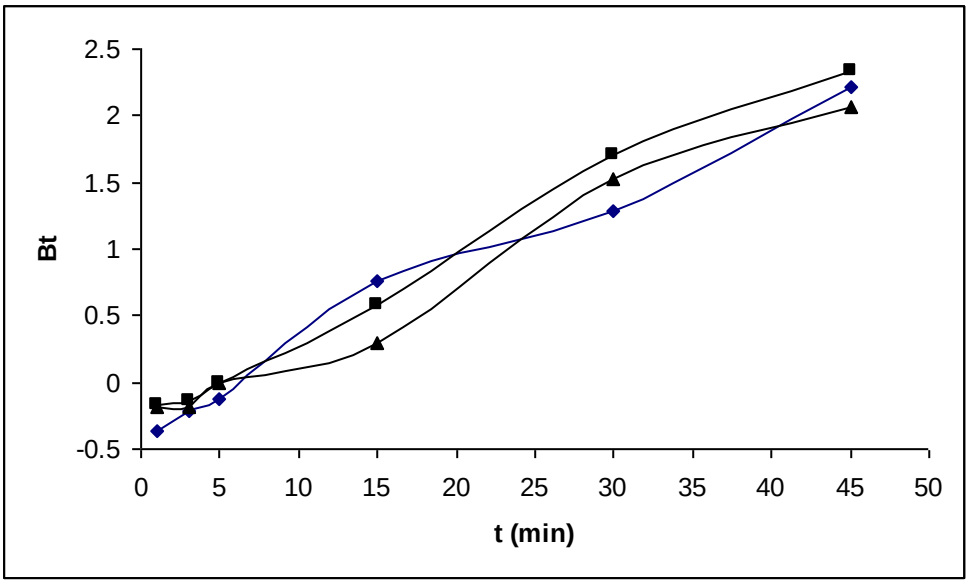

Fig. 11: Boyd kinetic plots on the adsorption of fluoride on IZHO at pH 6.8 (± 0.1) and at 303(±2) K. Initial fluoride concentration (mg/dm^3) used: ♦5.0, ■12.5 and ▲25.0.

Chapter 4

ISOTHERM STUDY BY IRON (III), ZIRCONIUM (IV) AND BINARY IRON (III)-ZIRCONIUM (IV) OXIDES

.

4.1. **Synthesis of the material**: Described in the earlier section.

4.2. **Physicochemical characterizations**

The Fourier Transform Infrared (FTIR) spectra shown (Fig. 1) reveal the closeness of the peak positions excepting the additional peaks of wave numbers (cm^{-1}) at ~2926 and 2075 in spectrum for HZFO (A). These two peaks are presumably due to the stretching and bending modes of hetero bridged hydroxyl group in HZFO. Additional notable change of peak positions obtained in three spectra at wave number below 1000 cm^{-1} indicates the HZFO is the hybrid form of HFO and HZO. The X-ray diffraction patterns (Fig. 2) indicate both HFO and HZFO were of crystalline nature, and HZO was amorphous. The scanning electron microscopic (SEM) images shown (Fig. 3) indicate the irregular surface morphology of the oxide particles. The other characteristic parameters determined are shown in Table 1. The BET surface area values obtained for the oxides are very close with each other. However, the pH_{zpc} values determined are differed notably depending upon the metal ion basicity. The percentage of surface water content as obtained from the thermo gravimetric (TG) analyses showed the synthetic oxides are hydrated compound.

4.3. Effect of pH

The results of sorption amount (mg/g) against final solution pH (pH_F) for fluoride sorption at 303 (±2) K on the HZFO, HFO and HZO are shown in Fig.4. Results showed that the fluoride sorption increased with increasing pH from $pH_F \geq 2.0$ to ~5.0, ~4.6 and ~6.8 for HFO, HZO and HZFO, respectively. In acid pH range, hydrous oxides surfaces remain positively charged due to the reaction either (i) or (ii). The available anion (here

F^-) in solution gets to be associated on the hydrous oxide surface with electrostatic forces via outer or inner sphere complex reaction.

$MOH_{(s)} + H_3O^+ \rightarrow MOH_2^+{}_{(s)} + H_2O$ ---------- (i)

$MOH_{(s)} + H_3O^+ \rightarrow M^+{}_{(s)} + 2H_2O$ ---------- (ii)

Less fluoride sorption in strong acid pH can be attributed due to (i) less available fluoride concentration in solution for adsorption as the equilibrium, $HF_{(aq)} \leftrightarrow H^+{}_{(aq)} + F^-{}_{(aq)}$, shifts left for common-ion effect ($pK_a{}^{HF} = 2.95$), and (ii) slight solubilization loss of hydrous oxides. Though the fluoride sorption capacity was found to increase from pH_F 2.2 (±0.1), and that decreased at $pH_F \geq 6.8$, ≥ 5.0 and ≥ 4.6 on HZFO, HFO and HZO, respectively. This is due to the change of surface nature of the sorbents. At $pH_F \geq pH_{zpc}$, the oxides surfaces become negative; and fluoride sorbs via the sorption of cation available (here Na^+) in solution competing with hydroxyl ion. Thus, the sorption of fluoride takes place on sorbent surfaces in the secondary sorption sphere, and the sorption amount (q_e, mg/g) decreases. The fluoride sorption amount obtained for HZFO was found higher than that for HFO at pH_F >3.0, but that was clearly lesser than HZO up to pH_F ~7.0. Thus, the use of mixed oxide (HZFO) might be more and less profitable than HFO and HZO, respectively for fluoride contaminated water treatment at pH_F ranged 6.5 to 8.0.

4.4. Equilibrium sorption studies:

The equilibrium sorption isotherm is fundamentally important in the design of sorption systems. Equilibrium studies give the capacity of the sorbent and describe the sorption isotherm by constants whose values express the surface properties and affinity of the sorbent. Thus, the equilibrium data obtained at three different temperatures (283, 293 and 303 K) for fluoride sorption on hydrous oxides, namely HZFO, HFO and HZO at pH 6.8(±0.2) are shown in Figs. 5a-5c. These data (Figs.5a-5c) are analyzed using the described isotherm model equations.

4.4.1. The Langmuir isotherm

The widely used linear Langmuir equation (Eq.2) was applied for analysis of data (Figs. 5a-5c). The isotherm parameters evaluated from the slopes and intercepts of linear plots of the specific sorption, C_e/q_e (g/L) against the equilibrium concentration, C_e (mg/L) for fluoride sorption onto the studied oxides are shown in Table-2. These plots were found to be linear over the entire concentration range studied with high R^2 values (≥0.95). It was

found in general that the monolayer sorption capacity (θ, mg/g) of fluoride increases with increasing temperature from 283 to 303 K. However, the equilibrium sorption constant (b, L/mg) of fluoride increases for HZFO while that decreases for HFO and HZO with rising temperature. The R^2-values suggest that the Langmuir isotherm provides increasingly a good model for the sorption system on HZFO with rise of temperature. Although the fluoride sorption data on HFO and HZO describe fairly well the Langmuir model (R^2 = 0.9545- 0.9910) over the concentration and temperature range studied, the effect of temperature on the sorption system reflected from the data of isotherm parameters is notable.

The essential features of the Langmuir isotherm can be expressed in terms of a dimensionless constant separation factor or equilibrium parameter, R_L which is defined by the following relationship:

$$R_L = 1/ (1 + bC_0) \text{ ---------- (11)}$$

where C_0 and b are the initial sorbate concentration (mg/L) and the Langmuir equilibrium constant (L/mg), respectively. The R_L value indicates the shape of the isotherm as:

Values of R_L	Type of isotherm
$R_L > 1$	Unfavourable
$R_L = 1$	Linear
$0 < R_L < 1$	Favourable
$R_L = 0$	Irreversible

The calculated R_L values were found in the range of 0 to 1 for all studied temperatures and concentrations at pH 6.8 (±0.2) on all the hydrous oxides. The sharp increase of Langmuir equilibrium constant (b) value with increasing temperature on sorption process suggest the fluoride sorption at higher temperature is more favourable on HZFO compared to that on HFO.

4.4.2. **The Freundlich isotherm**

The related Freundlich isotherm (Eq. 4) parameters evaluated from the slopes and intercepts of linear plots of the fluoride sorption data (Figs. 5a-5c) are shown in Table 2. The values suggest that the linear Freundlich isotherm is also fairly good model for describing the fluoride sorption data on HFO (R^2 = 0.9496-0.9696) and HZO (R^2 = 0.9178-0.9926), and the fit of data increases with increasing temperature of the sorption

process. Based on R^2-values, it can be generalized that the sorption data on HFO and HZO fit increasingly well, while that on HZFO fit poorly with rising temperature from 283 to 303 K. The general order of the present sorption data fit with rising temperature is: HZO > HFO > HZFO. The values of n lie between 1 and 10 in all the cases indicate the surface heterogeneity. Although the fluoride sorption data on HZFO describe the Freundlich isotherm badly with increasing temperature, the increase of k_F and n values suggest the favourable sorption of fluoride onto the mixed oxide compared with the pure oxides.

4.4.3. The Temkin isotherm

The isotherm parameters evaluated from the linear plots of Temkin isotherm (Eq. 6) of the present data are shown in Table 2. Results show that the sorption data obtained for HFO describe the Temkin model increasingly well while that for HZO and HZFO show, in general, the opposite trend with increasing temperature. Based on the R^2-values, the order of sorption data fit with increasing temperature is: HFO > HZO > HZFO at pH 6.8 (±0.2).

4.4.4. The Redlich-Peterson isotherm

The equilibrium isotherm data shown in Figs. 5a-5c have been analyzed by the Redlich-Peterson equation (Eq. 8). The evaluated isotherm parameters related to the used model equation are also shown in Table 2. The linear regression coefficient, R^2-values are very high (>0.96 to <1.0) at all the temperatures studied for fluoride sorption on the hydrous oxides. This is obvious since the method used to evaluate the Redlich-Peterson isotherm parameters was the trial and error adjustments of g value for maximize the linear coefficient, R^2. Contrast to present optimized trial and error adjustment of g-value, Ho et al.[28] used the adjustment of some other parameter for evaluating the constants of this model. For all the studied adsorbents at three different temperatures, the g-values are lied 0.901 to 0.921, that is, $0.90 < g < 0.93$. As the g-values somewhat away from 1.0, the fluoride sorption onto the hydrous oxides indicates the heterogeneity of sorbent surfaces. However, the fluoride sorption data for HZFO fit with the linear form of the present isotherm model increases (R^2 increases from 0.9934 to 0.9997), while those for HFO fit with this model was fairly well and remain nearly same (R^2 = 0.9720-0.9759) with increasing temperature on sorption reaction. However, the fluoride sorption data for HZO

describe the model well (R^2 = 0.9633 to 0.9949), and the data fit decreases with increasing temperature. The lower α and β values at 303K suggest that HZFO can be used more efficiently than HFO for fluoride sorption at pH 6.8 (± 0.2). This agrees well also with the observation found in the studies of pH effect.

4.5. Thermodynamic parameters

The thermodynamic parameter namely the Gibbs free energy change (ΔG^0) for the sorption process was calculated using Eq. (9). The results obtained are shown in Table 3. The negative Gibbs free energy change values for fluoride sorption on the synthetic hydrous oxides indicate the spontaneity of the sorption process. The significant increase in $-\Delta G^0$ value with increasing temperature for the sorption process on HZFO compared with that on HFO indicates the fluoride sorption on HZFO was thermodynamically more spontaneous. The decrease in $-\Delta G^0$ value obtained indicates the fluoride sorption on HZO is progressively less spontaneous with increasing temperature. The changes of enthalpy (ΔH^0) and entropy (ΔS^0) values were evaluated from the intercepts and slopes of the linear plots (plots not shown) of $-\Delta G^0$ (kJ/mol) versus T (K) as per Eq. (10) in the studied temperature range 283 to 303K. The results (Table 3) show that ΔH^0 value obtained for HZFO is much high (+ 65.043 kJ/mol) compared to that for HFO (+ 5.060 kJ/mol) while that for HZO is negative (- 37.206 kJ/mol). Thus, the fluoride sorption reaction on HZFO was much more endothermic than that on HFO; while that on HZO was clearly exothermic. Again, the positive ΔS^0 values obtained for HZFO and HFO indicated some structural change of sorbate and sorbent. Additionally, the positive ΔS^0-value also indicates the increase of randomness at the solid-liquid interface during the sorption of fluoride on the hydrous oxides, and the increase of randomness at the interface is much greater for HZFO (ΔS^0 =+0.2962 kJ/mol K) than that for HFO (ΔS^0 = +0.0828 kJ/mol K). The low negative ΔS^0-value for fluoride sorption reaction on HZO (ΔS^0 = -0.0636 kJ/mol K) suggests the decrease in sorbate concentration in solid-solution interface indicating thereby the increase in sorbate concentration onto the solid phase. This agrees well with the physical adsorption phenomenon that takes place through the columbic attraction.

4.6. Conclusion:

The synthetic oxides are of hydrated nature. The HZFO and HFO are crystalline and HZO is of amorphous type. The results of pH influence for fluoride

sorption on the hydrous oxides studied show the increase of fluoride sorption capacity from equilibrium pH 2.2 (±0.1) to pH ~5.0 for HFO, ~4.6 for HZO and ~6.8 for HZFO. The order of sorption capacity around neutral pH is HZO > HZFO > HFO. Analyzes of sorption isotherm data for fluoride on the hydrous oxides obtained at pH 6.8 (±0.2) and three different temperatures indicated that both the Langmuir and Redlich-Peterson models, in general, describe the sorption data well; and the fit of experimental data for HZFO increases with increasing temperature on the above model equations. However, the fit of the sorption data on HFO practically remained same with the models tested; and that on HZO decreases with the models excepting the Temkin equation with increasing temperature. The fluoride sorption onto HZFO and HFO is found endothermic while that onto HZO is exothermic in nature.

Table 1: Physicochemical characteristics of the synthetic oxides

Properties	HZFO	HZO	HFO
Nature	Crystalline	Amorphous	Crystalline
Metal Oxide (%)	71.88	68.24	72.13
Water Loss (using TGA)	16.68	15.32	16.50
Surface Morphology	Irregular	Irregular	Irregular
Particle Size(mm)	0.14-0.29	0.14-0.29	0.14-0.29
pH_{ZPC}	5.2-6.4	4.6-5.5	6.4-7.7
BETSA (m^2/g)	162.5	160.50	165.60

Table 2: Isotherm parameters for fluoride sorption at pH 6.8(±2) on HZFO, HZO and HFO

Isotherm Equations	Parameters	HZFO			HZO			HFO		
		Temperature(K)			Temperature(K)			Temperature(K)		
		283	293	303	283	293	303	283	293	303
Langmuir	R^2	0.9886	0.9909	0.9986	0.9910	0.9688	0.9545	0.9644	0.9641	0.9678
	θ	7.50	7.51	8.21	8.09	9.42	10.21	7.06	7.29	7.50

	b	0.1615	0.3593	0.9976	0.1797	0.1143	0.0634	0.1501	0.1477	0.1462
Freundlich	R^2	0.9773	0.9088	0.8500	0.9178	0.9658	0.9926	0.9496	0.9546	0.9696
	K_F	1.69	2.76	4.72	2.009	1.6979	1.0619	1.54	1.55	1.57
	n	2.61	3.54	6.09	2.6903	2.2899	1.7602	2.55	2.50	2.48
Temkin	R^2	0.9602	0.9685	0.9164	0.9828	0.9552	0.9448	0.9560	0.9565	0.9649
	A	1.061	2.7697	5.1182	1.4023	0.8601	0.6519	0.9791	1.007	1.024
	B	1.45	1.21	0.81	1.5865	1.8329	2.2214	1.3787	1.4240	1.4742
Redlich-Peterson	R^2	0.9934	0.9952	0.9997	0.9949	0.9746	0.9633	0.9723	0.9720	0.9759
	α	0.6935	0.2677	0.0619	0.5504	0.7978	1.3159	0.7843	0.778	0.7621
	β	0.1808	0.1791	0.1613	0.1793	0.1554	0.1331	0.1995	0.1922	0.1851
	g	0.920	0.921	0.921	0.901	0.901	0.901	0.911	0.912	0.912

Table 3: Thermodynamic parameters for fluoride sorption at pH 6.8 (±2) on HZFO,HZO and HFO

Parameters	HZFO			HZO			HFO		
	Temperature(K)			Temperature(K)			Temperature(K)		
	283	293	303	283	293	303	283	293	303
b(L/mg)	0.1615	0.3593	0.9976	0.1797	0.1143	0.0634	0.1501	0.1477	0.1462
b(L/mol)x10^4	0.3068	0.6827	0.1895	0.3414	0.2172	0.1205	0.2831	0.2806	0.2778
$-\Delta G^0$(kJ/mol)	18.8895	21.5071	24.8130	19.1422	18.7159	17.8705	18.3188	19.3409	19.9753
ΔH^0(kJ/mol)	+ 65.0430			-37.2060			+5.06		
ΔS^0(kJ/mol.K)	0.2962			-0.0636			+ 0.0828		

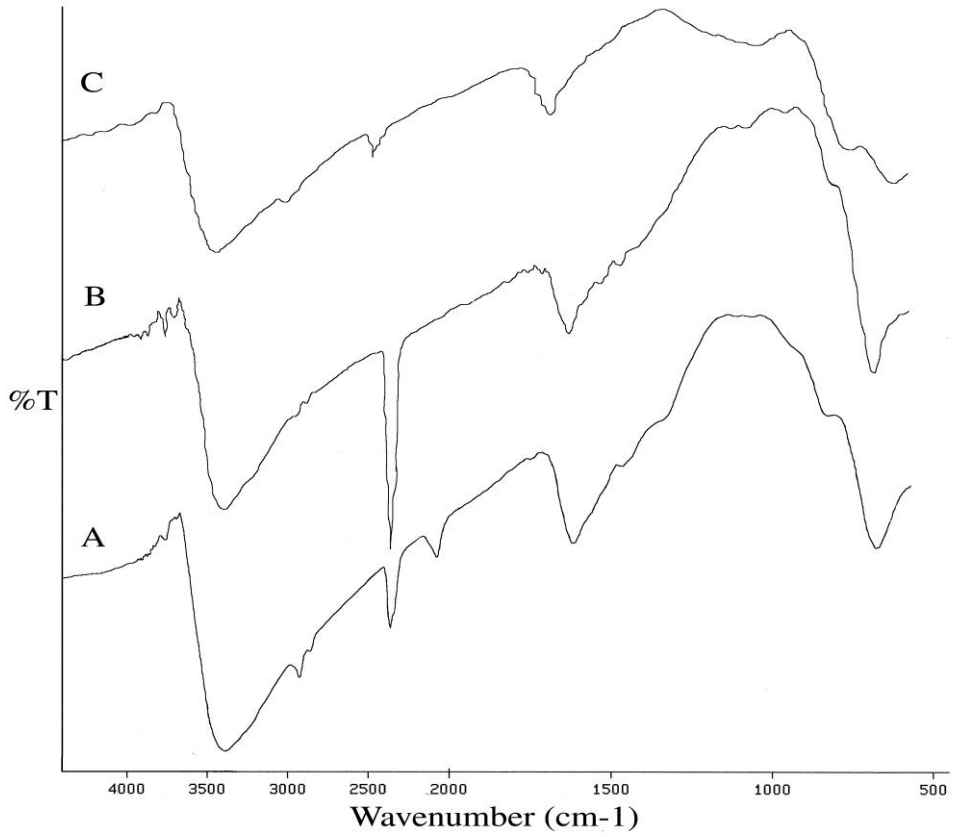

Fig. 1: The Fourier Transform Infrared (FTIR) spectrum of (A) HZFO (B) HFO and (C) HZO.

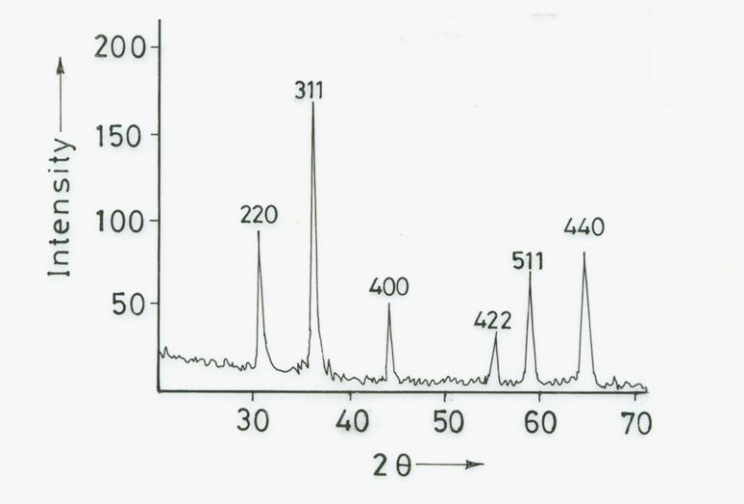

(a)

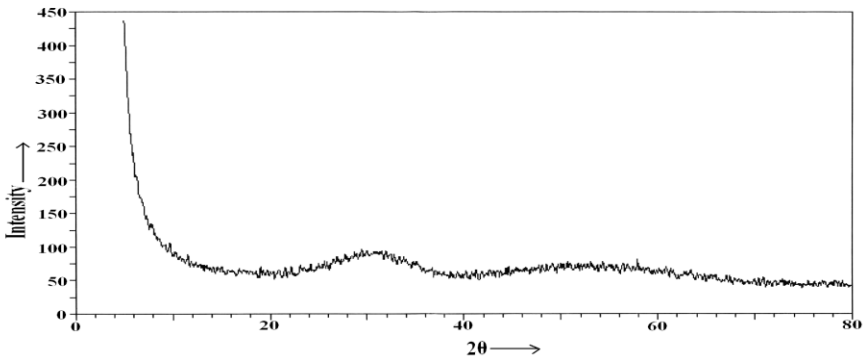

(b)

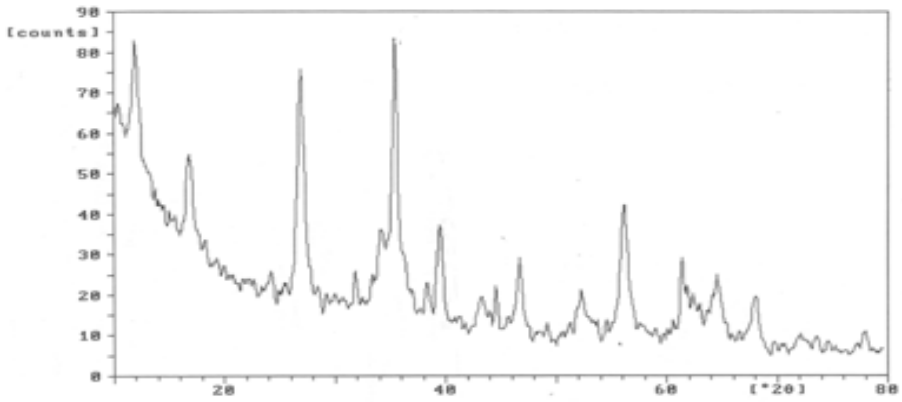

(c)

Fig. 2: The X-ray diffraction patterns of (a) HFO (b) HZO (c) HZFO

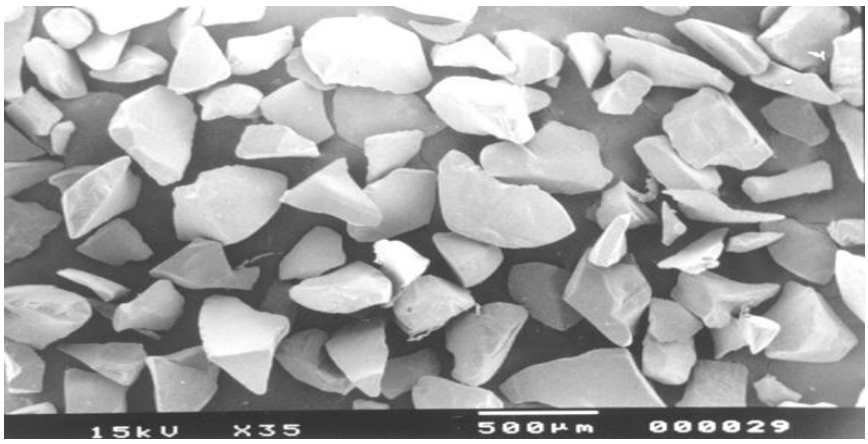
15kV X35 500µm 000029

(a)

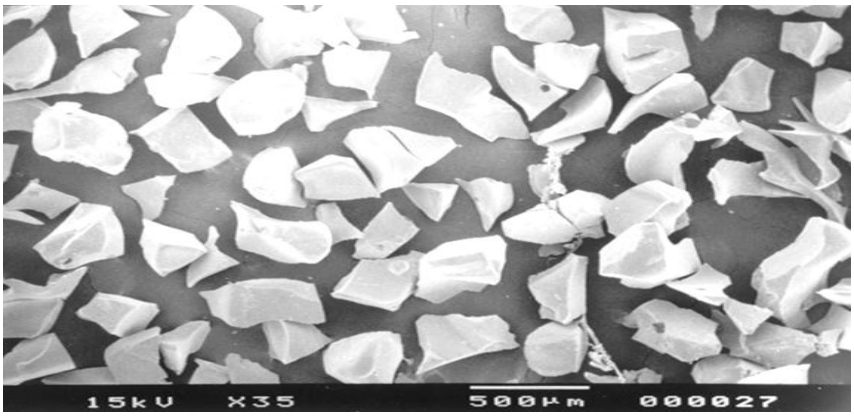
15kV X35 500µm 000027

(b)

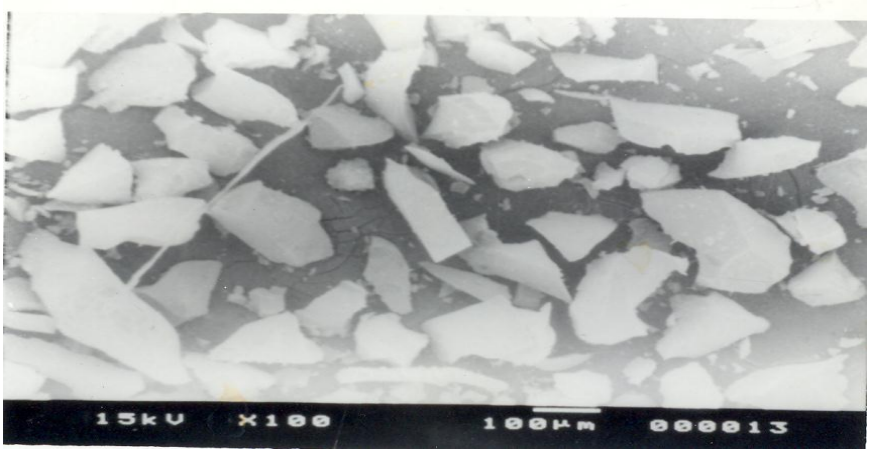
15kV X100 100µm 000013

(c)

Fig. 3: The scanning electron microscopic (SEM) images of (a) HFO (b) HZO and (c) HZFO

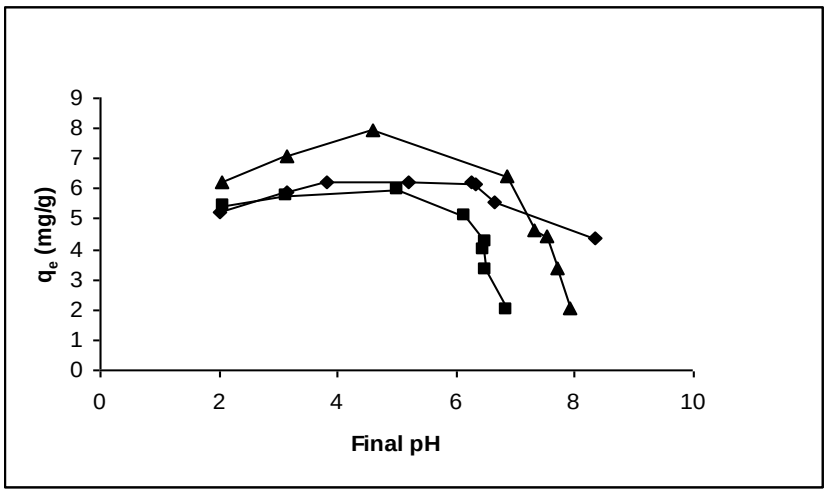

Fig. 4: The plot of fluoride sorption data versus final solution pH at 303 (±2) ºK by ♦ HZFO, ■ HFO and ▲ HZO. Initial Fluoride load used was10.0 mg/g hydrous oxide.

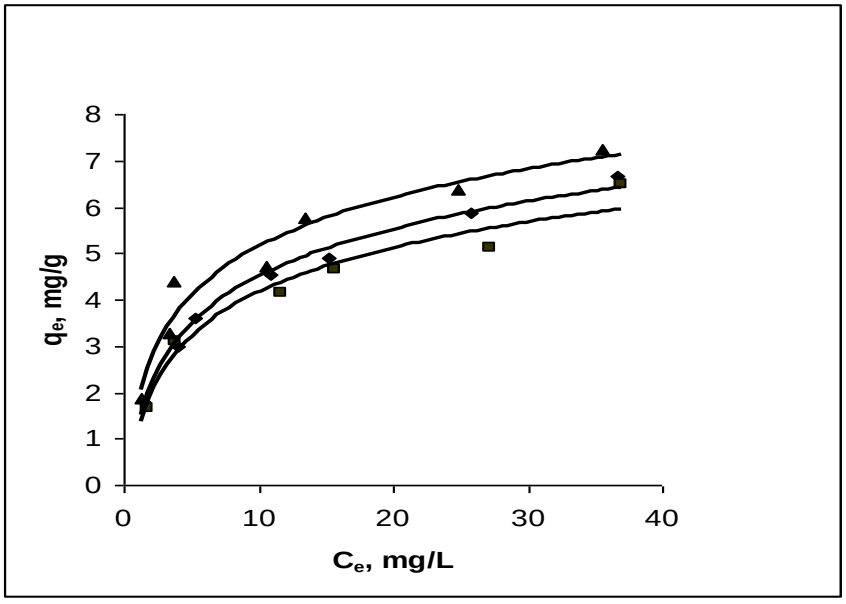

Fig.5a: The equilibrium isotherm data of fluoride sorption at final pH 6.8(±0.2) at 283(±2) K by ♦ HZFO, ■ HFO and ▲ HZO.

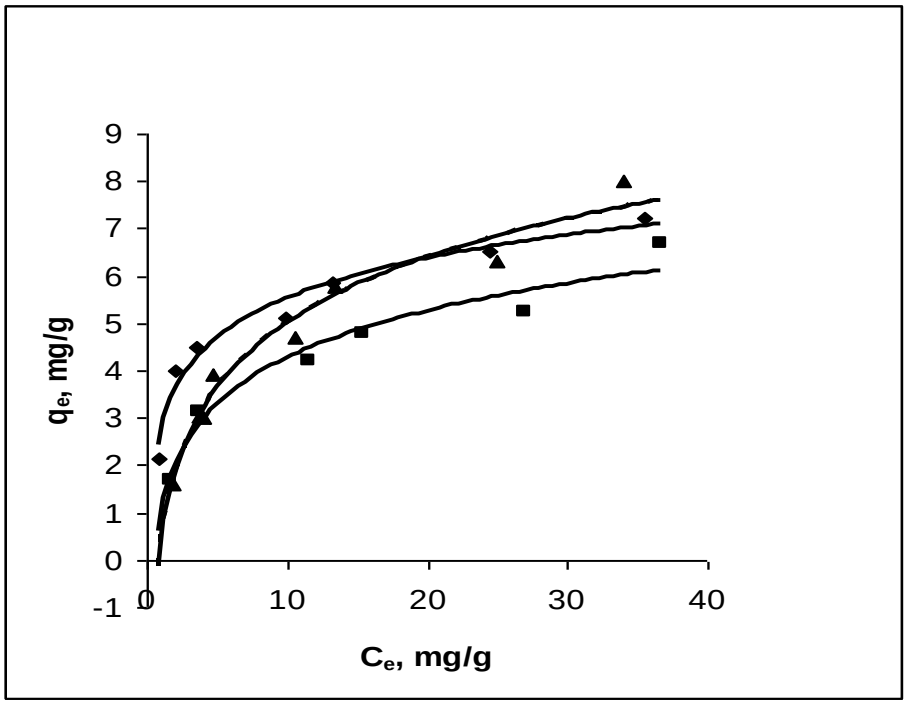

Fig.5b: The equilibrium isotherm data of fluoride sorption at final pH 6.8(±0.2) and at 293(±2)ºK by ♦ HZFO, ■ HFO and ▲ HZO.

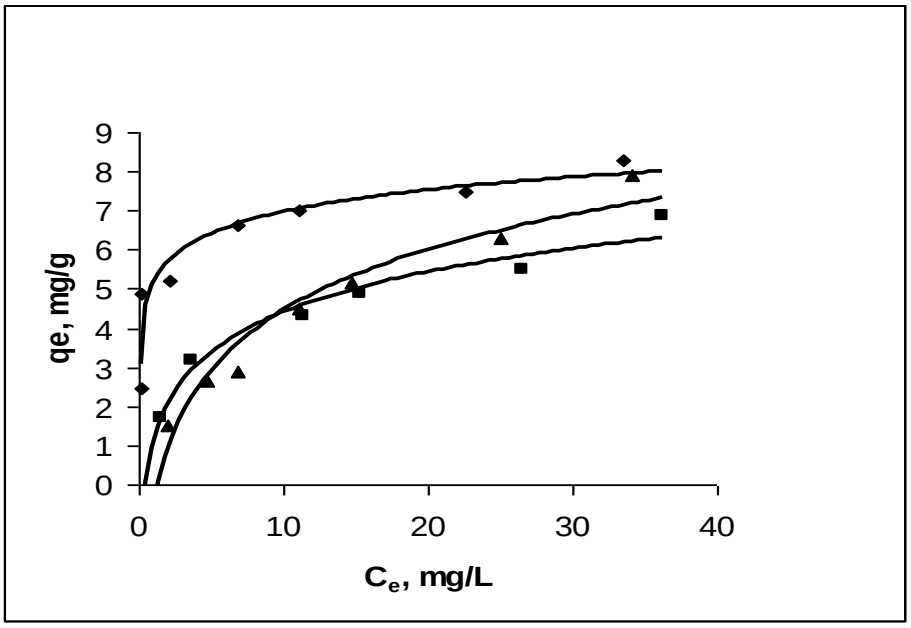

Fig.5c: The equilibrium isotherm data of fluoride sorption at final pH 6.8(±0.2) and

at 303 (±2)ºK by ♦ HZFO, ■ HFO and▲ HZO

Chapter 5

Adsorption of Fluoride from Aqueous Solution by Synthetic Iron (III)-Aluminum (III) Mixed Oxide.

5.1. Synthesis of iron (III)-aluminum (III) binary mixed oxide

Solutions of 0.1 mol L^{-1} $FeCl_3$ in 0.01mol L^{-1} of HCl and 0.1 mol L^{-1} $AlCl_3$ in .01mol L^{-1} of HCl were mixed together (v/v = 1:1), and the mixture was heated at 60 to 65 ºC. Aqueous ammonia solution (1:1) was added drop wise onto the hot solution until the pH of the solution including gel precipitate reached to 6.5-7.0. The hydrolyzed precipitate with supernatant liquid was aged for 45 h. Decantation off, thereafter, the supernatant liquid; the solid mass was washed thrice with deionised water, and filtered. The washed and filtered precipitate was dried in an air oven at 60 to 70 ºC. The dried product was grounded to the particles of size 140-290 µm and heated for 2 h at 120 ºC. Finally, the particles were homogenized to pH 7.0, and used for the adsorption experiments.

5.2. Results and Discussion

5.2.1. Characterization of the Mixed Oxide:

The X-ray diffraction pattern obtained (**Fig.1**) for the mixed oxide showed nine peaks at the angle º2θ values between 16.9 and 68.6. The relative intensity values of five peaks out of nine were 67.8%, 100%, 47.1%, 36.9% and 52.6% at º2θ angle values 27.23, 35.67, 39.67, 46.87 and 56.25 respectively which indicates the crystalline nature of the synthetic mixed oxide. The Fourier Transform Infra Red (FTIR) spectra of the hydrous iron(III)-aluminum(III) binary oxide (A), pure hydrous oxides of iron(III) (B) and

aluminum(III) (C) are shown in **Fig-2**. The wave number values (cm^1) for adsorption peaks around or above 3400 are for the water (symmetrically and asymmetrically bounded) molecules and at around 1620-1655 for OH-bending group. The adsorption peak at ~2360-2370 cm^{-1} was found to be present in all three different synthetics oxides which are presumably for CO_2 adsorbed from air during preparation. The adsorption peaks obtained below wave number 1500 cm^{-1} showed characteristic differences in spectrum of mixed oxide (A) from those of the spectra obtained for the pure oxides (B and C). The wave number values (cm^{-1}) for symmetrical and asymmetrical stretching vibration modes of M-O bonds (**Fig.2**) were found for the synthetic mixed oxide (A) to be intermediate (690 and 476.9) between those found for hydrous aluminum oxide (730.2 and 583.4) (C) and hydrous ferric oxide (670.6 and 461.1) (B). The additional wave number values (cm^{-1}) presumably for the symmetrical and asymmetrical bending of O-$H_{bridging}$ in mixed oxide were at 983.9 and 1465. The notable shifting of wave number values for the synthetic mixed oxide from either of the pure oxides indicates the presence of hydroxide bridge between two heterometal ions in the synthetic iron(III)-aluminum(III) mixed oxide. The scanning electron micrograph (SEM) images obtained for two different magnifications (**Fig. 3)** showed irregular surface morphology with high porosity indicating high surface area of the mixed oxide. The thermo gravimetric analysis (TGA) for the mixed oxide showed (figure not given) total weight loss of ~28.12% when dried up to 700ºC, and ~80% of the total weight loss was found at around 90-110ºC. The differential thermal analysis (DTA) showed the synthetic mixed oxide was stable up to 700ºC as the thermal spectrum showed (figure not given) no exothermic or endothermic peak. The results of thermal analysis indicate the hydrous nature of the mixed oxide.

Some determined physicochemical parameters of the mixed oxides are: Fe:Al = 1:1 (mole/mole), specific surface area = 195.6 m^2 g^{-1}, pH_{zpc} = 5.9-7.5, particle size = 140-290 µm, and monolayer adsorption capacity, obtained from the Langmuir isotherm plot of equilibrium data**,** for fluoride at pH~7.0 = 17.73 mg g^{-1}.

5.2.2. Effect of pH:

The effect of pH on the adsorption of fluoride is shown in Fig.4. The results showed that the adsorption of fluoride (mg g^{-1}) onto the synthetic binary mixed oxide was increased with increasing initial solution pH (pH_i) from 3.0 to 4.0, and remained, thereafter, nearly constant up to pH_i 10.0 at concentrations 10.0 and 25.0 mg L^{-1}, while that decreased slightly above pH_i 4.0 for the concentration 50.0 mg F^- L^{-1}. The less fluoride adsorption at pH_i 3.0 is presumably due to slight solubility loss of the adsorbent. At pH_i 4.0, the mixed oxide surface should be strongly positive (pH_{zpc} = 5.9-7.5) and adsorbs fluoride with strong electrostatic forces (Eq. R4).

$$MOH_{(S)} + H_3O^+ + F^- \rightarrow MOH_2^+ \text{---} F^-_{(S)} + H_2O \text{ ---------- (R4)}$$

The mechanism suggested is similar to that for arsenate adsorption onto the different metal oxides. The fluoride adsorption reaction suggested (Eq. R4) agrees well to the observe increase in equilibrium solution pH. The noted decrease of fluoride adsorption capacity (Fig. 4) at above pH_i 4.0 for the solution of concentration 50.0 mg L^{-1} is peculiar, and that may be due to the error in experimental measurements or abstraction of metal ion as $[MF_{6-x}(OH)_x]^{(x-3)-}$ (M = Fe and/Al) from the surface at high fluoride level in solution.

5.2.3. Adsorption isotherm analysis:

The equilibrium data for fluoride adsorption onto the synthetic iron(III)–aluminum(III) binary mixed oxide at pH 6.9 (±0.2) and temperature 28ºC are shown in **Fig**. **5**. Results indicated that the mixed oxide has high affinity for fluoride adsorption under these conditions. The equilibrium data (**Fig. 5**) had been analyzed by linear regression of isotherm model equations viz. Langmuir (Eq. 2), Freundlich (Eq. 4), Temkin (Eq. 5) and Redlich-Peterson (Eq.7). The related parameters obtained by calculation from the values of slopes and intercepts of respective linear plots (only best fit plot given) are shown in Table 1. The present data fitted well ($r^2 > 0.99$) with the Langmuir and the Redlich-Peterson models (**Fig. 5a and 5b**). The monolayer adsorption capacity (θ) obtained for mixed oxide is 17.73 mg g^{-1} which is found to be much higher than that of either of the pure oxides iron (III) (θ =7.50 mg g^{-1}) and aluminum (III) (θ = 11.42 mg g^{-1}) (determined in our laboratory), and that agrees fairly well with their specific surface area values (BET surface area in m^2 g^{-1}, respectively, for the present mixed oxide, hydrous ferric oxide and hydrous aluminum oxide were 195.6, 165.6 and 172.4**).** Thus, it is suggested that the present mixed oxide could be a better adsorbent than either of the pure oxides. The value for the Redlich-Peterson constant, β, obtained is high (15.66 mg L^{-1}) for the maximum optimized value for g (0.96), which indicates the high affinity for fluoride of iron(III)-aluminum(III) mixed oxide. The high g-value (0.96) of the Redlich-Petreson model required to describe the best fit of the present data, indicated that the adsorption of fluoride is due to the Langmuir monolayer surface adsorption. However, the Freundlich isotherm model based on multilayer adsorption described the data fairly well (r^2= 0.9489). The Freundlich adsorption constant (K_F) obtained from the linear plot (not shown) was also high (12.03 L mg^{-1}). The Freundlich coefficient, n, which should have

values ranging from 1 to 10, is high (7.80), and that also supports favorable adsorption of fluoride onto the mixed oxide.

The linear plot (not shown) for Temkin adsorption isotherm, which contains the features of chemisorption, described poorly the present isotherm adsorption data (r^2 = 0.9414). This indicated the adsorption of fluoride onto the mixed oxide took place mainly with physical forces. Hence the order of isotherm equations obeyed by the present data is:

Redlich-Peterson ≥ Langmuir > Freundlich > Temkin.

Another essential feature of the Langmuir model can be given in terms of dimensionless separation factor, R_L, which was defined by Weber and Chakravorti[1] as:

$R_L = 1/ (1+ bC_0)$ …… (20)

where C_0 and b are the initial solute concentration and a Langmuir constant, respectively.The value of R_L indicates the shape of the isotherm to be (i) unfavorable (R_L>1), (ii) linear (R_L=1), (iii) favorable (0<R_L<1), and (iv) irreversible (R_L = 0). In this work, the R_L–values calculated in the studied range of fluoride concentration are found to be in the range 0 to 1.0; which suggest the favorable adsorption of fluoride onto the studied mixed oxide under the conditions used for the experiments.

5.2.4. Thermodynamic parameters

Assuming the activity coefficient as unity at low concentration of solute (Henry's law sense), the thermodynamic parameters for the adsorption process in solution was calculated using the following thermodynamic relations:

$\Delta G^0 = \Delta H^0 - T\Delta S^0$ …… (.21) and $\Delta G^0 = -2.303RT \log K_c$ …….. (22)

Combining Eq. (21) with Eq. (22), the Eq. (23) is obtained.

$\log K_c = \Delta S^0/ 2.303R - (\Delta H^0/2.303R)\ 1/T$ ----------(23)

where K_c is the equilibrium constant at temperature T and K_c was calculated as

$K_c = q_e / C_e$, where q_e/C_e is called the adsorption affinity, which is the ratio of the amount adsorbed per unit mass (q_e) to the solute concentration in solution (C_e) at equilibrium, ΔG^0, ΔH^0 and ΔS^0 are the change in free energy, enthalpy and entropy under standard states respectively. So the above relation (Eq. 23) can be written as (Eq. 24**)**

$$\log(q_e/C_e) = \Delta S^0/2.303R - (\Delta H^0/2.303R)1/T \quad \ldots\ldots\ldots\ldots\ldots\ldots(.24)$$

Assuming ΔS^0 and ΔH^0 to be constant within the temperature range studied, the values have been calculated from the slope and intercept of the straight line obtained from the plot of log (q_e/C_e) versus 1/T, and ΔG^0, the change of free energy, at various temperatures were calculated from the relation above (Eq. 21). When the adsorption was carried out within the temperature range 10º to 40ºC, the extent of adsorption improved with an increase in the adsorption temperature. So the fluoride adsorption on iron(III)–aluminum(III) mixed oxide was definitely endothermic in nature.

The thermodynamic parameters for the fluoride adsorption (Table 2) were computed from the plot of log (q_e/C_e) versus 1/T (**Fig.6**) for an initial fluoride concentration (25.0 mg L^{-1}). The plot has good linearity with regression coefficient ($r^2 = 0.9864$) over the range of 1/T values .The value of ΔH^0 calculated was +29.31 kJ mol^{-1}, and that indicates the endothermic nature of fluoride adsorption process.

The results showed the increase in adsorption capacity of fluoride with increasing temperature which is presumably due to control of adsorption process by diffusion phenomenon. Thus, the result indicates the endothermic nature of diffusion controlled adsorption process.

The entropy change (ΔS^0) obtained for the present system was +116.75 J mol^{-1} K^{-1}. This indicated the fluoride adsorption on the mixed oxide leads to the increase in entropy of the system. The adsorption of fluoride from aqueous solution on the solid surface takes place with increase in entropy, which is probably due to the release of greater number of water molecules at the solid–liquid interface during adsorption of fluoride ion. Using the values of ΔH^0 and ΔS^0 (Table 2), the values of ΔG^0 have been calculated by the Eq. (21). The values of ΔG^0 obtained (Table 2) indicated the adsorption of fluoride is spontaneous and, the spontaneity of the process is enhanced with increasing temperature. The similar trend in increase in the values of ΔG^0 was reported by some other workers[2-4].

5.3. Analysis of kinetic data:

5.3.1. Effect of initial fluoride concentration:

The results on the rate of fluoride adsorption on iron (III)-aluminum (III) mixed oxide surface as a function of initial fluoride concentration are shown in **Fig. 7**. The fluoride adsorption was fast up to 20 minutes and then it was slow. The time required to reach equilibrium was 90 minutes for higher concentrations. The initial rapid adsorption was presumably due to ion-exchange with surface hydroxyl ions of the adsorbent. The slow adsorption in the later stage represents a gradual uptake of fluoride at the inner surface[5]. However the later part of the adsorption step was found insignificant for the lowest solute concentration (10 mg L^{-1}). These data (Fig.7) were analyzed using kinetic equations viz. pseudo-first order (Eq.9), pseudo-second order (Eq. 12), intra particle diffusion (Eq.14), Elovich (Eq. 15) and Boyd chemical phenomenon (Eq. 19) models. The various related kinetic parameters, obtained by calculation from the slopes and intercepts of the plots (best fit plot given), are shown in Table 3. The Lagergren pseudo-

first order kinetic equation (Eq. 9) described the kinetic data fairly well (r^2 = 0.9890 and 0.9641) for the fluoride concentrations of 25.0 and 50.0 mg L^{-1}, and that described too poorly (r^2 = 0.6775) the kinetic data obtained for the fluoride concentrations of 10.0 mg L^{-1}. The pseudo-second order kinetic equation (Eq. 12) described the present data best (r^2 = 0.9990-1.0000) in the concentration range of fluoride used for the adsorption study (**Fig. 7a**). The pseudo-second order rate constant k_2, initial adsorption rate h_0 and equilibrium adsorption capacity q_e obtained (Table 3) by calculation from the slopes and intercepts of the plots (**Fig. 7a**) showed the decrease in k_2 and h_0 and increase in q_e values with the increase of initial fluoride concentration. The similar type of observations was reported by Ho et al.[6], Demirbas et al.[7] and Uzun [8].

The equilibrium adsorption capacity (q_e) evaluated from the pseudo-second order plot was found to increase from 4.78 to 18.18 mg g^{-1} with increasing fluoride concentration from 10.0 to 50.0 mg L^{-1} which suggests the studied mixed oxide adsorbent should be a well adsorbent for scavenging fluoride from contaminated water.

The data (Fig 7) were analyzed by the intra-particle diffusion kinetic equation (Eq. 14). Figure 7b shows the plot of mass of fluoride adsorbed per unit mass of iron(III)-aluminum(III) mixed oxide (q_t, mg g^{-1}) versus square root of contact time ($t^{1/2}$, $min^{1/2}$). The data points appeared in Fig. 7b could be connected by two straight lines – the first linear portion for macro pore diffusion and the second depicting micro-pore diffusion[2, 5, 9-12]. The extrapolation of the first linear portion of the plots back to the axis showing q_t (mg g^{-1}) gives positive intercept which provide the idea about boundary layer thickness. It is indicated that the extrapolation of first linear portion of plots (Fig. 7b) should not pass through the origin, so the adsorption rate of fluoride on to the mixed oxide is not solely

pore diffusion controlled. If the data points shown in Fig. 7b be connected from zero, the initial sharp line showing variation of q_t versus $t^{1/2}$ values in Fig.7b should attribute to the boundary layer diffusion effect or external mass transfer effect[2, 3, 9-12]. Thus, the adsorption data indicated the removal of fluoride from aqueous phase on to the studied mixed oxide was rather complex process, involving both boundary layer diffusion and intra-particle diffusion. The increase of k_{id} (average pore diffusion rate constant, mg g^{-1} $min^{-0.5}$) with increasing concentration (Table 3) indicated the higher pore sorption possibility of fluoride on to the adsorbent at room temperature. However, the pore-diffusion coefficient (D_P) and film diffusion coefficient (D_F) were calculated using the following standard relations [13, 14]:

$D_P = (0.03\ r_0^2) / t_{1/2}$ and $D_F = (0.23 \times r_0 \times \partial \times C_s) / t_{1/2} \times C_L$, where r_0 is mean radius of adsorbent particles (assumed spherical), ∂ is the film thickness (0.001 cm), and C_s and C_L are the concentrations of solute in solid and liquid phases at t = t and t = 0, respectively. Here, $t_{1/2}$ (the time for 50% adsorption) values used for calculation were obtained from the relation, $t_{1/2} = 1/ (q_e\ k_2)$, where k_2 is the pseudo-second order rate constant and q_e has same meaning mentioned elsewhere. It has been known[13] that if D_p-value be ranged in 10^{-11} to 10^{-13} $cm^2\ s^{-1}$, the pore-diffusion is the rate limiting and if D_F- value be ranged in 10^{-6} to 10^{-8} $cm^2\ s^{-1}$, the boundary layer (film) diffusion is the rate limiting step. The D_p and D_F values ($cm^2\ s^{-1}$) calculated, respectively, for the present case were in the range 1.16×10^{-7} to 7.10×10^{-9} and 3.44×10^{-5} to 4.57×10^{-6} at the concentration range of fluoride ion studied. It has been found that the values of either D_p or D_F are not lied in appropriate range, so obviously the fluoride adsorption rate is multi-stage controlled phenomena.

5.3.2. Effect of temperature on adsorption kinetics:

The time dependent fluoride adsorption kinetic studies on iron(III)-aluminum(III) binary mixed oxide surface are carried out at four different temperatures and, the results are shown in **Fig. 8**. The data were analyzed by using the same kinetic equations described earlier, and the parameters obtained are shown in Table 4.

The pseudo-first order kinetic equation (Eq. 9) described (graph not shown) the temperature dependent fluoride adsorption kinetic data fairly well (r^2 = 0.9807-0.9873) except the data obtained at a temperature of 10º C (r^2 = 0.9085). In contrast, the pseudo-second order plot (**Fig. 8a**) according to Eq. (12) described the data of **Fig. 8** best (r^2 = 0.9906-0.9990). The equilibrium adsorption capacity qe (mg g^{-1}), which was calculated from the plot according to Eq. (12), increased from 13.76 to 19.27, and the initial adsorption rate h_0 was also increased from 1.02 to 2.56 with increase of temperature from 10º to 40 ºC. So, from the above q_e and h_0 values, the endothermic nature of the adsorption was also verified. On the other hand, the values of pseudo-second order rate constant (Table 4) were found to increase from 5.38 x 10^{-3} to 6.90 x 10^{-3} g mg^{-1} min^{-1} for the increase of temperature from 10º to 40 ºC, and the result is similar to that due to Ho et al.[6]. The time dependent fluoride adsorption capacity values of the mixed oxide obtained with increasing temperature on the reactions were plotted against the square root of contact time (Fig. 8b) according to the Eq. (14) showed, as in the earlier section, the adsorption rates were also multiple stage controlled process which is similar to the conclusion drawn by some other authors [2, 3, 9-12]. Furthermore, the D_p and D_F -values (cm^2 s^{-1}) calculated for the temperature range studied were (4.50 - 7.95) ×10^{-9} and (0.81 – 1.98) ×10^{-6}, respectively which indicated the kinetic rate of the fluoride adsorption was

controlled by the process of multistage diffusion. Table 4 shows the kinetic parameters obtained by analyzing the data using other kinetic equations also. It has been found that the present data within the studied temperature range described the Elovich equation (Eq. 15) fairly well (r^2 = 0.9630- 0.9950) (plots not given), indicating adsorption as chemisorption. The Boyd (chemical phenomenon) kinetic equation (Eq.16) described the kinetic data fairly well (r^2 = 0.9807- 0.9859, plots not shown), excepting the data obtained at 10ºC (r^2 = 0.9086). Thus the analytical data (Table 4) reveal that the both pseudo-first order and Boyd (chemical phenomenon) kinetic equations is basically the same model.

5.3.3. Activation parameters:

The increase in second order rate constant with increase in temperature may be described by the Arrhenius equation:

$k_2 = A \exp(-E_a / RT)$ …….. (25)

k_2 is the pseudo second order rate constant (g mg $^{-1}$ min $^{-1}$), A is a temperature-independent factor (g mg $^{-1}$min^{-1}), Ea the activation energy of adsorption (kJ mol^{-1}), R the gas constant (8.314 J mol $^{-1}$ K^{-1}) and T the absolute temperature (K). Taking logarithmic of Eq. (25), the following Arrhenius type linear relationship (Eq. 26) is obtained.

$\ln k_2 = \ln A + (-E_a/ R)\ 1/T$ …….(26)

The plot of lnk_2 against 1/T shows a linear (**Fig. 9**) variation with a correlation coefficient (r^2) of 0.9605. The intercept and slope of the plot give the temperature independent parameter, A (1.34 x 10^{-3}g mg $^{-1}$s^{-1}) and the activation energy, E_a (6.35 kJ mol^{-1}), respectively.

5.3.4. Effect of some other ions:

The effect of some other ions viz. sulfate, phosphate, chloride, bicarbonate, magnesium and calcium on fluoride adsorption by iron(III) – aluminium(III) mixed oxide was tested by batch method. The results (Fig. 10) showed that the presence of bicarbonate and sulfate decreases the adsorption capacity of fluoride from 11.04 to 8.25 and 11.22 to 8.55, respectively. The presence of other tested ions has almost no significant effect on fluoride adsorption by iron(III) – aluminium(III) mixed oxide.

5.3.5. Fixed bed column study:

A fixed bed column study was performed using iron(III) – aluminium(III) mixed oxide paced column. For this experiment a glass column of 1 cm diameter, bed height 4.2 cm (bed volume: 3.3 cm^3) was used. The down flow rate used in this experiment was 1.0 $ml.min^{-1}$. In three similar columns, the fluoride solution concentration ($mg.L^{-1}$) of 12.0, 6.0 and 3.0 were passed down and effluent was collected in 50 ml fraction and, the collected fraction was analyzed for residual amount of fluoride. From the result (Fig. 11) it was found that with decrease of initial fluoride concentration in throughput solution, the effluent volume with fluoride concentration below toxic level (1.5 mgL^{-1}) was increased and result shows that the treated volume (Fig. 11) 500 ml, 2500 ml and 4000 ml were collected.

5.4. Conclusion

The iron(III)-aluminum(III) mixed oxide is crystalline which was synthesized by simple method. The FTIR spectra indicate the presence of Fe-O-Al bond. The SEM image shows almost irregular surface morphology with high porosity indicating high surface area. The fluoride adsorption onto the mixed oxide is found to be pH dependent, and the optimum initial pH range obtained is 4.0 – 10.0 for fluoride adsorption except for the

solute concentration of 50 mg L^{-1}. The equilibrium time is 1.5 h for fluoride adsorption on the synthetic iron(III)-aluminum(III) mixed oxide. The isotherm data obtained have been described best by both the Redlich-Peterson and the Langmuir isotherm model equations. The monolayer adsorption capacity (θ) obtained is found to be higher than that of either of the pure oxides. The thermodynamic analysis shows the adsorption process is endothermic and spontaneous in nature. The adsorption kinetic data is described best by the pseudo-second order model in the range of fluoride concentration and temperature studied, and the rate is controlled by multistage diffusion. The value of the activation energy calculated is 6.35 kJ mol^{-1}. Bicarbonate and sulphate showed adverse effect on fluoride removal. The adsorbent packed column gave high treated volume when input fluoride concentration was 6.0 mgL^{-1} and 3.0 mgL^{-1}.

5.5. References

(1) Weber, T. W.; Chakravorti, R. K. Pore and Solid Diffusion Models for Fixed Bed Adsorbents. *AIChE J*. **1974**, *20*, 228.

(2) Srivastava, V. C; Swamy, M. M.; Mall, I. D.; Parasad, B.; .Mishra, I. M. Adsorptive Removal of Phenol by Bagasse Fly Ash Activated Carbon: Equilibrium, Kinetics and Thermodynamics. *J of Colloids Surf. A: Physicochem. Eng. Aspects* **2006**, *272*, 89.

(3) Bhattacharyya, K.G.; Sharma, A. Kinetics and Thermodynamics of Methylene Blue Adsorption on Neem (Azadirachta Indica) Leaf Powder. *Dyes Pigments* **2005,** *65*, 51.

(4) Singh, K. K.; Rastigo, R.; Hasan, S. H. Removal of Cr(VI) from Waste Water Using Rice Bran. *J. Colloid Interf. Sci.* **2005**, *290*, 61.

(5) Low, K. S.; Lee, C. K. The Removal of Cationic Dyes using Coconut Husk as an Adsorbent. *Pertanika* **1990**, *13*, 221.

(6) Ho, Y. S.; Chiang, T.H.; Hsueh, Y.M. Removal of Basic Dye from Aqueous Solution Using Tree Fern as a Biosorbent. *Process Biochem.* **2005**, *40*, 119.

(7) Demirbas, E.; Kobya, M.; Senturk, E.; Ozkan T. Adsorption Kinetics for the Removal of Chromium(VI) from Aqueous Solutions on the Activated Carbons Prepared from Agricultural Waste. *Water SA* **2004,** *30*, 533.

(8) Uzun, I. Kinetics of the Adsorption of Reactive Dyes by Chitosan. *Dyes Pigments* **2006,** *70*, 76.

(9) Kumar, V. K.; Ramamurthi, V.; Sivanesan, S. Modeling The Mechanism Involved During the Sorption of Methylene Blue onto Fly Ash. *J. Colloid Interf. Sci.* **2005**, *284*, 14.

(10) Sing, T. V.; Pant, K. K. Equilibrium, Kinetics and Thermodynamics Studies for Adsorption of As(III) on Activated Alumina. *Sep. Purif. Technol.* **2004**, *36*, 139.

(11) Mahramanlioglu, M.; Kizilcikli, I.; Bicer, I. O. Adsorption of Fluoride from Aqueous Solution by Acid Treated Spent Bleaching Earth. *J. Fluorine Chem*. **2002**, *115*, 41.

(12) Mohan, S. V.; Ramanaiah, S. V.; Rajkumar, B.; Sarma, P. N. Removal of Fluoride from Aqueous Phase by Biosorption on to Algal Biosorbent

Spirogyra Sp. – 102: Sorption Mechanism Elucidation. *J. Hazard. Mater.* **2006**, *Available online,* www. Elsevier. Com /locate/jhazmat.

(13) Helfferich, F. *Ion Exchange*, McGraw-Hill: New York, 1962.

(14) Boyd, G.E.; Adamson, A.W.; Mayers Jr., L.S. The Exchange Adsorption of Ions from Aqueous Solutions on Organic Zeolites. Kinetic II. *J. Am. Chem. Soc.* **1947**, *69*, 2836.

Table-1: Various Isotherm Parameters for Fluoride Adsorption onto Iron(III)-Aluminum(III) Mixed Oxide at Temperature 28(±1)°C and pH 6.9 (±0.2).

Isotherm Models	**Parameters**	**Values**
Langmuir	θ (mg g^{-1})	17.73
	b (L mg^{-1})	1.1701
	r^2	0.9929
Freundlich	K_F ($mg^{1-1/n}$ $L^{1/n}$ g^{-1})	12.0337
	n	7.80
	r^2	0.9489
Temkin	a	11.91
	b	1.8423
	r^2	0.9414
	α (g L^{-1})	-0.5122

Redlich-Peterson (g = 0.96)	β (mg L^{-1})^g	15.659
	r^2	0.9944

Table-2: Thermodynamic Parameters for Adsorption of Fluoride onto Iron(III)-Aluminum(III) Mixed Oxide at pH 6.9 (±0.2).

Initial fluoride concentration (mg L^{-1})	**ΔH^0 (kJmol^{-1})**	**ΔS^0 (J mol^{-}K^{-} ^{1})**	**r^2**	**- ΔG^0 (kJmol^{-1}) at temperatures (ºC)**			
				10	19	28	40
25.0	29.31	116.75	0.9864	3.73	4.78	5.83	7.23

Table-3: Various Kinetics Parameters for Fluoride Adsorption onto Iron(III)-Aluminum(III) Mixed Oxide at Different Initial Fluoride Concentrations at Temperature 28 (± 1) ºC and at pH 6.9 (±0.2).

Kinetic equations	**Parameters**	**10 mg L^{-1}**	**25 mg L^{-1}**	**50 mg L^{-1}**
Pseudo second order	k_2 (g mg^{-1} min^{-1})	38.7 x 10 $^{-2}$	1.77 x 10^{-2}	0.659 x 10^{-2}
	q_e (mg g^{-1})	4.78	12.71	18.18
	h_o (mg g^{-1} min^{-1})	8.85	2.85	2.18
	r^2	1.00	0.9999	0.9990
Pseudo first order	k_1 (min^{-1})	2.90 x 10^{-2}	4.40 x 10^{-2}	4.35 x 10^{-2}
	q_e (mg g^{-1})	0.2267	5.2312	12.1899
	r^2	0.6775	0.9890	0.9641
Intraparticle diffusion	k_{id} (mg g^{-1} min$^{-0.5}$)	0.055	0.536	0.989
	r^2	0.4589	0.8469	0.9238
	A_1	3.9848	4.9889	3.6645

Elovich	B_1	0.1816	1.6152	2.8956
	r^2	0.6252	0.9589	0.9881
Boyd	k_R (min^{-1})	0.0290	0.0439	0.0435
	r^2	0.6777	0.9890	0.9641

Table-4: Kinetic Parameters for Fluoride Adsorption onto Iron(III)-Aluminum(III) Mixed Oxide at Different Temperature with an Initial Fluoride Concentration of 50 mg L^{-1} and at pH 6.9 (±0.2)

Kinetic equations	**Parameters**	**10°C**	**19°C**	**28°C**	**40°C**
Pseudo second order	k_2 (g mg^{-1} min^{-1})	5.38 x 10^{-3}	5.86 x 10^{-3}	6.59 x 10^{-3}	6.90 x 10^{-3}
	q_e (mg g^{-1})	13.76	17.36	18.18	19.27
	h_o (mg g^{-1} min^{-1})	1.02	1.77	2.18	2.56
	r^2	0.9906	0.9976	0.9990	0.9990
Pseudo first order	k_1 (min^{-1})	2.07 x 10^{-2}	2.56 x 10^{-2}	3.82 x 10^{-2}	3.45 x 10^{-2}
	q_e (mg g^{-1})	8.06	8.21	10.66	9.86
	r^2	0.9085	0.9807	0.9873	0.9858
Intraparticle Diffusion	k_{id} (mg g^{-1} $min^{-0.5}$)	0.9144	0.8707	0.9889	0.9739
	r^2	0.8850	0.9544	0.9237	0.9346
Elovich	A_1	-0.1121	4.2375	3.6645	5.0013

	B_1	2.6998	2.5185	2.8956	2.8432
	r^2	0.9630	0.9950	0.9881	0.9939
Boyd	k_R (min^{-1})	2.07×10^{-2}	2.56×10^{-2}	3.79×10^{-2}	3.45×10^{-2}
	r^2	0.9086	0.9807	0.9856	0.9859

Table-5: Activation Parameters for Fluoride Adsorption onto Iron(III)-Aluminum(III) Mixed Oxide at pH 6.9 (±0.2).

Initial fluoride concentration ($mg\ L^{-1}$)	**Temperature (ºC)**	**Pseudo second order rate constant k_2 ($g\ mg^{-1}\ s^{-1}$)**	**E_a ($kJ\ mol^{-1}$)**	**A ($gmg^{-1}\ s^{-1}$)**	**r^2**
50.0	10	8.97×10^{-5}	6.35	1.34×10^{-3}	0.9605
	19	9.77×10^{-5}			
	28	10.98×10^{-5}			
	40	11.50×10^{-5}			

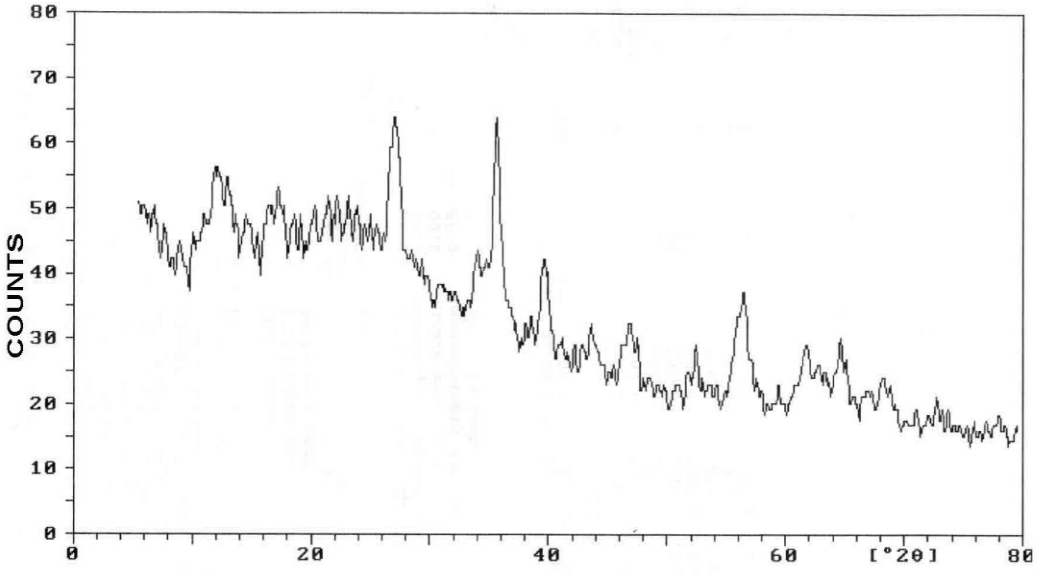

Fig. 1: X-ray diffraction pattern of hydrous Iron(III)-Aluminium(III) mixed oxide

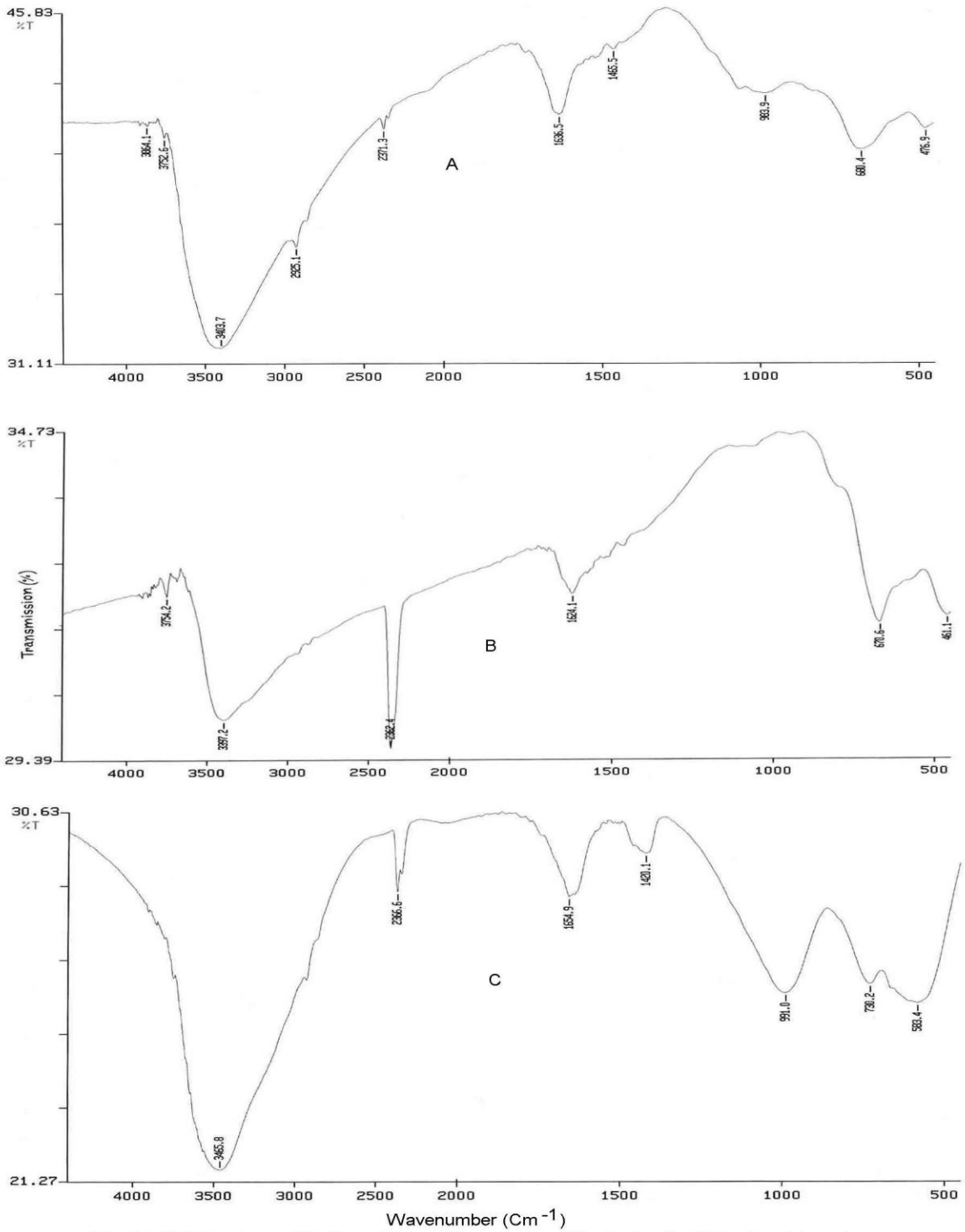

Fig. 2: FTIR Spectrum of Hydrous (A) Iron(III)-Aluminium(III) mixed oxide,(B)Ferric oxide and, (C)Aluminium oxide

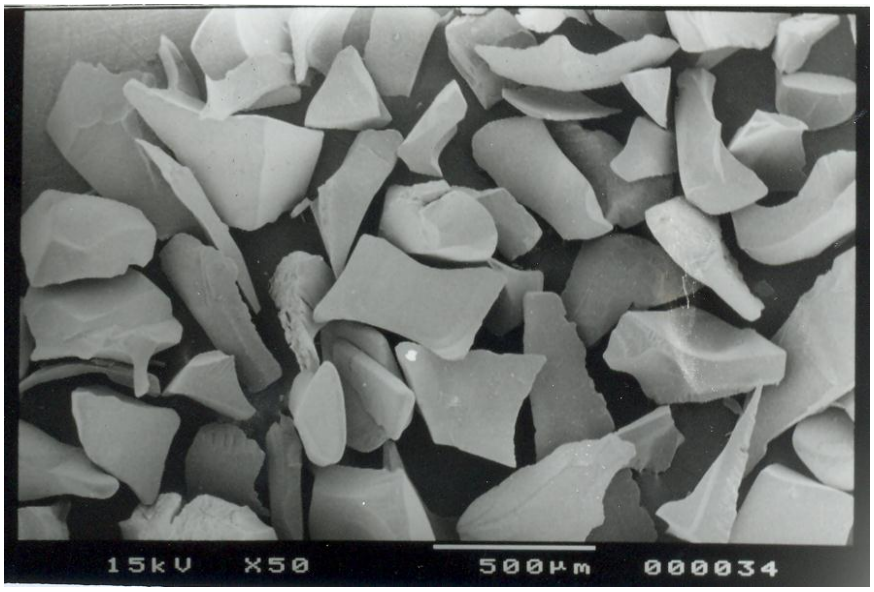

(a)

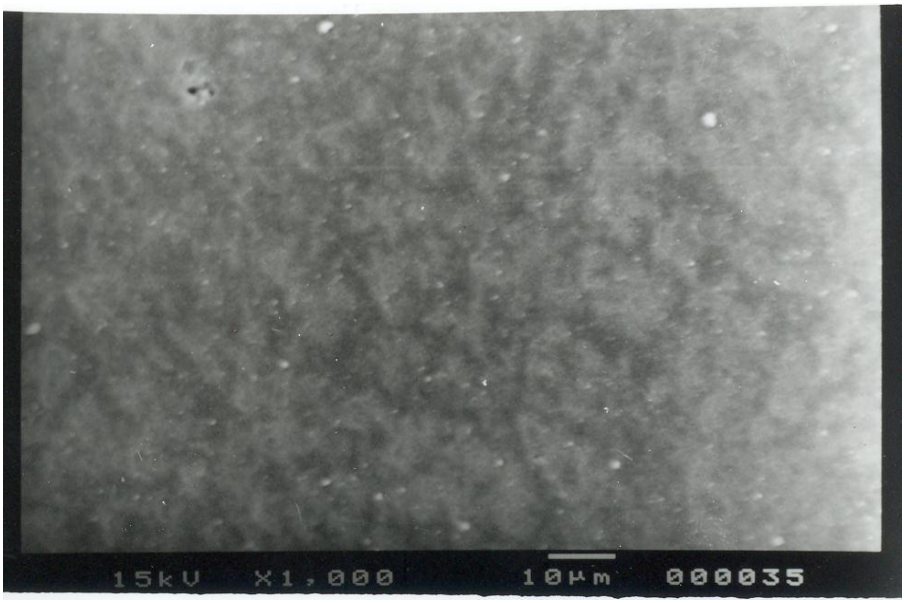

(b)

Fig. 3: Scanning Electron Micrograph of iron(III)-aluminum(III) mixed oxide (a) 50 times magnification (b) 1000 times magnification.

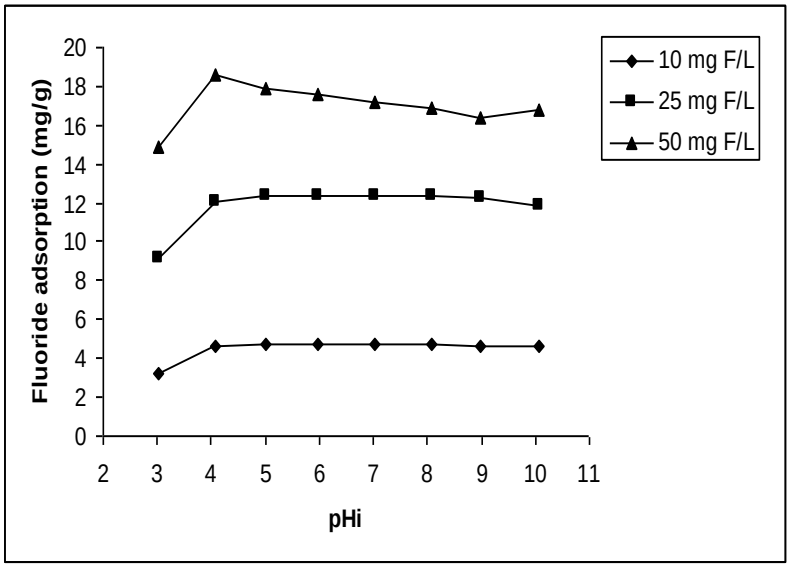

Fig. 4: Effect of initial pH (pHi) on adsorption of fluoride by iron(III)-aluminum(III) mixed oxide.

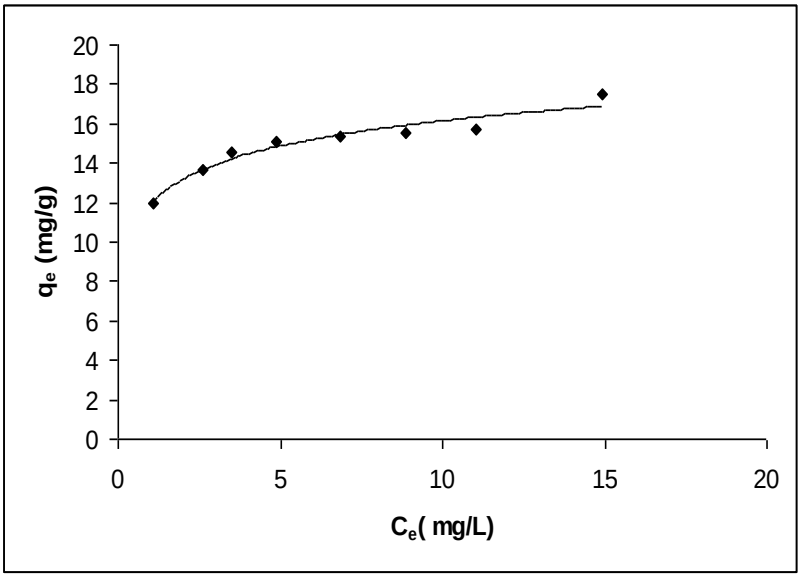

Fig.5: The plot of equilibrium adsorption capacity, q_e (mg g^{-1}) versus equilibrium concentration of fluoride, C_e(mg L^{-1}). Temperature: 28 (±1)ºC, pH: 6.9 (±0.2).

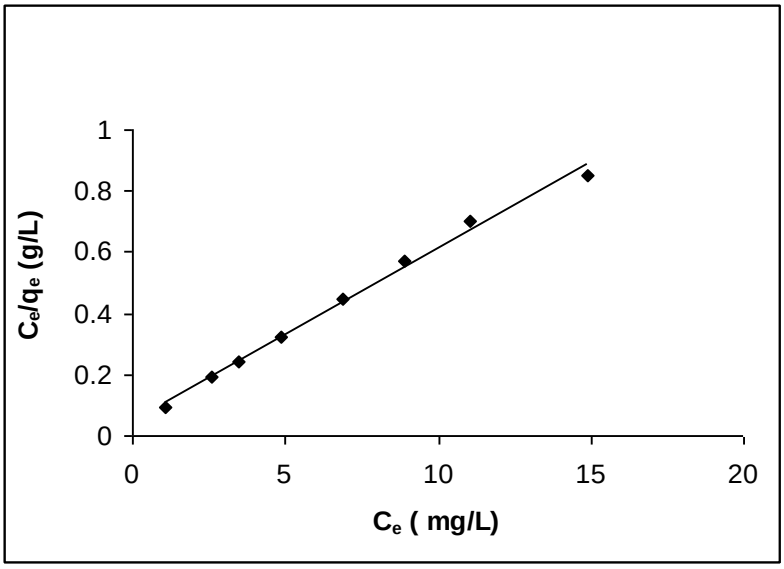

Fig. 5a: The plot of Langmuir isotherm for fluoride adsorption onto iron(III)-aluminum(III) mixed oxide.
Temperature: 28 (± 1)ºC, pH: 6.9 (±0.2).

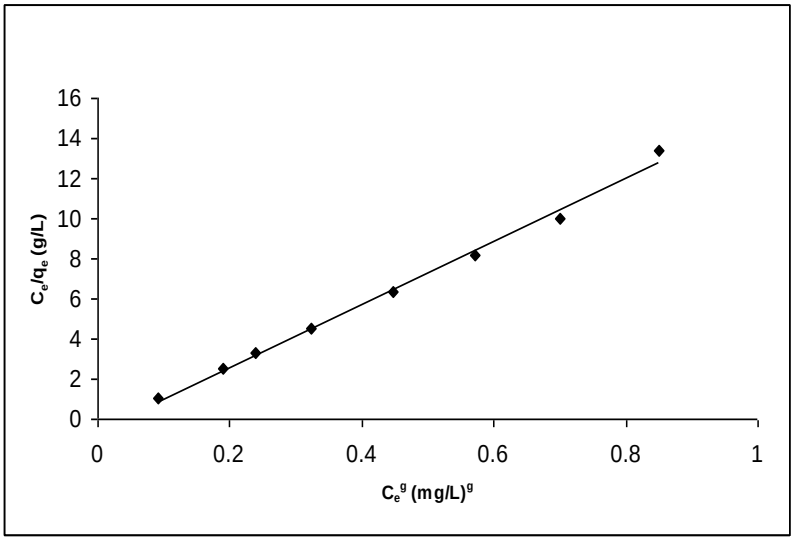

Fig. 5b: The plot of Redlich-Peterson isotherm for fluoride adsorption onto iron(III)-aluminum(III) mixed oxide.
Temperature: 28 (± 1)ºC, pH: 6.9 (±0.2).

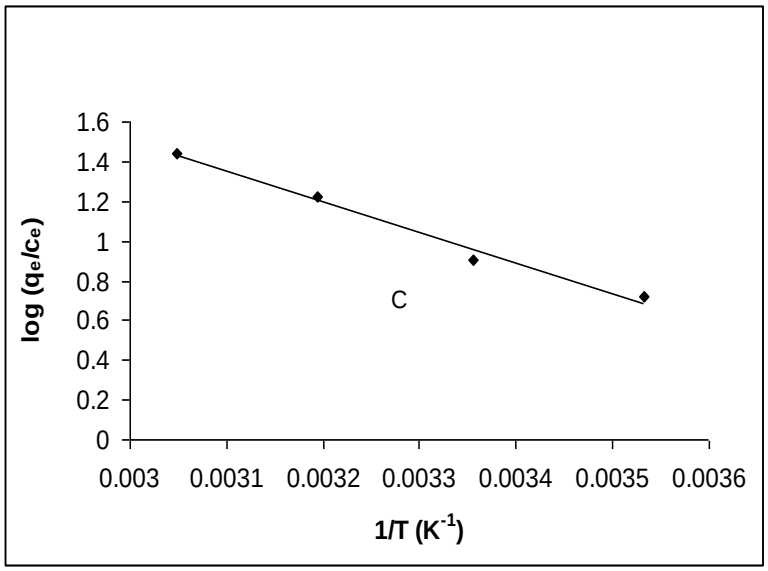

Fig.6: The plot of log (q_e/c_e) versus 1/T (K^{-1}) for adsorption of fluoride onto iron (III)-aluminum (III) mixed oxide.Temperature: 28 (±1)ºC, pH: 6.9 (±0.2).

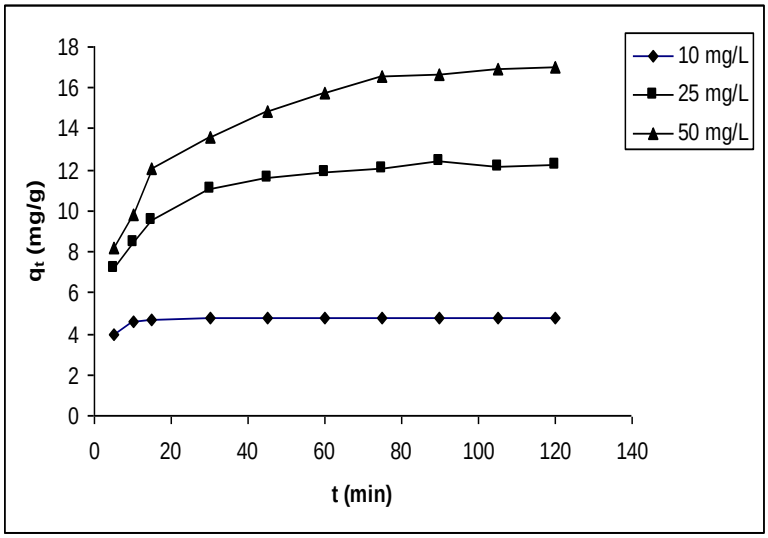

Fig.7: The plot of adsorption capacity q_t (mg g^{-1}) with time (min) for different initial fluoride concentration.
Temperature: 28 (±1)ºC, pH: 6.9 (±0.2).

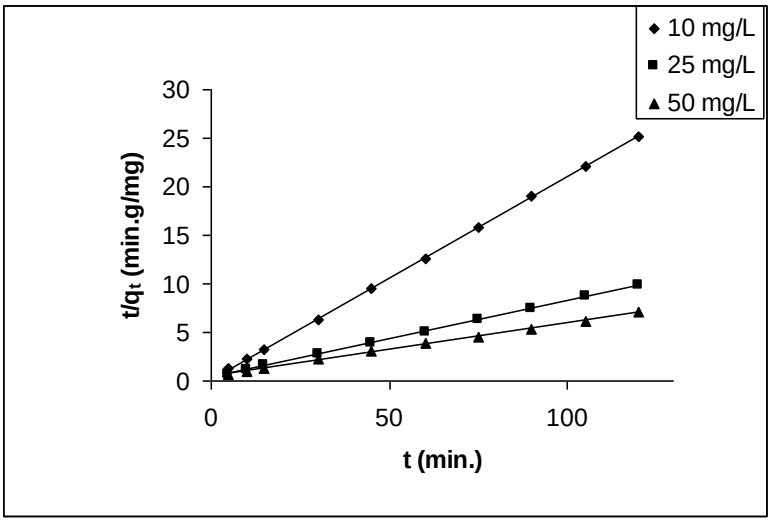

Fig. 7a: The pseudo-Second order kinetic plot for fluoride adsorption onto iron(III)-aluminum(III) mixed oxide.Temperature: 28 (±1)ºC, pH: 6.9 (±0.2).

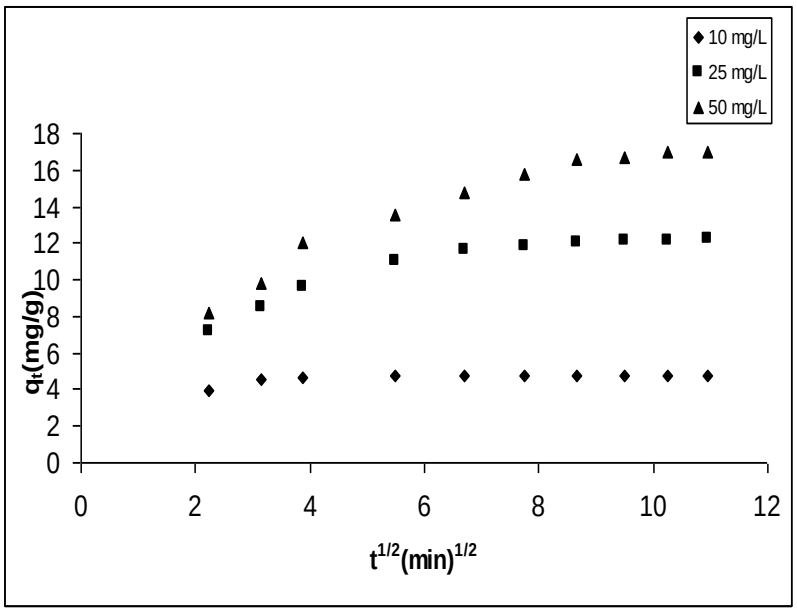

Fig.7b: Intraparticle diffusion kinetic plot for fluoride adsorption onto iron(III)-aluminum(III) mixed oxide.Temperature: 28 (±1)ºC, pH: 6.9 (±0.2).

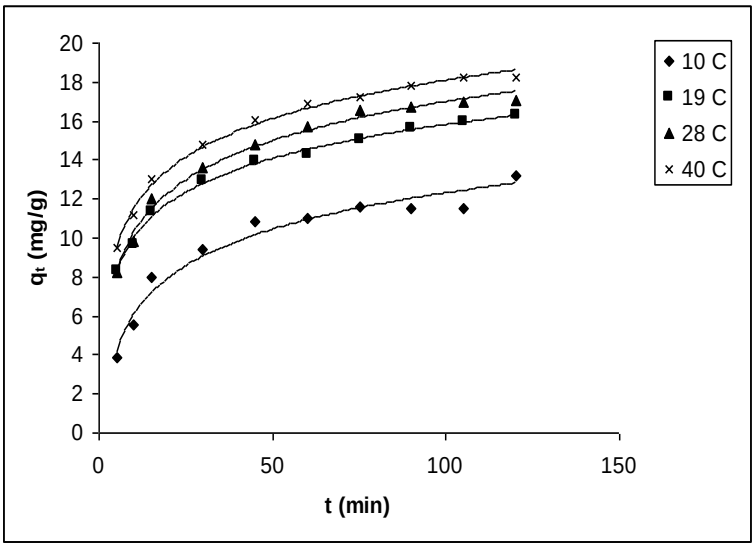

Fig.8: The plot of adsorption capacity, q_t (mg.g^{-1}) versus time, t (min) at different temperatures.The initial fluoride concentration: 50.0 mg L^{-1}, pH: 6.9 (±0.2).

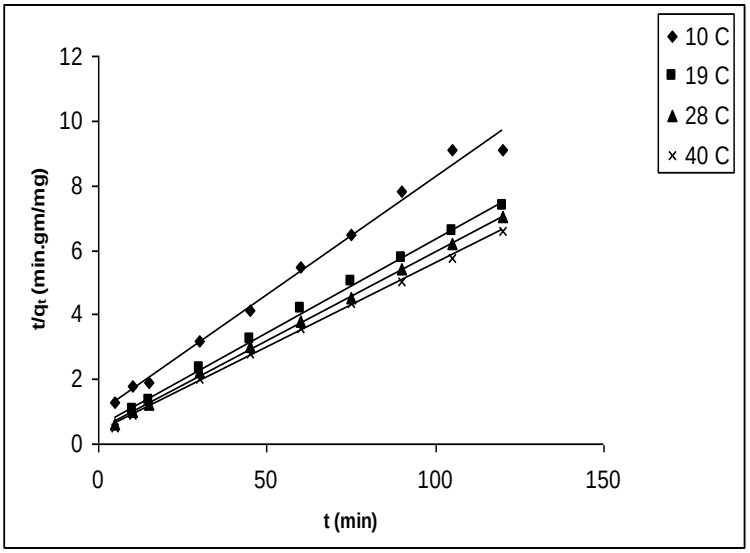

Fig.8a: The pseudo-second order kinetic plot for fluoride adsorption onto iron(III)-aluminum(III) mixed oxide at different temperatures. Initial fluoride concentration: 50.0 mg L^{-1}, pH: 6.9 (±0.2).

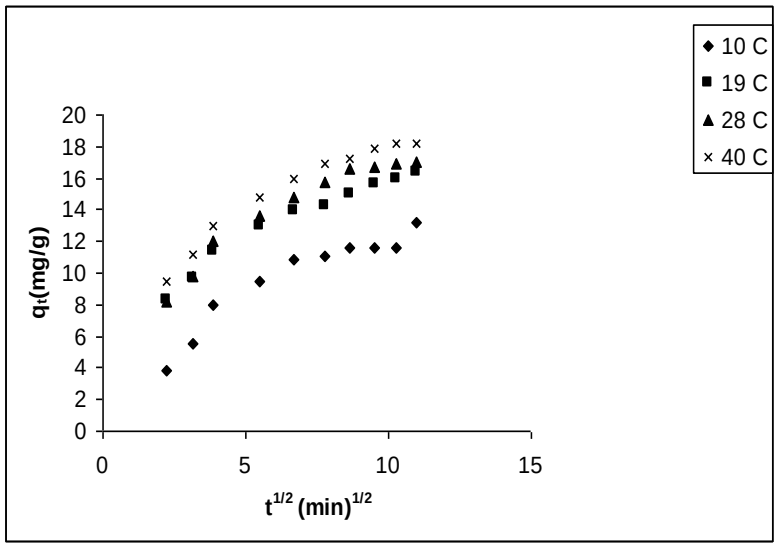

Fig.8b: Intra-particle diffusion plot for fluoride adsorption onto iron(III)-aluminum(III) mixed oxide at different temperatures. Initial fluoride concentration: 50.0 mg L^{-1}, pH: 6.9 (±0.2).

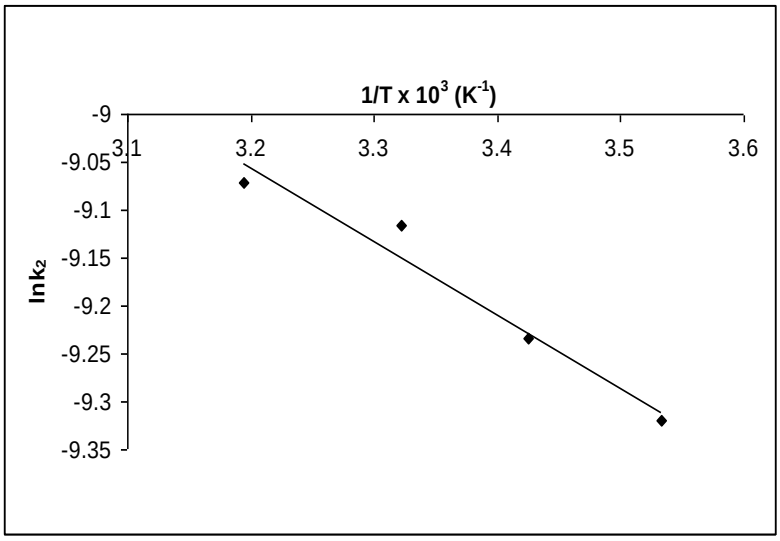

Fig. 9: The plot of ln k_2 versus 1/T for an initial fluoride concentration of 50.0 mg L^{-1} and pH 6.9 (±0.2).

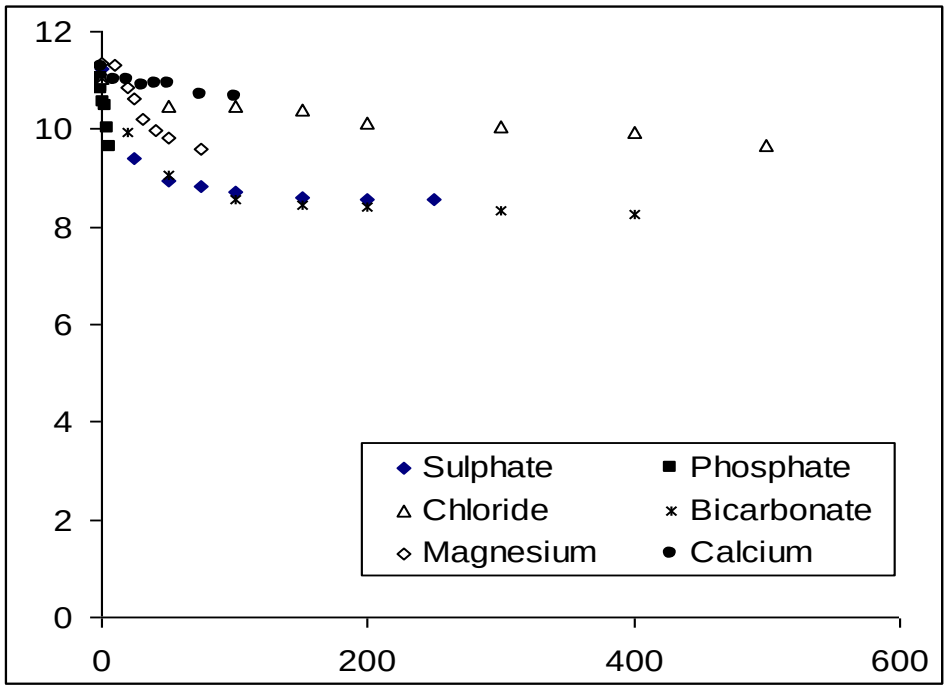

Fig. 10: Effect of foreign ions onto adsorption of fluoride by iron(III)-aluminum(III) mixed oxide as adsorbent.

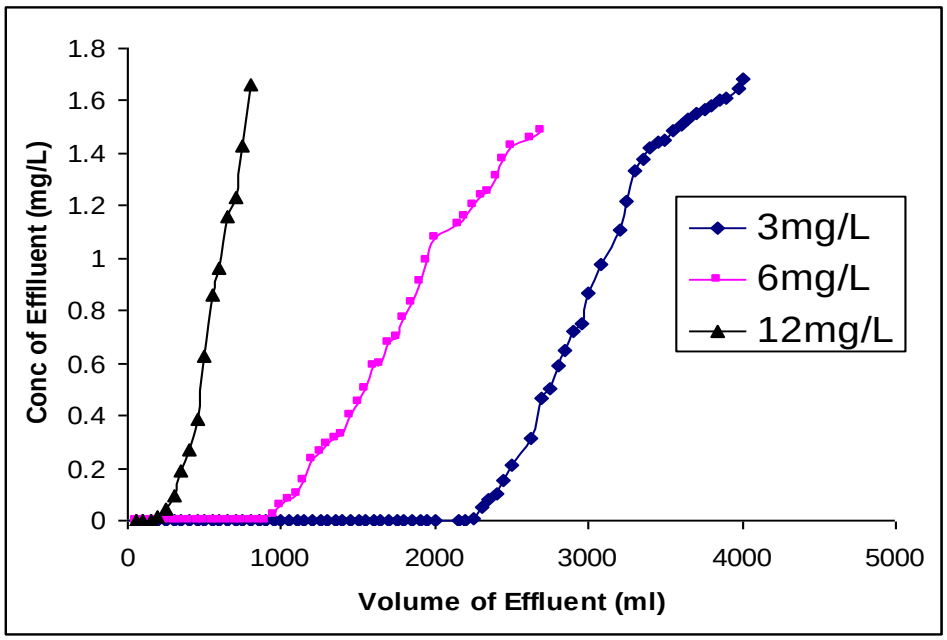

Fig. 11: Column study was performed by a fixed bed column of 1 cm diameter and 4.2 cm bed height at different fluoride concentration.

Chapter 6

Fluoride Adsorption for Removal by Hydrous Iron(III)-Tin(IV) Bimetal Mixed Oxide from the Aqueous Solutions.

6.1. Synthesis of hydrous iron(III)-tin(IV) binary mixed oxide (HITMO)

The synthesis of HITMO was made by hydrolyzing well stirred 0.1 M $FeCl_3$ (in 0.1M HCl) solution with 0.1 M Na_2SnO_3 (in 0.2 M NaOH) at room temperature followed by addition of 0.1 M NaOH to reach the supernatant liquid pH 5.3 (± 0.2). The brown gel precipitate, aged for three overnight, was filtered, washed with deionized water and dried at 70ºC in an air oven. The dried hot product when treated with cold water was broken to small particles. It was meshed (B. S. Sieve) for the fraction 50 to 100 meshes (particle size: 0.29 - 0.14 mm). This fraction was homogenized to a definite pH to be worked, and heat-treated at 250˚C for an hour into a muffle furnace for the use in the experiments.

6.2. Results and Discussion

6.2.1. Characterization of the Mixed Oxide

The FTIR spectra (Fig.1) of synthetic HITMO, hydrous ferric oxide (HFO) and hydrous stannic oxide (HSO) show the broad absorption peaks in the range of 3000-3750 cm^{-1} with maximum pointed at 3401.9, 3397.2, and 3429.6 cm^{-1}, respectively which are due to the stretching vibration of interstitial water and hydroxide groups. The bands found at 1624-1637 cm^{-1} for the OH bending vibration mode of water molecules. The broad peaks at 969.8, 842.7, 954.4 cm^{-1}, respectively, for HITMO, HFO and HSO are for the bending

vibration mode for bridging OH group. The peak obtained for HITMO at lower wave number (528.0 cm^{-1}) to that of HFO (682.6 cm^{-1}) and HSO (564.9 cm^{-1}) indicates the presence of some interactions between iron(III) and tin (IV) presumably through oxygen or hydroxide bridge. Thus, the synthetic HITMO is a hydrous binary composite mixture.

The X-ray diffraction (XRD) analysis (graph omitted) of HITMO shows the product is of amorphous type. The TG of HITMO shows (graph omitted) the weight loss percent 21.1 and 1.32 in the drying temperature (˚C) range, respectively, at 30-130 and >130- 900. The weight loss (21.1%) obtained up to130˚C is attributed to the physically adsorbed water molecules, and is the moisture content of HITMO. The absence of exothermic peak in DT analysis (graph omitted) indicated the material does not undergo polymerization or crystallization when dried up to 900˚C. The surface area (m^2 g^{-1}) determined for HITMO (127.0) was found to be lesser than either the HFO (165.6) or the HSO (140.8), and that indicates the diffusion of tin(IV) oxide into the lattice structure of the HFO. The analyzed iron to tin mole ratio and pH_{zpc} of the mixed oxide composite were 1:1 and 6.1 (± 0.2), respectively. The analysis of SEM images (Fig. 2**)** of HITMO shows irregularity in surface morphology (image-a: 35 times magnification), and agglomerated amorphous nano-powder (image-b: 1000 times magnification).

6.2.2. Effect of pH

Fig.3 shows the adsorption efficiency of fluoride on HITMO under different pH. The results showed that the fluoride adsorption capacity (mg g^{-1}) declined with increasing solution initial pH (pH_i) from 3.0 to 5.0, and remained nearly same up to pH_i 7.5 and that declined again with increasing pH_i. The greater fluoride adsorption capacity at lower pH_i is presumably due to the strong columbic attraction (R4) as the mixed oxide surface

should be positive (pH_{zpc} = 6.1 ± 0.2), and the surface positive charge density reduces with increasing pH and becomes neutral in the range of pH_{zpc}-value.

$MOH_{(S)} + H_3O^+ + F^- \rightarrow MOH_2^+ \text{---} F^-_{(S)} + H_2O$ ---------- (R4)

At pH > pH_{zpc}, the surface of the solid should be negative and, the fluoride adsorption capacity declined due to the columbic repulsion between the solute in solution and the solid surface. The suggested fluoride adsorption mechanism (R4) agrees well to the observed increase in equilibrium solution pH.

6.2.3. Effect of HITMO dose

Fig. 4 shows the effect of HITMO dose on the removal of fluoride at pH 6.40 (± 0.2). The percent of fluoride removal increased from 32.40 to 95.36 when the dose of HITMO was increased from 0.10 g to 0.80 g. However, there was only a small change in the extent of fluoride adsorption when adsorbent dose was increased over 0.80 g.

Furthermore, the adsorption capacity (q_e, mg g^{-1}) value decreased for a fixed fluoride concentration (25 mg. L^{-1}) with the increase of dose. This is agreed well with the increase of solid dose for a fixed solute load and surface sites heterogeneity of the adsorbent. According to surface site heterogeneity model, the surface is composed of sites with a spectrum of binding energies. At low adsorbent dose, all types of sites are entirely exposed and the adsorption on the surface is saturated faster showing a higher q_e value. But at higher adsorbent dose, the availability of higher energy sites decreases with a large fraction of lower energy sites occupied, resulting in a lower q_e value[1,2].

6.3. Kinetic modeling

6.3.1. Effect of concentration:

Fig. 5 shows the fluoride adsorption kinetic data at 303 (±1.6) K and pH 6.40 (± 0.20) on HITMO surface as a function of initial fluoride concentration. The fluoride adsorption was found to be rapid in the first 30 minutes of contact where ~ 90% of the equilibrium adsorbed amount was taken place by the adsorbent. From 30 to 120 minutes, the rate of adsorption became slow. The time required in reaching equilibrium increased with increasing solute concentration and that was 120 minutes for the highest concentration studied. The initial rapid adsorption was presumably due to ion exchange with surface hydroxyl ions of the adsorbent and, the later stage slow adsorption was for the gradual uptake of fluoride at the inner surface.

The time dependent adsorption data shown (Fig.5) were analyzed using the linear form of the kinetic equations[3-5] (Eqs. 3-5) shown in Table 1. The related kinetic equation parameters, obtained by calculation from the slopes and intercepts of the linear plots (best fit plots given), are shown in Table 2**.** The Lagergren pseudo-first order kinetic equation **(**Eq. 3) described the kinetic data fairly well (r^2 = ~0.900 to 0.970) but less well than the pseudo-second order kinetic equation (Eq. 4) (r^2 = 0.990-0.995) at the studied fluoride concentrations. The pseudo-second order rate constant (k_2), adsorption affinity ($h_0 = k_2 q_e^2$) and equilibrium capacity (q_e), obtained (Table 2**)** by calculation from the slopes and intercepts of the plots (Fig. 6), showed the decrease of pseudo-second order rate constant (k_2) values and the increase of h_0 and q_e values with increasing initial fluoride concentration. Thus, the rate of adsorption decreases with increasing the solute concentration. Ho et al[6]., Demirbas et al[7]. and Uzun[8] reported similar trends in their results using different systems.

The data shown in Fig 5 were also analyzed by the intra-particle diffusion kinetic equation (Eq.5) for evaluating rate-controlling step. Fig. 7 shows the plots of mass of fluoride adsorbed per unit mass of HITMO (q_t, mg g^{-1}) versus square root of contact time ($t^{0.5}$, $min^{0.5}$). The data points appeared in Fig. 7 could be joined by two straight lines those indicate the first linear portion for the macro-pore diffusion and the second depicting the micro-pore diffusion[9-14]. The extrapolation of the first linear portion of the plots (excluding the point at zero) back to the axis showing q_t (mg g^{-1}) gives positive intercept which provide the idea about boundary layer thickness, and to be found the boundary layer thickness increases with concentration. The extrapolation of first linear portion of plots (Fig. 7) should not pass through the origin, so the adsorption rate for the present case is not solely pore-diffusion controlled. If the data points shown in Fig. 7 be connected from zero, the initial sharp line showing variation of q_t versus $t^{0.5}$ values in Fig.7 should attribute to the boundary layer diffusion effect or external mass transfer effect[9-14]. Thus, the adsorption data indicated the fluoride removal from aqueous phase on to the studied mixed oxide was rather complex process, involving both boundary layer diffusion and intra-particle diffusion. The k_{id} (average pore diffusion rate constant, mg g^{-1} $min^{-0.5}$) value increased with increasing concentration (Table 2) indicating the higher pore sorption possibility of the solute on to the adsorbent at room temperature. However, the pore-diffusion coefficient (D_P, cm^2 s^{-1}) and film diffusion coefficient (D_F, cm^2 s^{-1}) were calculated using the following standard relations (Eqs. 6, 7)[15,16].

$$D_P = (0.03\ r_0^2) / t_{1/2} \quad \text{---------- (6)}$$

$$D_F = (0.23 \times r_0 \times \partial \times C_s) / t_{1/2} \times C_L \quad \text{---------- (7)}$$

where r_0 is the mean radius of adsorbent particles (assumed spherical), ∂ is the film thickness (0.001 cm)[15], and C_s and C_L are the concentrations of solute in solid and liquid phases at t = t and t = 0, respectively. Here, $t_{1/2}$ (the time for 50% adsorption) values used for calculation were calculated from the relation, $t_{1/2} = 1/ (q_e k_2)$, where k_2 is the pseudo-second order rate constant and q_e has same meaning mentioned elsewhere. It has been known[15] that if the D_p-values be ranged in 10^{-11} to 10^{-13}cm^2 s^{-1}, the pore-diffusion is the rate limiting and if the D_F- values be ranged in 10^{-6} to 10^{-8} cm^2 s^{-1}, the boundary layer (film) diffusion is the rate limiting step. The D_p and D_F values (cm^2 s^{-1}) calculated, respectively, for the present case were in the range (4.49 – 7,27) $\times 10^{-9}$ and 5.48 –8.2) $\times 10^{-10}$ for the studied concentrations of fluoride. It has been found that the values of either D_p or D_F are not laid in appropriate range indicating the fluoride adsorption rate was multi-stage controlled phenomena.

6.3.2. Effect of temperature

Fig. 8 shows the fluoride adsorption kinetic data obtained at studied four different temperatures and at pH 6.40 (± 0.20) on HITMO surface The data were analyzed by using the linear form of the kinetic equations (Eqs. 3-5) (Table 1)[3-5], and the parameters calculated from the slopes and intercepts of the linear plots (Fig. 9**)** are given in Table 3**.**

The pseudo-first order kinetic equation (Eq. 3) described (plots not shown) the present adsorption kinetic data much less well (r^2 = 0.799-0.931). In contrast, the pseudo-second order equation (Eq.4) described the data of Fig. 8 quite well (r^2 = 0.958 - 0.983). The equilibrium adsorption capacity (q_e, mg g^{-1}), which was calculated from the linear plots according to Eq. 4 (Fig. 9**)** increased from 5.29 to 5.84 and the initial adsorption rate ($h_0 = k_2 q_e^2$) was also found to increase from 0.095 to1.667 with the increase of temperature

from 283 (± 1.6) K to 328 (± 1.6) K. So, from the above q_e and h_0 values (Table 3**)**, the endothermic nature of the adsorption process has been indicated. In addition, the pseudo-second order rate constant (k_2 X 10^{-3}, $g.mg^{-1}.min^{-1}$) values (Table 3**)** were found to increase with increasing temperature from 283 (± 1.6) K to 328 (± 1.6) K, and the result obtained has been found to be similar to that due to Ho et al.[6]. Figure 10 shows the plots of the time dependent adsorption capacity (q_t, $mg.g^{-1}$) values obtained with increasing temperature on the reactions versus the square root of the contact time ($t^{0.5}$, $min^{0.5}$) according to the Eq. (5)**.** It has been found that the fit of the kinetic data were very good (r^2 = 0.989 – 0.996) and increasingly well with increasing temperature on the reaction. The initial sharp linear portion over the range of contact time indicated the fluoride adsorption was taken place with boundary-layer (film) diffusion, and the latter curved portion closer to the equilibrium time indicated the intra-particle (pore) diffusion controlled adsorption possibility of fluoride. Thus, the present adsorption kinetic reaction rate is the multistage controlled phenomena[9-14]**.** Furthermore, the calculated D_p and D_F values (cm^2 s^{-1}) for the studied temperature range using the equations (6) and (7), respectively, were (1.07 – 1.73) $\times 10^{-9}$ and (1.59 – 2.81) $\times 10^{-10}$ supported the conclusion drawn above.

6.4. Isotherm modeling

Figure 11 shows the equilibrium isotherm data as points for fluoride adsorption at pH 6.4 (±0.2) and temperature 303 (± 1.6) K on HITMO. The equilibrium data points (Fig. 11) were analyzed by using the most widely used two isotherm equations (Table 4; Eqs. 8, 9) viz. the Langmuir [49] and the Freundlich [50] models. Both the non-linear (plots shown in Fig. 11) and the linear (plots not shown) analyses show the data have been fitted well

with the Langmuir and the Freundlich models. The comparison of the computed isotherm parameters obtained from the linear and the non linear Langmuir and Freundlich isotherm models analyses (Table 5) showed the present data were fit better with the Langmuir ($r^2_{(non\text{-}linear)}$ = 0. 993, χ^2 = 0.0188 and $r^2_{(linear)}$ = 0.992) than the Freundlich ($r^2_{(non\text{-}linear)}$ = 0. 977, χ^2 = 0.0618 and $r^2_{(linear)}$ = 0.988). Thus, the Langmuir isotherm model is the better-fit model for the present data. This indicated the fluoride adsorption by HITMO took place with monolayer surface coverage. The monolayer adsorption capacity (θ, mg g^{-1}) of HITMO for fluoride obtained from either the linear analysis (10.47 $mg.g^{-1}$) or the non-linear analysis (10.58 $mg.g^{-1}$) of the present data was found to be higher than that of the pure iron (III) oxide (7.50 mg g^{-1}). Thus, it could be suggested that the present mixed oxide is a better adsorbent for scavenging the fluoride from water than the pure iron (III) oxide. The Freundlich adsorption constant (K_F, L mg^{-1}) obtained, respectively, from the linear and non-linear analyses were 0.99 and1.15. The Freundlich coefficient, n, which should have values ranging from 1 to 10, obtained from the linear and non-linear analyses were 1.79 and 1.56, respectively, and support the favorable adsorption of fluoride onto the mixed oxide.

6.5. Thermodynamic parameters

Assuming the activity coefficient as unity at low solute concentrations (Henry's law sense), the thermodynamic parameters for the adsorption process in solution was calculated using the following thermodynamic relations (Eqs. 10 and11):

$\Delta G^0 = \Delta H^0 - T\Delta S^0$ …… (10) and $\Delta G^0 = -2.303RT \log K_c$ …….. (11)

Combining the equations (10) and (11), the equation (12) is obtained.

$\log K_c = \Delta S^0 / 2.303R - (\Delta H^0/2.303R)\ 1/T$ ----------(12)

Each term in equations (10-12) has their usual significance and given in the nomenclature. The thermodynamic equilibrium constant, K_c was calculated by using equation (13),

$K_c = q_e / C_e$ ---------- (13) where q_e/C_e is called the adsorption affinity ($L.g^{-1}$), which is the ratio of the amount adsorbed per unit mass (q_e) to the solute concentration in solution (C_e) at equilibrium. So the above relation (Eq. 12) can be written as (Eq. 14)

$\log(q_e/C_e) = \Delta S^0/2.303R - (\Delta H^0/2.303R)1/T$ ……(14)

Assuming ΔS^0 and ΔH^0 to be constant within the range of studied temperature, the values were computed from the slope and intercept of the straight line of plots of log (q_e/C_e) versus 1/T (Fig.12), and ΔG^0, the free energy change for the reaction, at various temperatures was also calculated by using the equation (10). The plots showed good linearity with very good regression coefficients (r^2 = 0.992 and 0.993). The thermodynamic parameters computed for the present case for the studied solute concentrations (10.0 mg L^{-1} and 25.0 mg L^{-1}) are given in Table-6. The positive ΔH^0 ($kJ.mol^{-1}$) values indicated the fluoride adsorption on HITMO was an endothermic process. The positive entropy change (ΔS^0, J mol^{-1} K^{-1}) obtained (+8.72 and +24.17) for the present system for 10.0 and 25.0 $mg.L^{-1}$of fluoride solutions indicated the solute adsorption was taken place with increasing entropy of the system. This is presumably due to the release of greater number of water molecules at the solid–liquid interface during adsorption of hydrated fluoride ion. The positive ΔG^0 ($kJ.mol^{-1}$) values (Table.6) indicated the fluoride adsorption by HITMO is a non-spontaneous one and, that was governed by gaining energy from surroundings [22, 48].

6.6. Energy of adsorption

The equilibrium data shown as points in the Fig. 11 were analyzed by the Dubinin-Radushkevick (D-R) equation[2,16,17] (Eq.15) for evaluating the average adsorption energy of adsorption.

$$\ln q_e = \ln q_m - \beta\varepsilon^2 \quad (15)$$

$$\varepsilon = RT \ln (1+ 1/C_e) \quad (16)$$

The significance of each term present in equations (15) and (16) has been given elsewhere.

The q_m (mol.Kg^{-1}) and β (mol^2 kJ^{-2}) have been evaluated from the intercepts and slopes of the plots of ln q_e versus ε^2 (Fig. 13)**.** The mean free energy of adsorption (E_{DR}) is the free energy change when one mole of a solute is transferred to the surface of the adsorbent from infinity in the solution[17], and that has been calculated by the equation (Eq. 17)

$$E_{DR} = 1/ (2 \beta)^{1/2} \quad (17)$$

The D–R parameters and mean free energies evaluated are shown in Table 5**.** The magnitude of E_{DR} (kJ.mol^{-1}) is useful for estimating the type of adsorption reaction, and if it ranged between 8.0 and16.0 the adsorption should be taken place by ion exchange reaction[2,16]**.** In the present case, the E_{DR} value obtained (9.05 kJ.mol^{-1}) (Table 5) was ranged in 8.0 to16.0 kJ.mol^{-1} that indicated the adsorption of fluoride onto HITMO has taken place by ion exchange mechanism.

6.7. Activation parameters

The increase in pseudo-second order rate constant (k_2) with increasing temperature may be described by the Arrhenius equation (Eq. 18):

$$k_2 = A \exp (-E_a / RT) \quad \ldots\ldots\ldots\ldots\ldots\ldots\ldots\ldots (18)$$

k_2 is the pseudo second order rate constant (g.mg $^{-1}$.min^{-1}), A is a temperature-independent factor (g mg $^{-1}$min^{-1}), E_a the activation energy of adsorption (kJ mol^{-1}), R the gas constant (8.314 J mol $^{-1}$ K^{-1}) and T the absolute temperature (K). Taking logarithmic of equation (18), the following Arrhenius type linear relationship (Eq. 19) is obtained.

$$\ln k_2 = \ln A + (-E_a/R)\, 1/T \quad \ldots\ldots\ldots\ldots\ldots\ldots\ldots\ldots (19)$$

The plot of lnk_2 against 1/T shows a linear (Fig. 14) variation with a high regression coefficient (r^2 = 0.994) value. The intercept and slope of the plot gave the temperature independent parameter, A (7.2 x 10^{-4} g mg $^{-1}$s^{-1}) and the activation energy, E_a (6.02 kJ mol^{-1}), respectively, and are similar to the results reported by Ozcan et al.[2,16].

6.8. Desorption Study

From the results of pH effect on fluoride adsorption by HITMO, it was found that the fluoride adsorption capacity of HITMO was low in alkaline pH. Based on this, batch desorption test of fluoride from the solid surface was conducted by various pH solutions, and found that pH 13 (0.1M NaOH) solution is optimum one. The use of 25 ml of pH 13 solution per g fluoride rich HITMO (F^- content: 10.0 mg.g^{-1}) in five consecutive steps desorbed ~75% of adsorbed fluoride.

6.9. A case study

The fluoride removal efficiency of HITMO was tested by spiking fluoride up to a level 2.97 mg.L^{-1} into a ground water sample collected from a tube well (location: College Square, Kolkata, India). The initial parameters analyzed (mg.L^{-1} except pH) for the water sample were: pH 7.75, total hardness (as $CaCO_3$) 704,total alkalinity 727 , Ca^{2+} 221.24, Mg^{2+} 174.38, Fe (total) 0.05, TDS 1201, Cl^- 357.7, F^- 0.35 and As(total) 0.03. The natural water was spiked with fluoride to a concentration 2.97 mg.L^{-1}. The solid material,

HITMO, of a definite amount ranged in 0.5 to 3.0 g was added to the one liter of the fluoride spiked sample and stirred by a digital mechanical stirrer (speed:1000 rpm) for 2.0h. The filtrate of each experiment was analyzed for fluoride. The results (Fig.15) show when HITMO dose used was 2.0 $g.L^{-1}$, the fluoride concentration decreased to 1.49 $mg.L^{-1}$ which is below the toxic level of fluoride concentration in drinking water for the cooler climatic countries and, when the dose used was 2.5 $g.L^{-1}$ that goes to below 1.0 mg. L^{-1}, the permissible level for hotter climatic countries (WHO).

6.10. Conclusion

The HITMO has been synthesized by a simple method.The characterization of the material shows amorphous with irregular surface morphology .The pH zpc value determined is 6.5 ± 0.3. This material has been used for systematic fluoride adsorption for removal from water. The pH effect shows the decrease of the fluoride adsorption from pH 3.0- 5.0 and remains nearly same up to pH 7.5.The adsorption kinetic data obey the pseudo-second order model and the rate is multiple stage control.The equilibrium data are fit well with the Langmuir isotherm, and the monolayer adsorption capacity is 10.50 mg g^{-1}. The energy of adsorption (9.05 kJ mol^{-1}) computed from D-R isotherm suggest the fluoride adsorption took place by ion-exchange. The thermodynamic parameters evaluated for the present adsorption process shows ΔH^0, ΔS^0 and ΔG^0 values positive indicating the fluoride adsorption by HITMO is endothermic and non-spontaneous process. The fluoride rich material can be regenerated up to nearly 75% by a solution of pH 13.0. The application of HITMO for scavenging fluoride from the spiked (2.97 mg F^- L^{-1}) natural water shows 2 g material can reduce below 1.5 mg F^- L^{-1}.

6.11. References

[1] N.Das, P. Pattanaik, R. Das, Defluoridation of drinking water using activated titanium rich bauxite , Colloid. Interf. Sci. 292 (2005) 1-10.

[2] A.A.M. Daifullah, S.M Yakout, S.A. Elreefy, Adsorption of fluoride inaqueous solutions using $KMnO_4$ – modified activated carbon derived from stem pyrolysis of rich straw, J.Hazard. Mater. 147 (2007) 633-643.

[3] S. Largergren, Zur theorie der sogenannten adsorption gelöster stoffe, Kungliga Svenska Vetenskapsakademiens. Handlingar 24 (1898) 1-39.

[4] Y. S. Ho, G. McKay, Kinetic model for lead (II) sorption onto peat, Adsorp. Sci. Technol. 16 (1998) 243-255.

[5] W.J. Weber Jr., J.C. Morris. Kinetics of adsorption on carbon from solution, J. Sanit. Div. Am. Soc. Civ. Eng. 89 (1963) 31- 60.

[6] Y. S Ho, T.H. Chiang, Y.M. Hsueh, Removal of basic dye from aqueous solution using tree fern as a biosorbent, Process Biochem. 40 (2005) 119-124.

[7] E Demirbas, M. Kobya, E. Senturk, T Ozkan, Adsorption kinetics for the removal of chromium(VI) from aqueous solutions on the activated carbons prepared from agricultural waste, Water SA 30 (2004) 533-539**.**

[8] I Uzun, Kinetics of the adsorption of reactive dyes by chitosan, Dyes Pigments 70 (2006) 76-83.

[9] M. Maharamanlioglu, I. Kizilcikli, I. O. Bicer, Adsorption of fluoride from aqueous solution by acid treated spent bleaching earth, J. Fluorine Chem. 115 (2002) 41-47.

[10] S. V. Mohan, S. V. Ramanaiah, B. Rajkumar, P. N. Sarma, Removal of fluoride from aqueous phase by biosorption on to algal biosorbent spirogyra Sp.– 102: sorption mechanism elucidation, J. Hazard. Mater. 141(2007) 465-474.

[11] V. C. Srivastava, M. M. Swamy, I. D. Mall, B. Parasad, I. M. Mishra, Adsorptive removal of phenol by bagasse fly ash activated carbon: equilibrium, kinetics and thermodynamics, Colloids Surf. A: Physicochem. Eng. Aspects 272 (2006) 89-104.

[12] K. K. Singh, R. Rastigo, S. H. Hasan, Removal of Cr(VI) from waste water using rice bran, Colloid Interf. Sci. 290 (2005) 61-68.

[13] V. K. Kumar, V. Ramamurthi, S. Sivanesan, Modeling the mechanism involved during the sorption of methylene blue onto fly ash, Colloid Interf. Sci. 284 (2005) 14-21.

[14] T. S. Sing, K. K. Pant, Equilibrium, kinetics and thermodynamics studies for adsorption of As(III) on activated alumina, Sep. Purif. Technol. 36 (2004) 139-147.

[15] F. Helfferich, Ion Exchange, McGraw-Hill: New York, 1962.

[16] A. Ozcan, E. M. Oncu, S. Ozcan, Kinetics, isotherm and thermodynamic studies of adsorption of acid blue 193 from aqueous solutions onto natural sepiolite, Colloids and Surfaces A: physicochem. Eng. Aspects. 277 (2006) 90-97.

[17] M. M. Dubinin, L. V. Radushkevich, Proc. Acad. Sci.U. S. S. R. Phys. Chem. Sect. 55 (1947) 331.

Table-1: The kinetic equations used for analyzing time dependent fluoride adsorption data (significance of each term is given in nomenclature)

Equations	**Rate equation**	**Linear form used and plot made**	**Equation no.**	**Reference**
Pseudo-first order	$dq_t/dt = k_1 (q_e - q_t)$	$\log (q_e - q_t) = \log q_e - k_1 t / 2.303$, $\log (q_e - q_t)$ versus t	3	3
Pseudo-second order	$(dq_t/dt) = k_2 (q_e - q_t)^2$	$t/q_t = 1/(k_2 q_e^2) + t/q_e$, t/q_t versus t	4	4
Intra particle diffusion	----------	$q_t = k_{id} t^{1/2} + C$, q_t versus $t^{1/2}$	5	5

Kinetic equations	Parameters	Fluoride concentration ($mg.L^{-1}$)		
		10	15	25
Pseudo-second order	$k_2 \times 10^{-2}$	7.41	4.08	1.70
	q_e	1.62	2.41	4.37
	r^2	0.993	0.995	0.990
	h_0	0.200	0.238	0.333
	$k_1 \times 10^{-2}$	2.18	2.49	3.01

	q_e	0.75	1.31	3.03
Pseudo-first order	r^2	0.954	0.967	0.900
	k_{id} x 10^{-}	1.12	1.76	3.25
Intraparticle diffusion [1]	r^2	0.813	0.880	0.917

Table 2: The kinetic parameters obtained for fluoride adsorption on HITMO at different concentrations [temperature: 303 (± 1.6) K] and pH 6.4 (± 0.2).

Kinetic equations	**Parameters**	**Temperature (± 1.6 K)**			
		283	298	313	328
	k_2 x10^{-3}	3.37	3.82	4.19	4.89

Pseudo-second order	q_e	5.29	5.55	5.68	5.84
	r^2	0.983	0.965	0.960	0.958
	h_0	0.095	0.117	0.135	0.167
	$k_1 x\ 10^{-2}$	3.63	2.65	2.25	2.21
Pseudo-first order	q_e	5.54	4.80	4.35	4.61
	r^2	0.799	0.835	0.931	0.910
	$k_{id} x\ 10^{-1}$	3.56	3.81	3.88	4.18
Intraparticle diffusion	r^2	0.989	0.994	0.996	0.996

Table 3: The kinetic parameters on fluoride adsorption on HITMO at different temperatures and pH 6.4 (± 0.2). Fluoride concentration used: 25 $mg.L^{-1}$

Table 4: The isotherm model equations used for analysis of fluoride adsorption equilibrium data (significance of each term of equations is given in nomencluture).

	Equation.

Models	Non-linear form	Linear form	no.	Reference
Langmuir Isotherm	$q_e = \theta b C_e/(1+bC_e)$	$C_e/q_e = 1/(\theta b) + C_e/\theta$	8	15
Freundlich Isotherm	$q_e = K_F C_e^{1/n}$	$\log q_e = \log K_F + 1/n \log C_e$	9	16

Table 5: The evaluated isotherm parameters for fluoride adsorption on HITMO at 303 (± 1.6) K] and pH 6.4 (± 0.2).

Isotherm models	Linear analysis parameters	Non-linear analysis parameters

	θ	b	r^2	θ	b	r^2	χ^2
Langmuir							
	10.47	5.5×10^{-2}	0.992	10.58	5.36×10^{-2}	0.993	0.0188
Freundlich	K_F	n	r^2	K_F	n	r^2	χ^2
	0.99	1.79	0.988	1.15	1.56	0.977	0.0618
D-R Isotherm	q_m	β	E	r^2	……..		
	1.77×10^{-3}	6.1×10^{-3}	9.05	0.992			

Table 6: The thermodynamic parameters for adsorption of fluoride on HITMO.

Fluoride concentrations ($mg.\ L^{-1}$)	ΔH^0 ($kJmol^{-1}$)	ΔS^0 ($J\ mol^{-1}K^{-1}$)	ΔG^0 ($kJ\ mol^{-1}$) at different studied temperatures (± 1.6 K)			
			283	298	313	328
10.0	4.79	8.72	2.32	2.19	2.06	1.93
25.0	10.79	23.85	4.04	3.67	3.31	2.95

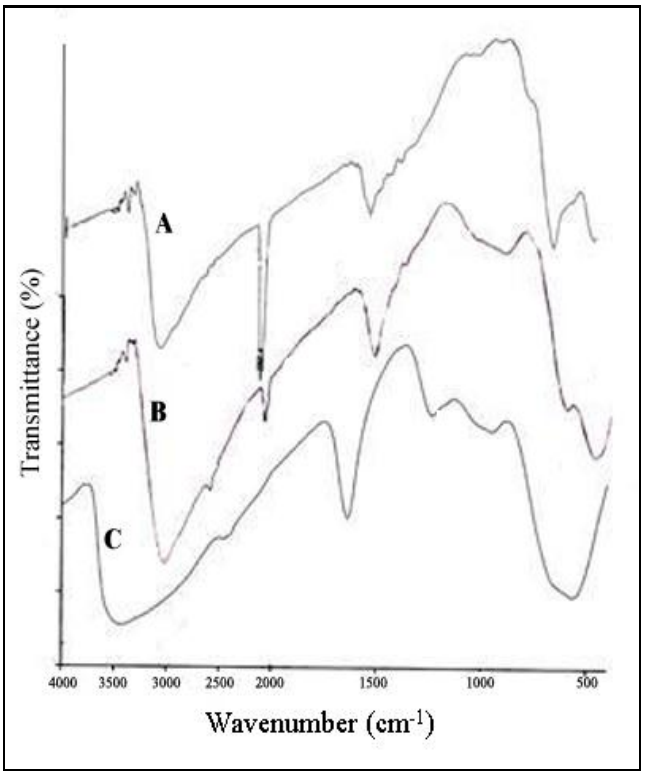

Fig.1: The FTIR spectra of (A) hydrous ferric oxide (HFO) (B) hydrous iron(III)-tin(IV) bimetallic mixed oxide (HITMO) and (C) hydrous stannic oxide (HSO).

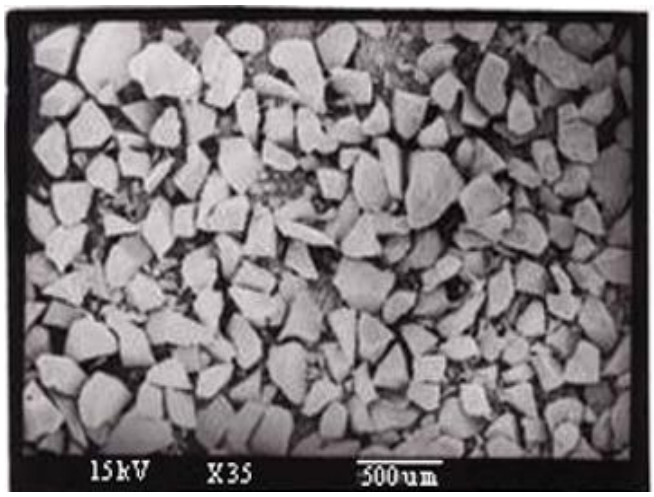

a

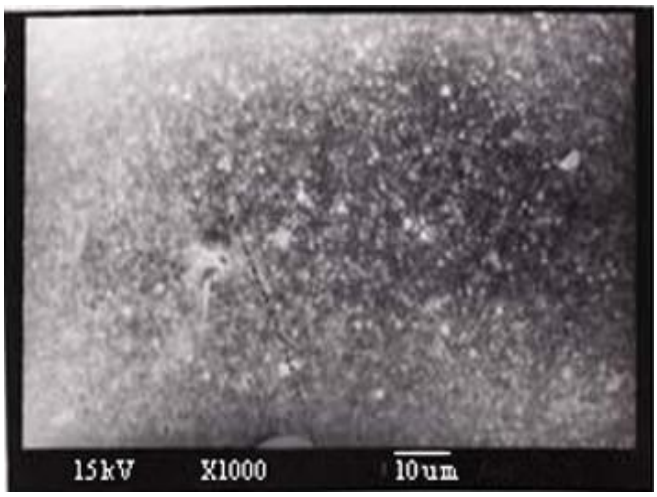

b

Fig. **2:** The scanning electron microscopic (SEM) image of HITMO of magnifications (a) 35 times (b) 1000 times.

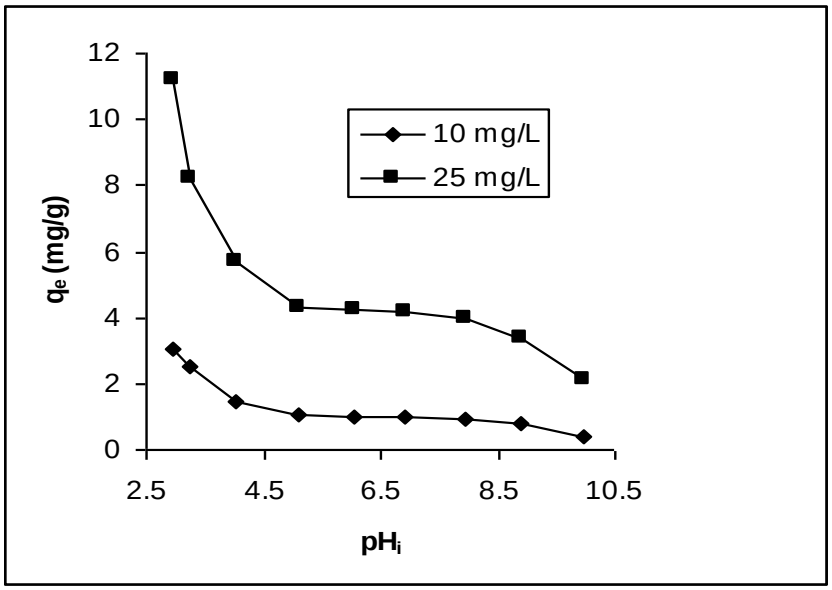

Fig.3: The effect of initial pH (pH_i) on fluoride adsorption by HITMO at 303 (± 1.6) K.

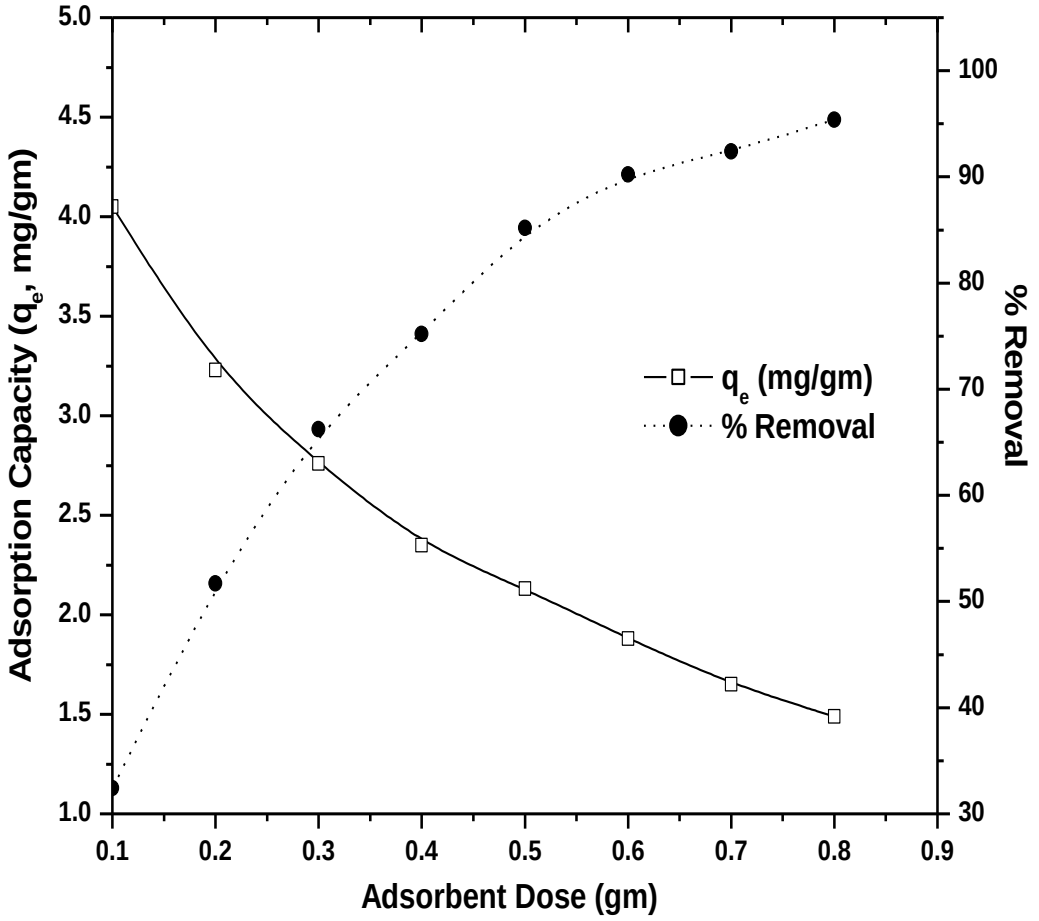

Fig.4: The effect of HITMO dose on fluoride removal at 303 (±1.6) K and at pH 6.40 (± 0.2) from the loaded 50 ml of 25.0 mg L^{-1} fluoride solution.

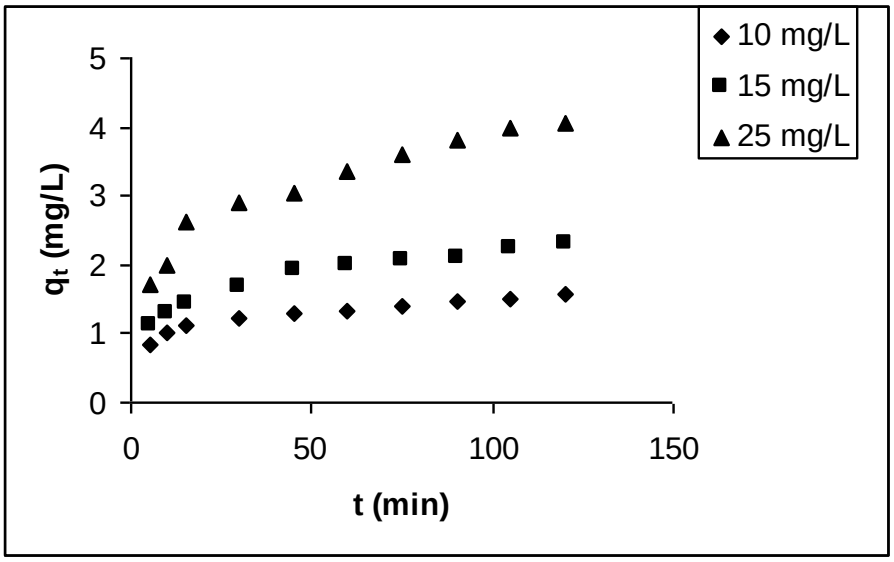

Fig. 5: The fluoride adsorption kinetics data on HITMO at 303 (±1.6) K and at pH 6.40 (± 0.2)

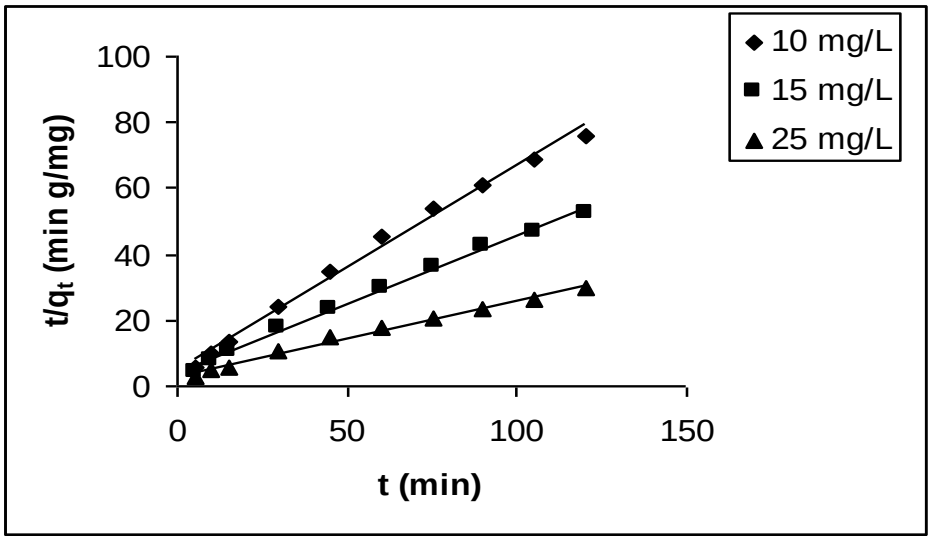

Fig. 6: The pseudo second order plots for the fluoride adsorption kinetic data obtained on HITMO at pH 6.40(±0.2) and 303 (± 1.6) K.

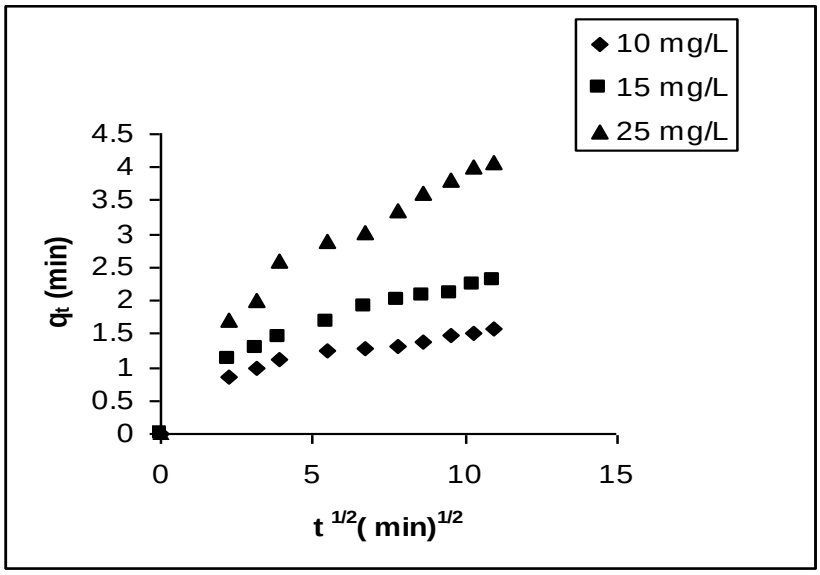

Fig.7: The intra-particle diffusion plots for the fluoride adsorption kinetic data obtained on HITMO at 303 (± 1.6) K and at pH 6.40(±0.2).

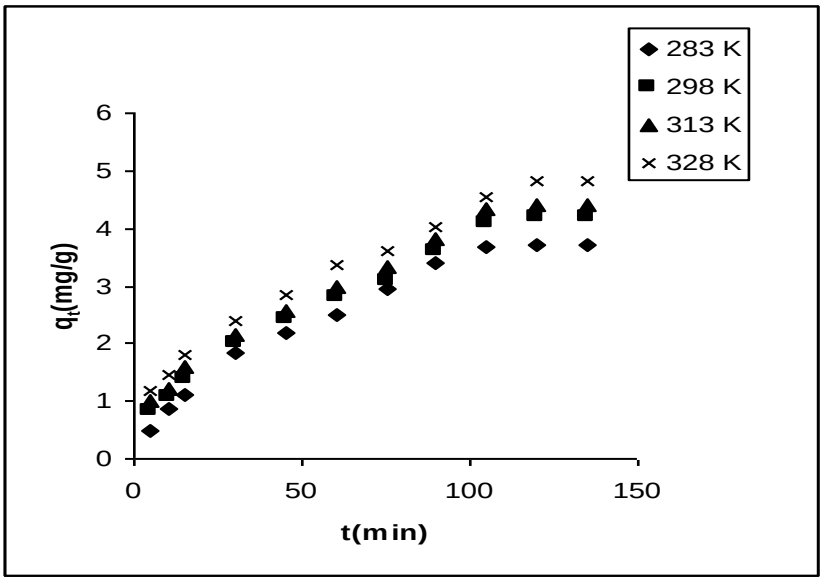

Fig. **8:** The temperature dependent fluoride adsorption kinetics data obtained on HITMO at pH 6.40(±0.2). Fluoride concentration: 25 mg L^{-1}.

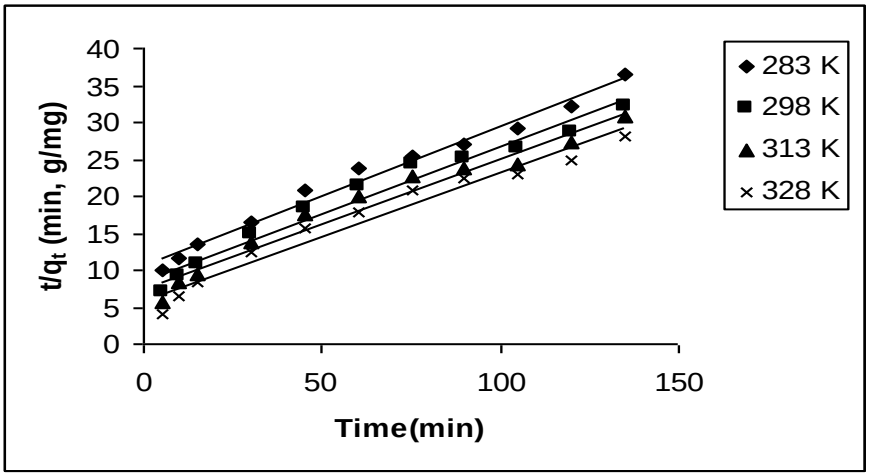

Fig. **9:** The pseudo-second order plots of the temperature dependent fluoride adsorption kinetic data obtained on HITMO at 6.40(±0.2). Fluoride concentration: 25 mg L^{-1}..

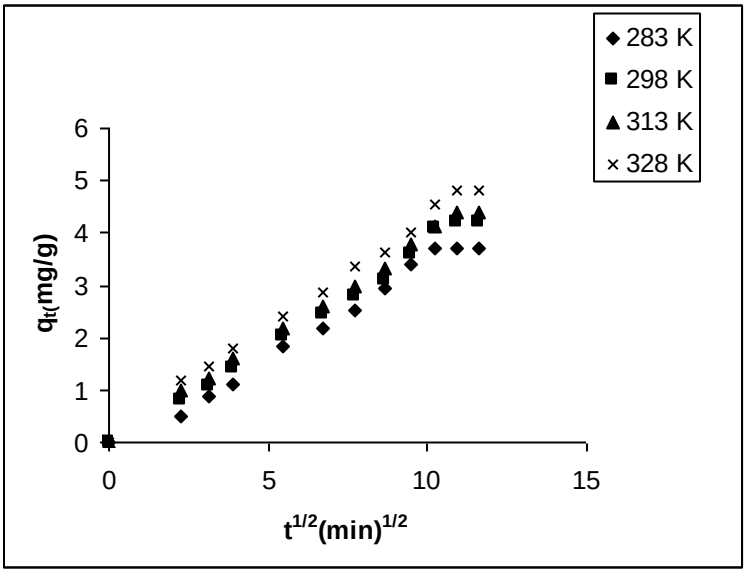

Fig.10: The intra-particle diffusion plots for the fluoride adsorption kinetic data obtained on HITMO at four different temperatures [pH 6.40(±0.2) and fluoride concentration of 25 mg L^{-1}.

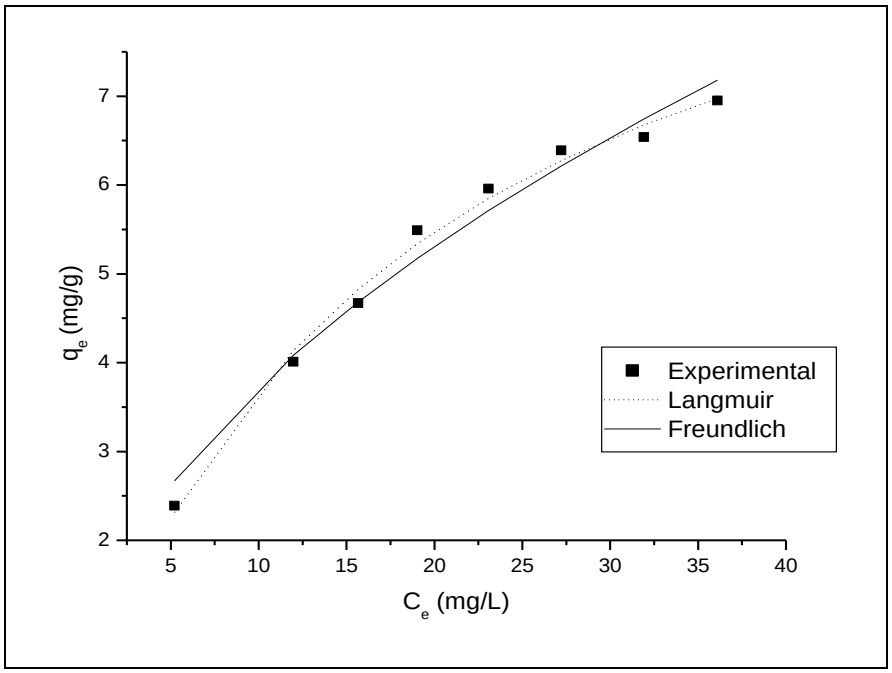

Fig.11: The plot of equilibrium adsorption capacity versus equilibrium concentration of fluoride on HITMO at 303 (± 1.6) K and at pH 6.40(±0.2) and the non-linear data fits with the Langmuir and Freundlich isotherm models.

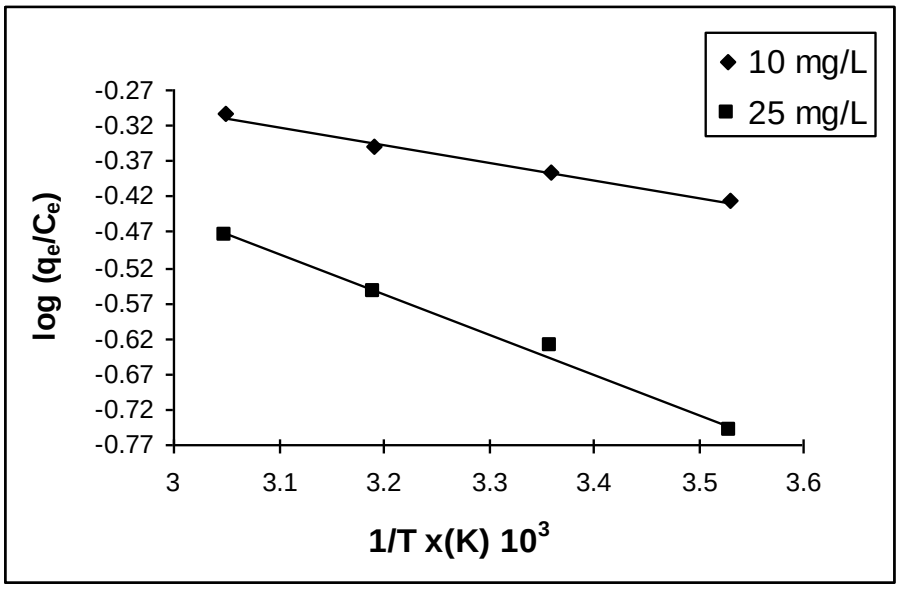

Fig.12: The plot of log (q_e/C_e) against 1/T (K) X 10^3 for thermodynamic parameters.

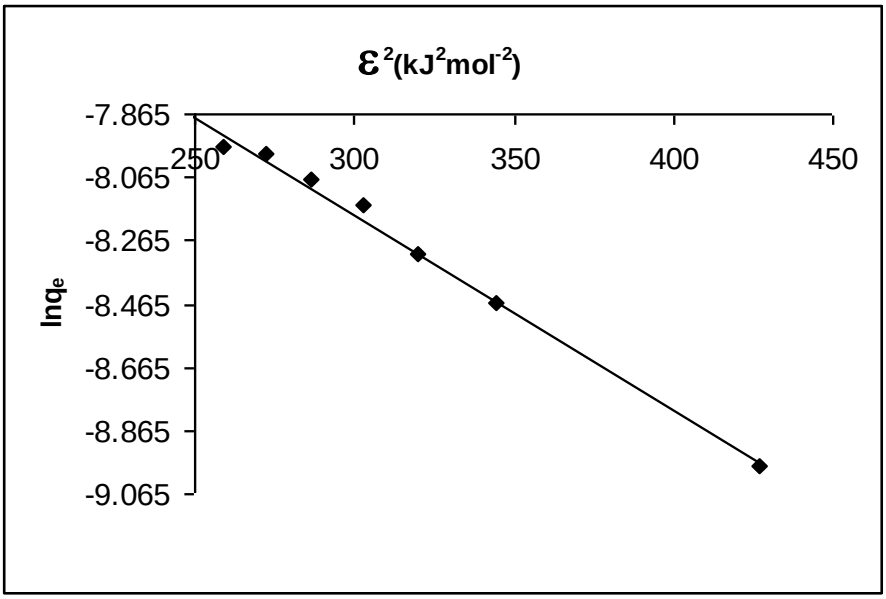

Fig.13: The Dubinin-Raduskevich (D-R) isotherm plot of the equilibrium data for the adsorption energy.

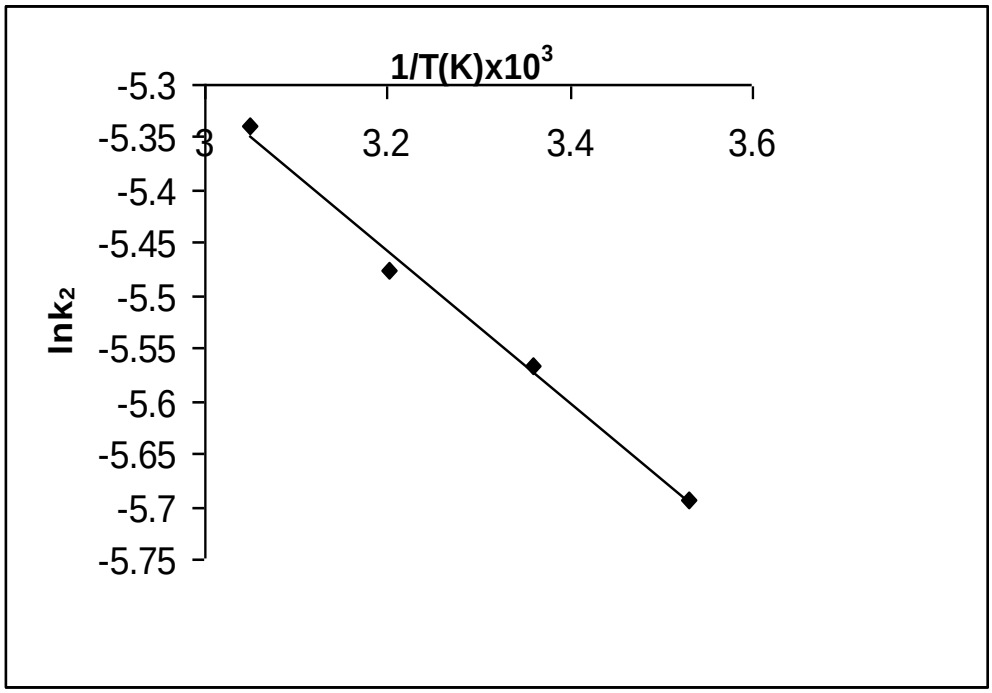

Fig.14: The plot of ln k_2 versus 1/T (K) X 103 for the activation parameter for fluoride adsorption on HITMO.

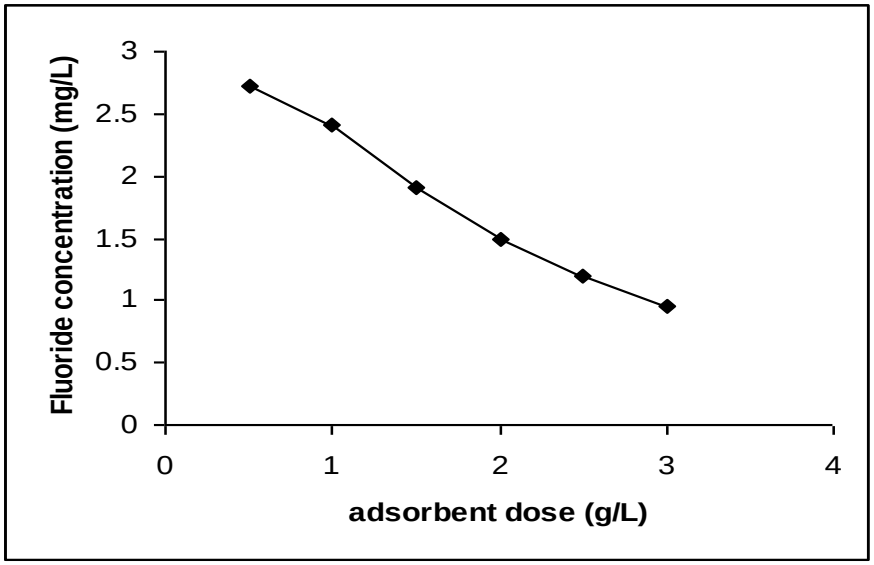

Fig.15**: The batch fluoride removal with varying HITMO dose per L of the natural water sample.**

Chapter 7

Field sample analysis for spot selection for field test

In order to selection of spot for the field application of our developed materials, field ground water samples were collected and analyzed for fluoride from some pockets of West Bengal. The results which we have obtained are presented in Table 1 – 3.

Table 1: Analysis of fluoride (mg/L) of some groundwater samples of **Nalhati** block of district **Birbhum**.

Place	Fluoride (mg/L)
Nasipur purbo-para	0.27
Nasipur paschim-para	0.44
Bhabanandapur	0.60
Kadashir durga mandir	0.32
Saotalpara kuya	0.17
Horritatoka primary school	0.25
Gobra jola	0.27
Asnai moszid	0.21
Bodhya uttor-para	0.43
Kasipur daspara	0.22
Lakshanaryanpur pathan-para	**4.21**
Kadashir mondal-para	0.14
Bahadurpur maszid	0.21
Bahadurpur kuya	0.43
Amlai	0.41
Saoutalpara Binaibabur tubewell	0.20
Bhabanandapur tap-water	0.27
Horitokka tubewell	0.22
Nasinu kuya	0.41

Horitokka Primary School	0.25
Udaynagar	0.27

Table 2: Analysis of fluoride (mg/L) in ground water samples of **Kolkata and adjoining area**.

Place	Fluoride Concentration (mg/L)
99/1B Bidhan Sarani, Kolkata-700004	0.42
P65 Krishnaram Bose Street,Shyambazar. kolkata-700004	**1.00**
87/B Arabinda Sarani, Hatibagan, Kolkata-700005	0.65
13/2A Micheal Madhusudan Sarani, Kidderpore, Kolkata-700023	0.39
69/5 B.B.sengupta Road, Behala, Kolkata-700034	0.26
Baguiati, Kolkata-700059	0.66
Maniktala	0.30
Girish Park	0.29
86/1 Suresh Sarkar road, Beleghata,kolkata-700010	0.37
Barasat	0.30
Barasat	0.21
Behala Joducoloni	0.55
56A/17 Banerjee para, paschim putiari, Kolkata-700041	0.44
Dhakuria	0.52
Barrackpore	0.48

Table 3: Analysis of fluoride of some water samples at **Ranigang cold field area**

Place	Fluoride Concentration (mg/L)
Open Well water	
Andal	1.09
Dakshinak	1.02
Siarsol	1.11
Raniganj	0.95
Shipur	1.34
Mine Water	
Nimcha	0.91
Parbelia	1.35
Dubeswari	1.11
Begunia	1.07
Tube Well water	
Ballavpur	1.01
Tapasi	1.23
Barakar	1.19
Shitalpur	0.99
Benipur	1.15
Goba	1.31

Results (Table 1) of Nalhati block show a spot with very high fluoride level. In this context it is said that many of the tube wells with high fluoride are sealed by the administration. The results of the ground water samples of Kolkata and adjoining area (Table 2) show the level of fluoride in the level of permissible value. However, most of the water samples of Raniganj coal field area is contaminated with fluoride above the permissible value (1.00 mg/L, WHO) for the tropical countries.

A comparative assessment among the mixed oxide which were prepared during the project tenure period:

The mixed oxides which were prepared are:

1. Iron(III) – Zirconium(IV)
2. Iron(III) – Aluminium (III)
3. Iron (III) – Tin(IV)
4. Iron(III) - Chromium(III)

Table 1

Mixed oxide	Langmuir monolayer adsorption (mg/g)
Iron(III) – Zirconium(IV)	8.1
Iron(III) – Aluminium (III)	17.73
Iron (III) – Tin(IV)	10.47
Iron(III) - Chromium(III)	16.73

The monolayer adsorption capacity obtained from the Langmuir equation for all the four adsorbents are shown in table 1. Among these adsorbents the minimum monolayer adsorption capacity is for Iron(III)-Zirconium(IV) and the capacity gradually increases for Iron(III)-Tin(IV) to Iron(III)-Chromium(III) to Iron(III)-Aluminium(III) which has the maximum adsorption capacity. The Iron(III)-Aluminium(III) is the best adsorbent for fluoride removal from ground water with highest monolayer adsorption capacity. Although the adsorption capacity for Iron(III)-Chromium(III) is little less than the Iron(III)-Aluminium(III), still it can be used effectively for removal of fluoride from ground water. In view of the toxicity of the metal ions, we can rate Iron (III)-Chromium (III) a better adsorbent for fluoride than Iron (III)-Aluminium (III). According to US EPA the toxicity level for aluminium (III) is 0.05mg/L, whereas chromium (III) is toxic at a level of 0.5mg/L (www.osha.gov). Al (III) is as much as 10 times more toxic than Cr(III)

in drinking water. Moreover, Cr (III) is an essential element for mammals in trace levels. So, according to the guidelines Cr (III) is much more acceptable than the Al (III). Keeping in mind the worse possibility of the constituent metal elements of the adsorbents to leach out in drinking water in the course of adsorption, the Cr (III) is more acceptable than the Al (III). Thus, although the Iron(III)-Aluminium(III) is little more effective than Iron(III)-Chromium(III), we can prefer the later one as best adsorbent for fluoride adsorption from drinking water. The final experiments with Iron (III)-Chromium (III) is being going on to conclude on this matter.

Publications

During the project tenure period, two papers have been published in two different international journals and one paper has been accepted for publication in a national journal. Another paper has been communicated for publication in an international journal and work for another paper, using Iron (III) - Chromium (III) mixed oxide as adsorbent is almost complete.

List of publication in details

Title of Work	Name of the Authors and Journals
Adsorption kinetics of fluoride on iron(III)-zirconium(IV) hybrid oxide	Krishna Biswas ,Durjoy Bandhoyapadhyay and Uday Chand Ghosh*; Adsorption (2007)**13**,83-94
Adsorption of Fluoride from Aqueous Solution by a Synthetic Iron(III)-Aluminum(III) Mixed Oxide	Krishna Biswas, Sanat Kumar Saha and Uday Chand Ghosh*; Ind.Eng.Chem.Res. (2007) **46**,5346-5356
Adsorption of fluoride on synthetic iron(III), zirconium (IV) and binary iron(III)-zirconium(IV) oxides: Comparative assessment on pH – effect and isotherm	Krishna Biswas ,Durjoy Bandhoyapadhyay and Uday Chand Ghosh*, Journal of Environmental Science and Engineering (2007)(**in press)**
Fluoride adsorption for Removal by Hydrous Iron (III) –Tin (IV) Bimetal Mixed Oxide from the aqueous Solutions.	Communicated in **Chemical Engineering Journal** (Under Review, Mans.No. CEJ-D-08-00163**)** **Authors:** Krishna Biswas , Kaushik Gupta and Uday Chand Ghosh*